Yuri Teixeira e Sousa

Kinematically exact elastoplastic analysis of steel rods with compact cross sections

A dissertation submitted in partial fullfilment of the requirements for the degree of Master of Science.
Area of concentration: Structural Engineering
Advisor: Eduardo M. B. Campello

University of São Paulo

Polytechnic School

Postgraduate Program in Civil Engineering

São Paulo
2017

Este exemplar foi revisado e corrigido em relação à versão original, sob responsabilidade única do autor e com a anuência de seu orientador.

São Paulo, _____ de _____ de _____

Assinatura do autor: _____

Assinatura do orientador: _____

Catalogação-na-publicação

Sousa, Yuri Teixeira e
Kinematically exact elastoplastic analysis of steel rods with compact cross sections / Y. T. Sousa -- versão corr. -- São Paulo, 2017.
78 p.

Dissertação (Mestrado) - Escola Politécnica da Universidade de São Paulo. Departamento de Engenharia de Construção Civil.

1.Elastoplasticity 2.Exact kinematics 3.Finite element 4.Steel structures I.Universidade de São Paulo. Escola Politécnica. Departamento de Engenharia de Construção Civil II.t.

Abstract

In this work, we present the formulation and implementation of two elastoplastic constitutive equations for kinematically exact thin-walled rod models. The first uses the fact that first order strains due to cross sectional shear stresses and warping are considered to formulate a small strains three-dimensional elastoplastic constitutive model. Given the kinematical hypothesis of non-deformability of the cross section in the projection of its plane, we may also assume that plastic deformations may occur due only to the cross sectional normal stresses, thereby allowing us to formulate a second, simple one-dimensional framework. Our approach adopts a standard additive decomposition of the strains together with a linear elastic relation for the elastic part of the deformation. Both ideal plasticity and plasticity with (linear) isotropic hardening are considered. The models have a computational implementation within a finite element thin-walled rod model and, following the kinematics adopted, we implement this equation on models with consideration of the warping of the cross sections, having 7 degrees of freedom. The formulation and implementation presented is validated by the analysis of problems known in the literature and comparison of the results. We believe that simple elastoplastic models combined with robust thin-walled rod finite element may be a useful tool for the analysis of thin-walled rod structures, such as, e.g., steel structures.

Keywords: Elastoplasticity, Exact kinematics, Finite element, Steel structures.

Resumo

Neste trabalho, apresentamos a formulação e implementação de duas equações constitutivas elastoplásticas simples para modelos de barra de parede fina cinematicamente exatos. O primeiro usa o fato de deformações de primeira ordem devido a esforço cortante na seção transversal e empenamento serem considerados para formular um modelo constitutivo elastoplástico tridimensional para pequenas deformações. Dada a hipótese cinemática de não deformabilidade da seção transversal da barra na projeção de seu plano, podemos também assumir que deformações plásticas ocorrem devido apenas às tensões normais à seção transversal, nos permitindo formular um segundo modelo unidimensional simples. Nossa abordagem adota uma decomposição aditiva padrão das deformações com uma relação elástica linear para a parte elástica das deformações. Tanto plasticidade ideal quanto plasticidade com encruamento isótropo (linear) são considerados. Os modelos resultantes têm uma implementação computacional com elementos finitos de barras e, de acordo com a cinemática adotada, implementamos esta equação com consideração do empenamento das seções transversais, possuindo 7 graus de liberdade. A formulação e implementação apresentadas são validadas pela análise de problemas conhecidos na literatura e comparação dos resultados. Acreditamos que modelos elastoplásticos simples combinados com um elemento finito de barras robusto podem ser uma ferramenta útil para a análise de estruturas reticuladas como, por exemplo, estruturas de aço.

Palavras-chave: Elastoplasticidade, Cinemática exata, Elemento finito, Estruturas de aço.

Contents

1 Introduction

One of the motivations for the development of scientific research in structural engineering is the optimization of material used in structural elements while maitaining their capacity to perform their functions in the structural system. This allows us to fulfill demands for ever stronger and lighter structures and in a wider range of applications. Greater efficiency is acquired through improvements in the fields of materials, manufacturing, fabrication and assembly, design and analysis, with ever more acurate models of physical behavior of the designed structure at an adequate level of practicality. This minimizes the excess of material used to attain the required performance and safety.

For structural steel elements, one of the biggest barriers to advancement in this area is the complexity of methods of analysis with consideration of geometrical nonlinearity (GNL) and the description of nonlinear elastic and inelastic material responses, i.e., consideration of material nonlinearity (MNL). Given the characteristics of the structural steel material and the slender geometry of steel rods, effects of GNL and MNL are relevant for many design criteria, most notably in statically indeterminate plane and spatial frames.

Of the most common methods used in structural design, the inelastic analysis methods consider deformation and load-carrying capacity greater than those in elastic regime due to direct consideration of inelastic redistribution of stresses. It allows a gain of efficiency while maintaining the necessary safety in design with adequate loading and geometric conditions without resorting to approximation through heuristic coefficients to account for this reserve capacity.

The classic methods of structural analysis with consideration of plasticity and GNL are laborious and have been giving way to analyses with mathematical models that are amenable to numerical methods, allowing the use of processing power of current computers. The development and implementation of constitutive equations with consistent kinematical formulations is, because of that, a subject that has attracted researchers. Computational nonlinear elastoplastic analysis methods for reticulated steel structures that have been developed in the last three dacades may be divided into two general groups based on either the plastic hinge or plastic zone representations of yielding.

The plastic hinge representation captures major effects of plastification by modeling the

occurence of points along the rod axis where the whole section is plastified. The rod is considered elastic except where a plastic hinge occurs. Because these hinges have zero-length and full sectional plastification happens at once, this approach neglects effects of the spread of yielding through the cross sections and along the rod axis, and thus is unable to directly simulate the interactions with residual stress and loss of stiffness in the neighborhood of the plastic hinge. Due to the general coarseness of the approach, this methods tend to be more efficient, and practical for many situations in structural design.

Variations of the plastic hinge methods have been proposed to overcome difficulties regarding specific phenomena such as the determination of the location of the plastic hinge under non-uniform distributed loads, approximation of partial sectional yielding and modeling of specific section shapes and connection types. Interactions due to geometric nonlinearities may be accounted for in stability functions, which may have different algeraic formulations and approximations but are not fully nonlinear. Implementation complexity may vary depending on the modifications adopted. These models tend to closely match the results of more refined methods when dealing with slender sections due to the increased likelihood of global instability in elastic regime. For rods with compact sections they tend to overestimate the load-carrying capacity due to the neglect of distributed stiffness degradation, requiring heuristic adjustments.

Analysis with plastic zones uses a finer discretization of the rods in finite elements and also auxiliary subdivisions of the cross sections into fibers or cells which encompass the domain of integration of each cross section. Numerical integration is performed on the discretized section to obtain the stresses and strains along each rod finite element. Incremental loading on the updated deformed configuration captures effects of geometric nonlinearities and completes the main characteristics of these methods. The spread of yielding is directly modeled on the rod finite element mesh and on each cell or fiber of the discretized section, motivating their refinement to capture smoother transitions and evolution of material states. Residual stresses can also be directly modeled on the cells of the cross-section, allowing interaction with the approximated local yielding. Due to the number of phenomena handled directly by these methods, they are often used as a hierarchically higher modeling approach, comparable to analyses using shell finite elements. This greater complexity implies a greater computational cost both in memory space and

processing time, and also more involved implementations. They perform well in calibrating and verifying simpler models but are not practical enough for routine professional structural analyses. In many works published about these methods, it is common to refer to the parts of the discretized cross section as fibers. However, in this work, we will refer to these pieces as *cells* of the discretized sections, emphasizing that they are but a tool for a numerical integration scheme.

Both the plastic hinge and plastic zone approaches fall under the class of advanced analysis methods. Advanced analysis encompasses methods that are able to assess the behavior of a structure without the need for separate individual checks on each member. They provide an alternative to stability and resistance interaction checks that rely on the effective length factor. By considering, even if approximately, geometric nonlinearities, material nonlinearities, residual stresses and geometric imperfections, structural analysis can be made in a single procedure with the advantage of determining specific failure modes of the structure.

This work develops a plastic zone method for the elastoplastic analysis of steel structures using exact rod kinematics. It provides the formulation and computational implementation of an elastoplastic constitutive equation to the kinematically exact rod finite element theories of Pimenta (1993) and Campello (2000), of which it may be regarded as an extension.

These theories assume, as usual in classic beam theories, that the cross sections are non-deformable in the projection of their planes, but consider that they may not remain orthogonal to the rod axis due to shear stress and also that they may no longer be plane due to non-uniform warping, treating the magnitude of the warping as one of the variables of the problem. Two rod constitutive models are proposed. In the first, full three-dimensional plasticity is considered to the extent permitted by the rod kinematics and the linear elastic constitutive equation. In the second model, the stresses acting on the cross sectional normal direction are assumed to dominate the behavior of the rod, which presents a path for simplifications of the yield criterion and the plastic flow law by regarding parts of the constitutive equation as one-dimensional.

The extension of nonlinear and kinematically exact rod theories with elastoplastic material models widens their applicability to many structural systems that require advanced

analysis for adequate design and modeling. This research intends to allow these already powerful rod kinematics to be applied to those cases. It also allows a better comparison with the many variations of advanced analysis methods and other hierarchically higher simulation methods, inserting them in a broad field of research.

Consistent with the literature on the subject, the rods will be considered as a material body mathematically represented by a one-dimensional domain embedded in a three-dimensional Euclidean space.In this work, we will only consider steel rods with compact cross sections, and assume that no sectional in-plane deformation occurs.

For integration of the stresses and strains over the cross section according to the plastic zone approach, we use a numerical integration scheme using an auxiliary mesh which is a discretization of the cross section over which the procedure is carried out. This discretization is also used to solve a boundary value problem to obtain an approximation of the warping function and its partial derivatives with respect to the spatial coordinates of the cross section. Lastly, it is also used to obtain approximations to all relevant geometric properties of the cross section, to be used when the integration over the cross section is performed analytically for comparison with elastic materials. For the update of stress states and internal variables, a simple radial return algorithm suffices for the needs of this work.

In an attempt to make a broad assessment of the developed sheme/model, we have implemented the elastoplastic constitutive equations developed here within the rod models of Pimenta (1993) and Campello (2000) with 7 degrees of freedom, i.e., within kinematical models with considereation of sectional warping. Their results are compared in numerical examples.

1.1 Literature review

Structural analysis of rod elements is a classic subject in engineering and continuum mechanics with vast research history. The first rigorous observations date back to Galileo Galilei and Leonardo da Vinci, with the first consistent formulations in the 18th century by Jacob and Daniel Bernoulli and Leonhard Euler. Dating to the 17th and 18th centuries are the first formilations of theories of elastic and plastic behavior of materials by Robert Hooke and Charles-Augustin de Coulomb. A while latter, in the 19th century when the

theory of elasticity and the theories of plates and shells were getting foundational developments, the first models for materials with plastic behavior came up by Adhémar Barré de Saint Venant, Maurice Lévy, Christian Otto Mohr, Henri Édouard Tresca and James J. Guest, along with the first yield criterion for ductile materials, known as Tresca-Guest yield criterion. Following this, the von Mises yield criterion, with contributions form Maxwell, Huber and Hencky, was formulated in the begining of the 20th century and is one of the main yield criteria used in mathematical modeling of ductile materials like structural steel. Along with this criterion, the first constitutive equations using increments of plastic strain were described by Lévy and von Mises.

In the decade of 1920, Prandtl and Reuss formulated the first equations in which the increments of elastic and plastic strain are treated separately, consisting of the elastoplastic model of Prandtl-Reuss. Also at that time, Timoshenko (1921) wrote the equations for rods with consideration of shear deformation and rotational bending. Years later, in 1940 Vlasov published his theory of thin-walled rods with consideration of non-uniform warping of cross sections (cf. Vlasov, 1959). In this period, great advances were made in the experimental research of materials and formulation of new physical models, notably the Drucker-Prager yield criterion, dislocation theory and other advancements that have not yet widely permeated structural theory (Osakada, 2010).

This work focuses on rod theories with geometrically exact formulations. In general, we can define such theories as

> ... when the relationships between the configuration and the strain measures are consistent with the virtual work principle and the equilibrium equations at the deformed state, regardless of the magnitude of the displacements, rotations and strains. (Crisfield and Jelenić, 1999, p. 1126 apud Tiago, 2007, p. 135)

However, the hypothesis of non-deformability of cross sections in the projection of their planes, assumed in these theories, effectively denies the possibility of truly large strains. In elastoplastic analysis, this is also true due to the fact that this assumption violates the conservation of volume.

The first formulation of a geometrically exact rod theory we owe to Antman (1974) based on a generalization of Kirchhoff's theory for plates. But only with Simo (1985) we had the first formulation consistent with the principles of the mechanics of deformable solids.

These initial developments were made after the formulation for plane frames by Reissner (1972). However, for spatial frames, as pointed by Reissner (1973, 1981) himself, the non-comutative property of tridimensional rotations complicates the derivation of the rotation measures and assuming them as being small renders geometric exactness impossible.

Argyris (1982) presented his seminal paper with results for consistent parameterization of large rotations in tridimensional space. This made possible for Simo (1985) to formulate his already mentioned theory with some important characteristics: (1) being geometrically exact, it takes into consideration all geometrical effects without restriction to the magnitude of displacements and rotations, without resorting to series expansion or truncation of terms of higher order; (2) great simplicity, not needing to involve dual spaces or to distinguish covariance and contravariance of tensors. However, it has the disadvantage of requiring many update procedures at each iteration, with complicated algorithms and it is not frame-invariant, its convergence depending on the path of iterations.

An alternative theory was presented by Cardona and Géradin (1988) in which the primary variables of the problem are the incremental displacements and incremental spin vector of the solid. This work also proposes the use of a rotation vector to parameterize the rotation tensor with the advantage of having a clear geometrical meaning and a smaller number of parameters (three), but unable to avoid singularities in case of large rotations. Furthermore, the linearization of the equilibrium equations shows clear asymmetry, possibly due to neglecting terms of second derivatives of the tensor that relates the spin and rotation vectors.

The first geometrically exact rod theory in tridimensional space in which the rotation tensor is parameterised with the rotation vector and the weak form of the equilibrium equation is presented exactly appeared in Pimenta (1993), having its numerical implementation in Pimenta and Yojo (1993a). In this theory, for conservative loadings, the tangent form of equilibrium is always symmetric, even in a state far from equilibrium. This symmetry is important for the numerical implementation of the equations, simplifying the algorithms a lot. Among the later enhancements of this formulation we can highlight the consideration of cross sectional warping that allows handling of finite strains in Campello (2000), Pimenta and Campello (2001, 2003) and Corrêa (2004). A while later,

various researchers addopted the parameterization of the rotation tensor with the rotation vector to obtain a symmetric weak form of equilibrium, even if this symmetry is not always evident. We can cite Ibrahimbegović et al. (1995), Géradin and Cardona (2001) and Ritto-Corrêa and Camotim (2002).

As a result of the uninterrupted interest in geometrically exact theories based on finite rotations since then, the scope of applications and research has widened. We have the first formulations for elastoplastic behavior for plane frames in Saje et al. (1997) and for spatial frames in Planinc and Saje (1999) and Gruttmann et al. (2000) (the last ones applicable to small elastic and plastic strains); anisotropic materials in Petrov and Géradin (1998); stability bifurcation points in Cardona nad Huespe (1998), Planinc and Saje (1999), Ibrahimbecović and Mikdad (2000); dynamic effects in Armero and Romero (2003), Betsch and Steinmann (2003) and Gams et al. (2007).

1.2 Notation

Throughout this text, italic Latin or Greek letters lowercase or uppercase (a, b, ..., α, β, ..., A, B, ..., Γ, Δ, ...) denote scalar quantities, bold italic Latin or Greek lowercase letters ($\boldsymbol{a}$, $\boldsymbol{b}$, ..., $\boldsymbol{\alpha}$, $\boldsymbol{\beta}$, ...) denote column vectors and bold italic Latin or Greek uppercase letters ($\boldsymbol{A}$, $\boldsymbol{B}$, ..., $\boldsymbol{\Gamma}$, $\boldsymbol{\Delta}$, ...) denote second-order tensors in a three-dimensional Euclidean space. Summation convention over repeated indices is adopted, with Greek indices ranging from 1 to 2 and Latin indices from 1 to 3.

2 Rod kinematics and equilibrium

The following is a short description of the kinematical model and equilibrium equations based on the theorem of virtual work that are adopted as basis for the developments of this work. It consists in a geometrically exact formulation in which shear deformation due to bending and warping of the cross section due to combined bending and non-uniform torsion are explicitly taken into account. For a detailed formulation we refer to the works of Pimenta and Yojo (1993a, 1993b) that was first implemented by Campello (2000). We assume a reference configuration with a straight rod axis. Initially curved rods may be considered as stress-free deformed initial configurations (Campello and Pimenta, 2003). Let $\{\boldsymbol{e}_1^r, \boldsymbol{e}_2^r, \boldsymbol{e}_3^r\}$ be a local orthonormal basis with corresponding coordinates $\{x_1, x_2, x_3\}$ in the reference configuration. Vectors $\boldsymbol{e}_\alpha^r$ are placed on the rod's cross section and $\boldsymbol{e}_3^r$ is placed along the rod axis as shown in Figure 1. Points in this configuration are described by the vector field $\boldsymbol{\xi} = \boldsymbol{\zeta} + \boldsymbol{a}^r$, where $\boldsymbol{\zeta} = x_3\boldsymbol{e}_3^r$ describes the position of points on the rod axis and $\boldsymbol{a}^r = x_\alpha \boldsymbol{e}_\alpha^r$ defines de positions of points on the cross section relative to the axis. Note that $x_3 \in L = [0, l]$ is the axis coordinate, with l being the rod's reference length. Let $\{\boldsymbol{e}_1, \boldsymbol{e}_2, \boldsymbol{e}_3\}$ be a local orthonormal basis in the deformed configuration as seen in

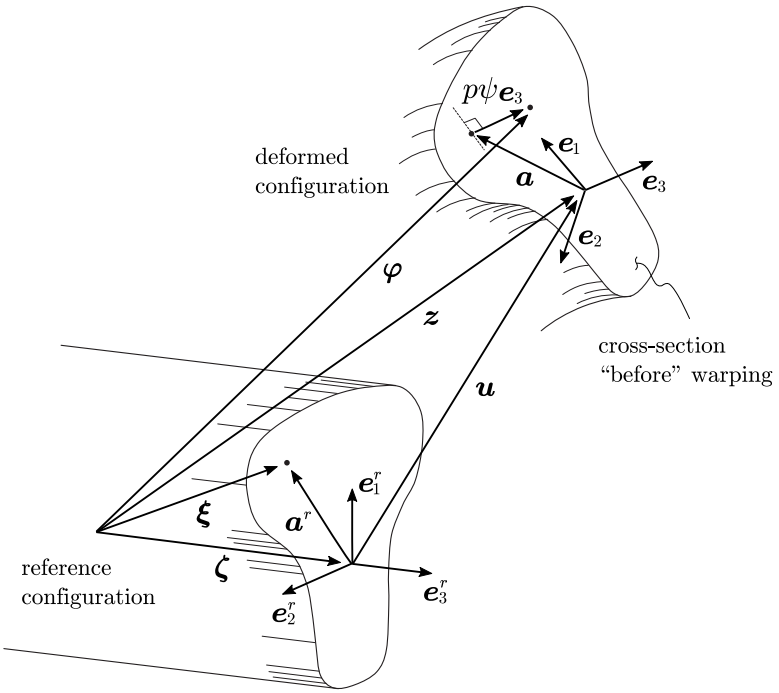

Figure 1: Description of reference and deformed configurations and rod kinematics. Source: the author, derived from figure provided as courtesy by Campello (2014).

Figure 1. We can make a Lagrangian description of the deformation of the rod by a vector

field $\boldsymbol{\varphi}(\boldsymbol{\xi})$ such that the position of the material points in the deformed configuration is expressed by

$$\boldsymbol{\varphi} = \boldsymbol{z} + \boldsymbol{a} + p\psi\boldsymbol{e}_3, \tag{1}$$

where $\boldsymbol{z} = \boldsymbol{z}(x_3)$ describes the position of points at the deformed axis, $\boldsymbol{a} = \boldsymbol{a}(x_i)$ defines the position of points at the deformed cross section *in the projection of its plane*, $\psi = \psi(x_\alpha)$ is a function defining the warping of the cross section with respect to its shear center (the so-called warping function) and $p = p(x_3)$ is a scalar parameter that gives ψ its amplitude. In the next section, we describe a method used to obtain ψ for arbitrary cross sections. Having defined all the basic elements of our deformed configuration seen in equation (1), we will continue the description of the kinematics with the deformation gradient.

2.1 Warping function

To express the warping or deplanation of the cross section mathematically, there are many possible functions ψ to choose from. We have, for example, the classic St. Venant warping function, with expressions derived on a case by case basis for each sectional shape or, for thin-walled cross sections, e.g., the Vlasov sectorial area (Vlasov, 1959), or any other function that adequately describes the out-of-plane deformation of the cross section. In the present work, ψ is approximated using the finite element method. We define the rotation matrix $\boldsymbol{R} = \left[\begin{smallmatrix} 0 & 1 \\ -1 & 0 \end{smallmatrix}\right]$ to be used in the next steps. First, we write the following boundary value problem used to obtain $\overline{\psi}$, the warping function relative to the origin of an arbitrary reference frame on the cross section:

$$\nabla^2\overline{\psi} = 0 \quad \text{in} \quad A \tag{2}$$

$$\nabla\overline{\psi}\cdot\boldsymbol{n} - \boldsymbol{R}\boldsymbol{x}\cdot\boldsymbol{n} = 0 \quad \text{on} \quad \partial A, \tag{3}$$

where $\boldsymbol{x}$ is the position vector of points on the cross section, A is the cross sectional area, ∂A is its boundary and $\boldsymbol{n}$ is the outward normal unit vector on the cross section boundary. Multiplying each equation by a test function v, integrating over their domains and using integration by parts in equation (2) and Green's theorem in equation (3), we can write

this problem in the following variational formulation:

$$\int_A \nabla\overline{\psi} \cdot \nabla v \; dA - \int_A \boldsymbol{Rx} \cdot \nabla v \; dA = 0 \qquad \forall \; v \in \hat{V} \qquad \text{with} \qquad \overline{\psi} \in V, \tag{4}$$

in which $V = \{v \in \mathrm{H}^1(A)\}$ and $\hat{V} = \{v \in \mathrm{H}^1(A) : v = 0 \text{ on } \partial A\}$, where H^1 is the Sobolev space of degree 1. This problem can be solved numerically with a relatively simple finite element implementation, whereby the cross section is discretized (see Pilkey, 2002, for an example).

With $\overline{\psi}$, we can solve a linear system $\boldsymbol{Cs} = \boldsymbol{b}$ to obtain $\boldsymbol{s}$, the position vector of the shear center of the cross section, with

$$\boldsymbol{C} = \int_A (\boldsymbol{x} - \boldsymbol{g}) \otimes \boldsymbol{Rx} \; dA \tag{5}$$

$$\boldsymbol{b} = \int_A \overline{\psi}(\boldsymbol{g} - \boldsymbol{x}) \; dA \tag{6}$$

where $\boldsymbol{g}$ is the position vector of the centroid. We can then obtain the warping function relative to the shear center of the cross section:

$$\psi = \overline{\psi} + \boldsymbol{Rs} \cdot (\boldsymbol{g} - \boldsymbol{x}) - \frac{1}{A} \int_A \overline{\psi} \; dA. \tag{7}$$

Examples of ψ functions as obtained here with the above procedure for arbitrary section shapes are shown in Figure 2. With it, we can obtain many geometric properties of the cross section as will be seen later. We refer to Gruttmann et al. (1999), Campello (2000) and Pilkey (2002) for detailed descriptions of the preceding steps. In this work we assume that ψ remains unchanged even after plastic deformation.

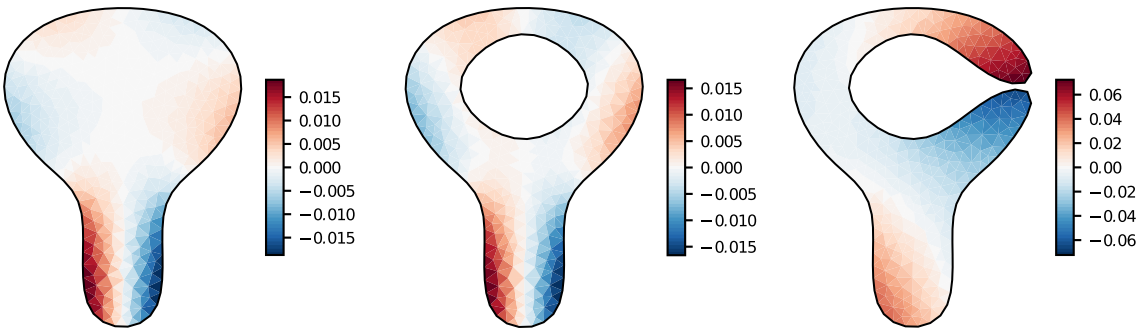

Figure 2: Warping functions relative to the shear centers of arbitrary sections.

2.2 Deformation gradient

Back to the description of the kinematics, let $\boldsymbol{Q}$ be the rotation tensor of the cross section. For local coordinate systems, we have that $\boldsymbol{e}_i = \boldsymbol{Q}\boldsymbol{e}_i^r$ and $\boldsymbol{Q} = \boldsymbol{e}_i \otimes \boldsymbol{e}_i^r$, which relate the bases of the reference and deformed configurations. We can then obtain vector $\boldsymbol{a} = x_\alpha \boldsymbol{e}_\alpha = \boldsymbol{Q}\boldsymbol{a}^r$. From equation (1) and from Figure 1, we can see that $\boldsymbol{z} = \boldsymbol{\zeta} + \boldsymbol{u}$, where $\boldsymbol{u}$ is the displacement vector of points on the rod axis. With these definitions, no cross sectional in-plane distortion is allowed. However, first order shear deformations are accounted for because $\boldsymbol{a}$ is not necessarily normal to the deformed axis, i.e., the deformed cross-section's unwarped plane is not necessarily perpendicular to the rod axis.

The rotation tensor $\boldsymbol{Q}$ may be written in terms of the classic Euler rotation vector $\boldsymbol{\theta} = \theta_i \boldsymbol{e}_i^r$, by means of the well-known Euler-Rodrigues formula

$$\boldsymbol{Q} = \boldsymbol{I} + \frac{\sin\|\boldsymbol{\theta}\|}{\|\boldsymbol{\theta}\|}\boldsymbol{\Theta} + \frac{1-\cos\|\boldsymbol{\theta}\|}{\|\boldsymbol{\theta}\|^2}\boldsymbol{\Theta}^2, \tag{8}$$

in which $\boldsymbol{\Theta} = \mathrm{skew}(\boldsymbol{\theta})$ is the skew-symmetric tensor whose axial vector is $\boldsymbol{\theta}$.

The final quantity needed in our description of the rod kinematics is the magnitude of the cross section warping, which can be constrained and is not *a priori* related to the rotation of the cross section, thus constituting an independent degree of freedom of the problem. We represent this degree of freedom by p, mentioned earlier in the description of the deformed configuration. Components of $\boldsymbol{u}$ and $\boldsymbol{\theta}$ on a global Cartesian system together with p constitute the seven degrees of freedom of this rod model. They are grouped in vector $\boldsymbol{d} = \begin{bmatrix} \boldsymbol{u} \\ \boldsymbol{\theta} \\ p \end{bmatrix}$.

The deformation gradient $\boldsymbol{F} = \nabla\boldsymbol{\varphi} = \partial\boldsymbol{\varphi}/\partial\boldsymbol{\xi}$ is obtained from differentiation of equation (1). We will use the notations $(\bullet)' = \partial(\bullet)/\partial x_3$, $(\bullet)_{,\alpha} = \partial(\bullet)/\partial x_\alpha$ and $\dot{(\bullet)} = \partial(\bullet)/\partial t$ for derivatives, where t is a time variable. With these notations, the deformation gradient is written as

$$\begin{aligned}\boldsymbol{F} &= \boldsymbol{\varphi}_{,\alpha} \otimes \boldsymbol{e}_\alpha^r + \boldsymbol{\varphi}' \otimes \boldsymbol{e}_3^r \\ &= (\boldsymbol{e}_\alpha + \psi_{,\alpha}\, p\boldsymbol{e}_3) \otimes \boldsymbol{e}_\alpha^r + (\boldsymbol{u}' + \boldsymbol{Q}^T\boldsymbol{e}_3 + \boldsymbol{Q}'\boldsymbol{Q}^T\boldsymbol{a} + \psi p'\boldsymbol{e}_3 + \psi p\boldsymbol{Q}'\boldsymbol{Q}^T\boldsymbol{e}_3) \otimes \boldsymbol{e}_3^r. \end{aligned} \tag{9}$$

Following the approach of Cardona and Géradin (1988), we define the axis' strain and curvature vectors respectively as $\boldsymbol{\eta} = \boldsymbol{u}' + \boldsymbol{Q}^T\boldsymbol{e}_3 - \boldsymbol{e}_3$ and $\boldsymbol{\kappa} = \text{axial}(\boldsymbol{Q}'\boldsymbol{Q})^T)$, where $\boldsymbol{\kappa}$ is the axial vector of the skew-symmetric tensor $\boldsymbol{K} = \boldsymbol{Q}'\boldsymbol{Q}^T$. Replacing them in equation (9) yields

$$\begin{aligned}\boldsymbol{F} &= (\boldsymbol{e}_\alpha + \psi_{,\alpha}\, p\boldsymbol{e}_3) \otimes \boldsymbol{e}_\alpha^r + (\boldsymbol{\eta} + \boldsymbol{e}_3 + \boldsymbol{\kappa} \times (\boldsymbol{a} + \psi p\boldsymbol{e}_3) + \psi p'\boldsymbol{e}_3) \otimes \boldsymbol{e}_3^r \\ &= \boldsymbol{Q} + \psi_{,\alpha}\, p\boldsymbol{e}_3 \otimes \boldsymbol{e}_\alpha^r + (\boldsymbol{\eta} + \boldsymbol{\kappa} \times (\boldsymbol{a} + \psi p\boldsymbol{e}_3) + \psi p'\boldsymbol{e}_3) \otimes \boldsymbol{e}_3^r. \end{aligned} \tag{10}$$

We can further group the variables in this equation by defining vectors

$$\boldsymbol{\gamma}_\alpha = \psi_{,\alpha}\, p\boldsymbol{e}_3 \tag{11}$$

$$\boldsymbol{\gamma}_3 = \boldsymbol{\eta} + \boldsymbol{\kappa} \times (\boldsymbol{a} + \psi p\boldsymbol{e}_3) + \psi p'\boldsymbol{e}_3. \tag{12}$$

By replacing equations (11) and (12) in equation (10), we can write a more succint expression:

$$\boldsymbol{F} = \boldsymbol{Q} + \boldsymbol{\gamma}_i \otimes \boldsymbol{e}_i^r. \tag{13}$$

Vectors $\boldsymbol{\eta}$, $\boldsymbol{\kappa}$, $\boldsymbol{\gamma}_\alpha$ and $\boldsymbol{\gamma}_3$ are affected by superposition of rigid body motions, making them inappropriate for the formulation of constitutive relations. To overcome this problem, we can define their respective back-rotated counterparts, which are frame-invariant, by left-multiplying them by $\boldsymbol{Q}^T$. Analogously to the notation for the reference local basis, we denote these quantities by a superscript r: $(\bullet)^r = \boldsymbol{Q}^T(\bullet)$. Performing some algebraic simplifications, we can write the back-rotated vectors with respect to the basis of the reference configuration:

$$\boldsymbol{\eta}^r = \boldsymbol{Q}^T(\boldsymbol{u}' + \boldsymbol{e}_3^r) - \boldsymbol{e}_3^r \tag{14}$$

$$\boldsymbol{\kappa}^r = \boldsymbol{\Gamma}^T\boldsymbol{\theta}' \tag{15}$$

$$\boldsymbol{\gamma}_\alpha^r = \psi_{,\alpha}\, p\boldsymbol{e}_3^r \tag{16}$$

$$\boldsymbol{\gamma}_3^r = \boldsymbol{\eta}^r + \boldsymbol{\kappa}^r \times (\boldsymbol{a}^r + \psi p\boldsymbol{e}_3^r) + \psi p'\boldsymbol{e}_3^r, \tag{17}$$

yielding

$$\boldsymbol{F} = \boldsymbol{Q}(\boldsymbol{I} + \boldsymbol{\gamma}_i^r \otimes \boldsymbol{e}_i^r). \tag{18}$$

In equation (15), tensor $\boldsymbol{\Gamma}$ relates the vector of angular velocities $\boldsymbol{\omega}$ to the temporal derivative of the rotation vector $\dot{\boldsymbol{\theta}}$. Recalling that the tensor of angular velocities $\boldsymbol{\Omega}$ in three dimensions is not the direct time derivative of the rotaion tensor, but is $\boldsymbol{\Omega} = \dot{\boldsymbol{Q}}\boldsymbol{Q}^T$ instead, it arises from this differentiation that $\boldsymbol{\omega} = \boldsymbol{\Gamma}\dot{\boldsymbol{\theta}}$, as seen in Campello (2000, p. 9). Tensor $\boldsymbol{\Gamma}$ is written as

$$\boldsymbol{\Gamma} = \boldsymbol{I} + \frac{1 - \cos\|\boldsymbol{\theta}\|}{\|\boldsymbol{\theta}\|^2}\boldsymbol{\Theta} + \frac{\|\boldsymbol{\theta}\| - \sin\|\boldsymbol{\theta}\|}{\|\boldsymbol{\theta}\|^3}\boldsymbol{\Theta}^2. \tag{19}$$

We refer to Tiago (2007, p. 107) for a description of some interesting properties and relations of $\boldsymbol{Q}$ and $\boldsymbol{\Gamma}$. Vector $\boldsymbol{\gamma}_3^r$ in equation (17) can be regarded as a generalized cross sectional strain vector. For an interpretation of the strain vectors $\boldsymbol{\eta}^r$ and $\boldsymbol{\kappa}^r$, encompassing axis elongation, cross sectional shear and specific rotations see, e.g., Géradin and Cardona (2001).

2.3 Virtual work

To obtain the weak form of the equilibrium equations using the virtual work theorem, we need the variation of equation (18). Henceforth, we use the symbol δ to denote either variations, virtual quantities or test functions related to the degrees of freedom. First, performing the variation of the back-rotated strain vectors, shown in full in Appendix A, we obtain

$$\delta\boldsymbol{\eta}^r = \boldsymbol{Q}^T(\delta\boldsymbol{u}' + (\boldsymbol{u}' + \boldsymbol{e}_3^r) \times \boldsymbol{\Gamma}\delta\boldsymbol{\theta}) \tag{20}$$

$$\delta\boldsymbol{\kappa}^r = \boldsymbol{Q}^T(\boldsymbol{\Gamma}'\delta\boldsymbol{\theta} + \boldsymbol{\Gamma}\delta\boldsymbol{\theta}') \tag{21}$$

$$\delta\boldsymbol{\gamma}_\alpha^r = \psi_{,\alpha}\,\delta p\boldsymbol{e}_3^r \tag{22}$$

$$\delta\boldsymbol{\gamma}_3^r = \delta\boldsymbol{\eta}^r + \delta\boldsymbol{\kappa}^r \times (\boldsymbol{a}^r + \psi p\boldsymbol{e}_3^r) + \psi\delta p\boldsymbol{\kappa}^r \times \boldsymbol{e}_3^r + \psi\delta p'\boldsymbol{e}_3^r, \tag{23}$$

where

$$\begin{aligned}\boldsymbol{\Gamma}' = &\frac{1-\cos\|\boldsymbol{\theta}\|}{\|\boldsymbol{\theta}\|^2}\boldsymbol{\Theta}' + \frac{\|\boldsymbol{\theta}\|-\sin\|\boldsymbol{\theta}\|}{\|\boldsymbol{\theta}\|^3}(\boldsymbol{\Theta}'\boldsymbol{\Theta}+\boldsymbol{\Theta}\boldsymbol{\Theta}') \\ &+ \frac{\|\boldsymbol{\theta}\|\sin\|\boldsymbol{\theta}\|+2\cos\|\boldsymbol{\theta}\|-2}{\|\boldsymbol{\theta}\|^4}(\boldsymbol{\theta}\cdot\boldsymbol{\theta}')\boldsymbol{\Theta} \\ &+ \frac{-\|\boldsymbol{\theta}\|\cos\|\boldsymbol{\theta}\|-2\|\boldsymbol{\theta}\|+3\sin\|\boldsymbol{\theta}\|}{\|\boldsymbol{\theta}\|^5}(\boldsymbol{\theta}\cdot\boldsymbol{\theta}')\boldsymbol{\Theta}^2. \end{aligned} \tag{24}$$

With these, the variation of the deformation gradient is

$$\delta\boldsymbol{F} = \boldsymbol{G}\boldsymbol{F} + \boldsymbol{Q}(\delta\boldsymbol{\gamma}_i^r \otimes \boldsymbol{e}_i^r) \tag{25}$$

where $\boldsymbol{G} = \delta\boldsymbol{Q}\boldsymbol{Q}^T$ is a skew-symmetric tensor whose axial vector is denoted by $\boldsymbol{g}$ and which is obtained analogously to the angular velocities tensor. We also have that $\boldsymbol{g} = \text{axial}(\delta\boldsymbol{Q}\boldsymbol{Q}^T) = \boldsymbol{\Gamma}\delta\boldsymbol{\theta}$ as seen in the work of Campello (2000), albeit with a different notation. From equation (18) we can also easily define the back-rotated counterpart of the deformation gradient and its variation:

$$\boldsymbol{F}^r = \boldsymbol{I} + \boldsymbol{\gamma}_i^r \otimes \boldsymbol{e}_i^r. \tag{26}$$

$$\delta\boldsymbol{F}^r = \delta\boldsymbol{\gamma}_i^r \otimes \boldsymbol{e}_i^r. \tag{27}$$

Now let $\boldsymbol{P}$ and $\boldsymbol{S}$ be the first and second Piola-Kirchhoff stress tensors, by definition related such that $\boldsymbol{P} = \boldsymbol{F}\boldsymbol{S}$. With the energy conjugate pair $(\boldsymbol{P}, \boldsymbol{F})$, the internal virtual work of our formulation is

$$\delta W_{int} = \int_\Omega \boldsymbol{P} : \delta\boldsymbol{F}\, d\Omega \tag{28}$$

$$= \int_\Omega (\boldsymbol{P} : \boldsymbol{G}\boldsymbol{F} + \boldsymbol{P} : \boldsymbol{Q}\delta\boldsymbol{F}^r)\, d\Omega. \tag{29}$$

In the above, the domain Ω denotes the volume of the rod in the reference configuration. Cauchy's second law of motion implies the symmetry $\boldsymbol{P}\boldsymbol{F}^T = (\boldsymbol{P}\boldsymbol{F}^T)^T$. From the orthogonality of $\boldsymbol{Q}$, in turn, we know that $\boldsymbol{G}$ is skew-symmetric, therefore $\boldsymbol{P} : \boldsymbol{G}\boldsymbol{F} = \boldsymbol{P}\boldsymbol{F}^T : \boldsymbol{G} = 0$

and equation (29) then simplifies to

$$\delta W_{int} = \int_\Omega \boldsymbol{P} : \boldsymbol{Q}\delta\boldsymbol{F}^r \, d\Omega = \int_\Omega \boldsymbol{Q}^T\boldsymbol{P} : \delta\boldsymbol{F}^r \, d\Omega \tag{30}$$

which suggests the definition of $\boldsymbol{P}^r = \boldsymbol{Q}^T\boldsymbol{P}$, yielding

$$\delta W_{int} = \int_\Omega \boldsymbol{P}^r : \delta\boldsymbol{F}^r \, d\Omega. \tag{31}$$

For the external virtual work, let $\overline{\boldsymbol{t}}$ be the external surface traction acting on the rod's surface per unit reference area and $\overline{\boldsymbol{b}}$ be the vector of external body forces per unit reference volume. It is then given by

$$\delta W_{ext} = \int_L \left(\int_C \overline{\boldsymbol{t}} \cdot \delta\boldsymbol{\varphi} \, dC + \int_A \overline{\boldsymbol{b}} \cdot \delta\boldsymbol{\varphi} \, dA \right) dL \tag{32}$$

in which C is the boundary of the cross sections. With $\delta\boldsymbol{\varphi}$ above given from the variation of equation (1), evaluation of the contour and area integrals in equation (32) renders the external force resultants. They are grouped in vector $\overline{\boldsymbol{q}}$ such that

$$\overline{\boldsymbol{q}} = \begin{bmatrix} \overline{\boldsymbol{n}} \\ \boldsymbol{\Gamma}^T\overline{\boldsymbol{m}} \\ \overline{B} \end{bmatrix}, \quad \text{where} \quad \begin{aligned} \overline{\boldsymbol{n}} &= \int_C \overline{\boldsymbol{t}} \, dC + \int_A \overline{\boldsymbol{b}} \, dA \\ \overline{\boldsymbol{m}} &= \int_C (\boldsymbol{a} + \psi p \boldsymbol{e}_3) \times \overline{\boldsymbol{t}} \, dC + \int_A (\boldsymbol{a} + \psi p \boldsymbol{e}_3) \times \overline{\boldsymbol{b}} \, dA \\ \overline{B} &= \int_C \psi \overline{\boldsymbol{t}} \cdot \boldsymbol{e}_3 \, dC + \int_A \psi \overline{\boldsymbol{b}} \boldsymbol{e}_3 \, dA. \end{aligned} \tag{33}$$

This allows us to rewrite equation (32) as

$$\delta W_{ext} = \int_L \overline{\boldsymbol{q}} \cdot \delta\boldsymbol{d} \, dL, \qquad \text{where} \qquad \delta\boldsymbol{d} = [\delta\boldsymbol{u} \;\; \delta\boldsymbol{\theta} \;\; \delta p]^T. \tag{34}$$

Components of $\overline{\boldsymbol{n}}$ and $\overline{\boldsymbol{m}}$ are respectively the resultant sectional external forces and moments, whereas $\overline{B}$ is the resultant sectional external bi-moment, all per unit reference length of the rod axis. For a detailed description of the effects of different loading types on each component as well as an extension of this model to include reaction forces on the kinematic boundary, although not considering the warping of the cross section, we refer to Tiago (2007, p. 148).

The equilibrium of the rod is enforced in a standard way by means of the virtual work

theorem:

$$\delta W = \delta W_{int} - \delta W_{ext} = 0 \quad \text{in } L, \quad \forall \delta \boldsymbol{d} \in V \tag{35}$$

where $V = \{v \in \mathrm{H}^1(\Omega) : v = 0 \text{ on } \partial\Omega\}$ with δW_{int} and δW_{ext} given by equations (28) and (32) or by equations (31) and (34). Henceforth, we use the notation $\Delta(\bullet)$ to mean a linearized or incremental counterpart of a function. To solve this weak form using the root finding method of Newton-Raphson, we linearize it by taking its Fréchet derivative over the field of increments of the degrees of freedom $\Delta\boldsymbol{d}$, which leads to the tangent formulation of this model:

$$\Delta\delta W = \int_\Omega (\Delta \boldsymbol{P}^r \colon \delta \boldsymbol{F}^r + \boldsymbol{P}^r \colon \Delta\delta \boldsymbol{F}^r - \boldsymbol{L}\Delta\boldsymbol{d} \cdot \delta\boldsymbol{d})\, d\Omega. \tag{36}$$

To obtain $\Delta\boldsymbol{P}^r$ and $\Delta\delta\boldsymbol{F}^r$ for this equation, we need the linearization of the relevant tensors, obtained analogously to their virtual couterparts as follows:

$$\Delta\boldsymbol{\eta}^r = \boldsymbol{Q}^T(\Delta\boldsymbol{u}' + (\boldsymbol{u}' + \boldsymbol{e}_3^r) \times \boldsymbol{\Gamma}\Delta\boldsymbol{\theta}) \tag{37}$$

$$\Delta\boldsymbol{\kappa}^r = \boldsymbol{Q}^T(\boldsymbol{\Gamma}'\Delta\boldsymbol{\theta} + \boldsymbol{\Gamma}\Delta\boldsymbol{\theta}') \tag{38}$$

$$\Delta\boldsymbol{\gamma}_\alpha^r = \psi_{,\alpha}\, \Delta p \boldsymbol{e}_3^r \tag{39}$$

$$\Delta\boldsymbol{\gamma}_3^r = \Delta\boldsymbol{\eta}^r + \Delta\boldsymbol{\kappa}^r \times (\boldsymbol{a}^r + \psi p \boldsymbol{e}_3^r) + \psi\Delta p \boldsymbol{\kappa}^r \times \boldsymbol{e}_3^r + \psi\Delta p' \boldsymbol{e}_3^r \tag{40}$$

$$\Delta\boldsymbol{F}^r = \Delta\boldsymbol{\gamma}_i^r \otimes \boldsymbol{e}_i^r \tag{41}$$

$$\Delta\boldsymbol{P}^r = \Delta\boldsymbol{F}^r\boldsymbol{S} + \boldsymbol{F}^r\Delta\boldsymbol{S}. \tag{42}$$

We also need the linearization of the virtual counterparts of some of the these tensors, which are given by

$$\begin{aligned}\Delta\delta\boldsymbol{\eta}^r = \boldsymbol{Q}^T\Big(&\delta\boldsymbol{u}' \times \boldsymbol{\Gamma}\Delta\boldsymbol{\theta} + \Delta\boldsymbol{u}' \times \boldsymbol{\Gamma}\delta\boldsymbol{\theta} + (\boldsymbol{u}' + \boldsymbol{e}_3^r) \times \Delta\boldsymbol{\Gamma}\delta\boldsymbol{\theta} \\ &- (\boldsymbol{\Gamma}\delta\boldsymbol{\theta} \cdot \boldsymbol{\Gamma}\Delta\boldsymbol{\theta})(\boldsymbol{u}' + \boldsymbol{e}_3^r) + (\boldsymbol{\Gamma}\Delta\boldsymbol{\theta} \cdot (\boldsymbol{u}' + \boldsymbol{e}_3^r))\boldsymbol{\Gamma}\delta\boldsymbol{\theta}\Big)\end{aligned} \tag{43}$$

$$\Delta\delta\boldsymbol{\kappa}^r = \boldsymbol{Q}^T\Big((\boldsymbol{\Gamma}'\delta\boldsymbol{\theta} + \boldsymbol{\Gamma}\delta\boldsymbol{\theta}') \times \boldsymbol{\Gamma}\Delta\boldsymbol{\theta} + \Delta\boldsymbol{\Gamma}\delta\boldsymbol{\theta}' + \Delta\boldsymbol{\Gamma}'\delta\boldsymbol{\theta}\Big) \tag{44}$$

$$\Delta\delta\boldsymbol{\gamma}_\alpha^r = \psi_{,\alpha}\, \Delta\delta p \boldsymbol{e}_3^r = \boldsymbol{o} \tag{45}$$

$$\Delta\delta\boldsymbol{\gamma}_3^r = \Delta\delta\boldsymbol{\eta}^r + \Delta\delta\boldsymbol{\kappa}^r \times (\boldsymbol{a}^r + \psi p \boldsymbol{e}_3^r) + \Delta\boldsymbol{\kappa}^r \times \psi\delta p \boldsymbol{e}_3^r + \delta\boldsymbol{\kappa}^r \times \psi\Delta p \boldsymbol{e}_3^r \tag{46}$$

$$\Delta\delta\boldsymbol{F}^r = \Delta\delta\boldsymbol{\gamma}_i^r \otimes \boldsymbol{e}_i^r, \tag{47}$$

where

$$\begin{aligned}\Delta\boldsymbol{\Gamma} = &\frac{1-\cos\|\boldsymbol{\theta}\|}{\|\boldsymbol{\theta}\|^2}\Delta\boldsymbol{\Theta} + \frac{\|\boldsymbol{\theta}\|-\sin\|\boldsymbol{\theta}\|}{\|\boldsymbol{\theta}\|^3}(\boldsymbol{\Theta}\Delta\boldsymbol{\Theta}+\Delta\boldsymbol{\Theta}\boldsymbol{\Theta})\\ &+\frac{\|\boldsymbol{\theta}\|\sin\|\boldsymbol{\theta}\|+2\cos\|\boldsymbol{\theta}\|-2}{\|\boldsymbol{\theta}\|^4}(\boldsymbol{\theta}\cdot\Delta\boldsymbol{\theta})\boldsymbol{\Theta}\\ &+\frac{-\|\boldsymbol{\theta}\|\cos\|\boldsymbol{\theta}\|-2\|\boldsymbol{\theta}\|+3\sin\|\boldsymbol{\theta}\|}{\|\boldsymbol{\theta}\|^5}(\boldsymbol{\theta}\cdot\Delta\boldsymbol{\theta})\boldsymbol{\Theta}^2, \end{aligned} \tag{48}$$

and

$$\begin{aligned}\Delta\boldsymbol{\Gamma}' = &\frac{1-\cos\|\boldsymbol{\theta}\|}{\|\boldsymbol{\theta}\|^2}\Delta\boldsymbol{\Theta}' + \frac{\|\boldsymbol{\theta}\|-\sin\|\boldsymbol{\theta}\|}{\|\boldsymbol{\theta}\|^3}(\Delta\boldsymbol{\Theta}'\boldsymbol{\Theta}+\boldsymbol{\Theta}'\Delta\boldsymbol{\Theta}+\Delta\boldsymbol{\Theta}\boldsymbol{\Theta}'+\boldsymbol{\Theta}\Delta\boldsymbol{\Theta}')\\ &+\frac{\|\boldsymbol{\theta}\|\sin\|\boldsymbol{\theta}\|+2\cos\|\boldsymbol{\theta}\|-2}{\|\boldsymbol{\theta}\|^4}\Big((\Delta\boldsymbol{\theta}\cdot\boldsymbol{\theta}')\boldsymbol{\Theta}+(\boldsymbol{\theta}\cdot\Delta\boldsymbol{\theta}')\boldsymbol{\Theta}\\ &\qquad+(\boldsymbol{\theta}\cdot\Delta\boldsymbol{\theta})\boldsymbol{\Theta}'+(\boldsymbol{\theta}\cdot\boldsymbol{\theta}')\Delta\boldsymbol{\Theta}\Big)\\ &+\frac{-\|\boldsymbol{\theta}\|\cos\|\boldsymbol{\theta}\|-2\|\boldsymbol{\theta}\|+3\sin\|\boldsymbol{\theta}\|}{\|\boldsymbol{\theta}\|^5}\Big((\Delta\boldsymbol{\theta}\cdot\boldsymbol{\theta}')\boldsymbol{\Theta}^2+(\boldsymbol{\theta}\cdot\Delta\boldsymbol{\theta}')\boldsymbol{\Theta}^2\\ &\qquad+(\boldsymbol{\theta}\cdot\boldsymbol{\theta}')\Delta\boldsymbol{\Theta}\boldsymbol{\Theta}+(\boldsymbol{\theta}\cdot\boldsymbol{\theta}')\boldsymbol{\Theta}\Delta\boldsymbol{\Theta}+(\boldsymbol{\theta}\cdot\Delta\boldsymbol{\theta})\boldsymbol{\Theta}'\boldsymbol{\Theta}+(\boldsymbol{\theta}\cdot\Delta\boldsymbol{\theta})\boldsymbol{\Theta}\boldsymbol{\Theta}'\Big)\\ &+\frac{\|\boldsymbol{\theta}\|^2\cos\|\boldsymbol{\theta}\|-8\cos\|\boldsymbol{\theta}\|-5\|\boldsymbol{\theta}\|\sin\|\boldsymbol{\theta}\|+8}{\|\boldsymbol{\theta}\|^6}(\boldsymbol{\theta}\cdot\boldsymbol{\theta}')\boldsymbol{\Theta}\\ &+\frac{\|\boldsymbol{\theta}\|^2\sin\|\boldsymbol{\theta}\|+7\|\boldsymbol{\theta}\|\cos\|\boldsymbol{\theta}\|+8\|\boldsymbol{\theta}\|-15\sin\|\boldsymbol{\theta}\|}{\|\boldsymbol{\theta}\|^7}(\boldsymbol{\theta}\cdot\Delta\boldsymbol{\theta})(\boldsymbol{\theta}\cdot\boldsymbol{\theta}')\boldsymbol{\Theta}^2. \end{aligned} \tag{49}$$

The steps of algebraic simplification for equations (43) and (44) are shown in full in Appendix A and the others easily follow from those. As usual, it was considered that $\Delta\delta\boldsymbol{d}=0$ and $\Delta\delta\boldsymbol{d}'=0$. Operator $\boldsymbol{L}$ in equation (35), in turn, is obtained by linearization of the external forces: $\boldsymbol{L}=\partial\overline{\boldsymbol{q}}/\partial\boldsymbol{d}$. Note that, due to the presence of $\boldsymbol{\Gamma}^T$ in the vector that is conjugate to the rotations, this operator is non-zero whenever there are external moments, even for loads that don't depend on the displacements and rotations. At least for conservative loading, it is, however, always symmetric (Campello, 2000, p. 43).

2.4 *A priori* integration over the cross section

Just as we have done above a formulation for the external virtual work with *a priori* integration over the cross section, this rod theory is usually formulated with an energy conjugate pair of vectors of generalized cross sectional stresses and strains. For detailed descriptions, the reader can refer to the works of Pimenta and Yojo (1993) and Campello (2000),

among others. We can start by taking the column vectors $\boldsymbol{\tau}_i^r$ of the back-rotated first Piola-Kirchhoff stress tensor such that $\boldsymbol{P}^r = \boldsymbol{\tau}_i^r \otimes \boldsymbol{e}_i^r$. Manipulating equation (31) with the terms defined in equations (20) through (23), and with $\boldsymbol{\tau}_i^r$, we obtain

$$\begin{aligned}\delta W_{int} &= \int_\Omega (\boldsymbol{\tau}_\alpha^r \cdot \delta\boldsymbol{\gamma}_\alpha^r + \boldsymbol{\tau}_3^r \cdot \delta\boldsymbol{\gamma}_3^r)\, d\Omega \\ &= \int_\Omega \boldsymbol{\tau}_\alpha^r \cdot \psi_{,\alpha}\, \delta p \boldsymbol{e}_3^r + \boldsymbol{\tau}_3^r \cdot \left(\delta\boldsymbol{\eta}^r + \boldsymbol{\kappa}^r \times (\boldsymbol{a}^r + \psi p \boldsymbol{e}_3^r) + \psi \delta p \boldsymbol{\kappa}^r \times \boldsymbol{e}_3^r + \psi \delta p' \boldsymbol{e}_3^r\right) d\Omega.\end{aligned} \tag{50}$$

Rearranging these inner products to gather the stress vectors $\boldsymbol{\tau}_i^r$ and the terms that depend on the position $\boldsymbol{a}^r$ of points on the cross section relative to the rod axis, we can integrate them over the area A of the cross section at the reference configuration, defining the following cross sectional stresses:

$$\boldsymbol{n}^r = \int_A \boldsymbol{\tau}_3^r\, dA = V_\alpha \boldsymbol{e}_\alpha^r + N \boldsymbol{e}_3^r \tag{51}$$

$$\boldsymbol{m}^r = \int_A (\boldsymbol{a}^r + \psi p \boldsymbol{e}_3^r) \times \boldsymbol{\tau}_3^r\, dA = M_\alpha \boldsymbol{e}_\alpha^r + T \boldsymbol{e}_3^r \tag{52}$$

$$Q = \int_A \left((\boldsymbol{\tau}_\alpha^r \cdot \boldsymbol{e}_3^r)\psi_{,\alpha} + \boldsymbol{\tau}_3^r \cdot (\boldsymbol{\kappa}^r \times \boldsymbol{e}_3^r)\psi\right) dA \tag{53}$$

$$B = \int_A (\boldsymbol{\tau}_3^r \cdot \boldsymbol{e}_3^r)\psi\, dA. \tag{54}$$

We can then write equation (31) as

$$\delta W_{int} = \int_L (\boldsymbol{n}^r \cdot \delta\boldsymbol{\eta}^r + \boldsymbol{m}^r \cdot \delta\boldsymbol{\kappa}^r + Q\delta p + B\delta p')\, dL. \tag{55}$$

Components of $\boldsymbol{n}^r$ are the resultant shear forces (V_α) and normal force (N) of the cross sections. Components of $\boldsymbol{m}^r$ are the sectional bending moments (M_α) and torsional moment (T), while Q and B are sectional the bi-shear and bi-moment due to the consideration of cross sectional warping. By grouping them in a generalized stress vector $\boldsymbol{\sigma}^r$ and matching with their work conjugate virtual strains in vector $\delta\boldsymbol{\varepsilon}^r$, we obtain

$$\boldsymbol{\sigma}^r = \begin{bmatrix} \boldsymbol{n}^r \\ \boldsymbol{m}^r \\ Q \\ B \end{bmatrix} \quad \text{and} \quad \delta\boldsymbol{\varepsilon}^r = \begin{bmatrix} \delta\boldsymbol{\eta}^r \\ \delta\boldsymbol{\kappa}^r \\ \delta p \\ \delta p' \end{bmatrix}, \tag{56}$$

which are 8×1 vectors that can be used to rewrite equation (31) again as

$$\delta W_{int} = \int_L \boldsymbol{\sigma}^r \cdot \delta \boldsymbol{\varepsilon}^r \, dL. \tag{57}$$

With this formulation, the tangent operator of our problem reads

$$\Delta\delta W = \int_L \left(\Delta\boldsymbol{\sigma}^r \cdot \delta\boldsymbol{\varepsilon}^r + \boldsymbol{\sigma}^r \Delta\delta\boldsymbol{\varepsilon}^r - \boldsymbol{L}\delta\boldsymbol{d} \right) dL. \tag{58}$$

To factor this expression into products with the degrees of freedom and their test functions, or virtual couterparts, first we define the following operators

$$\boldsymbol{\Psi} = \begin{bmatrix} \boldsymbol{Q}^T & \boldsymbol{Q}^T\boldsymbol{Z}'\boldsymbol{\Gamma} & \boldsymbol{O} & \boldsymbol{o} & \boldsymbol{o} \\ \boldsymbol{O} & \boldsymbol{Q}^T\boldsymbol{\Gamma}' & \boldsymbol{Q}^T\boldsymbol{\Gamma} & \boldsymbol{o} & \boldsymbol{o} \\ \boldsymbol{o}^T & \boldsymbol{o}^T & \boldsymbol{o}^T & 1 & 0 \\ \boldsymbol{o}^T & \boldsymbol{o}^T & \boldsymbol{o}^T & 0 & 1 \end{bmatrix} \quad \text{and} \quad \boldsymbol{\Upsilon} = \begin{bmatrix} \boldsymbol{I}\frac{\partial}{\partial x_3} & \boldsymbol{O} & \boldsymbol{o} \\ \boldsymbol{O} & \boldsymbol{I} & \boldsymbol{o} \\ \boldsymbol{O} & \boldsymbol{I}\frac{\partial}{\partial x_3} & \boldsymbol{o} \\ \boldsymbol{o}^T & \boldsymbol{o}^T & 1 \\ \boldsymbol{o}^T & \boldsymbol{o}^T & \frac{\partial}{\partial x_3} \end{bmatrix}, \tag{59}$$

where we have used the skew-symmetric tensor $\boldsymbol{Z}' = \text{skew}(\boldsymbol{u}' + \boldsymbol{e}_3^r)$. Operator $\boldsymbol{\Psi}$ gathers the effects of rotations and specific displacements on vector $\boldsymbol{\Upsilon d}$ containing the degrees of freedom and their derivatives with respect to the coordinate along the rod axis, which is, in turn, given by the action of the differential operator $\boldsymbol{\Upsilon}$ on the degrees of freedom $\boldsymbol{d}$. It is not difficult to see that vector $\delta\boldsymbol{\varepsilon}^r$ may now be written as $\delta\boldsymbol{\varepsilon}^r = \boldsymbol{\Psi}\boldsymbol{\Upsilon}\delta\boldsymbol{d}$. With these definitions and aiming at the linearization of equation (57), we can also define the operator $\boldsymbol{\Lambda} = \partial(\boldsymbol{\Psi}^T\boldsymbol{\sigma}^r)/\partial(\boldsymbol{\Upsilon d})$. All that is left is to define a constitutive operator relating our generalized stresses vector to the generalized strains as $\boldsymbol{D} = \partial\boldsymbol{\sigma}^r/\partial\boldsymbol{\varepsilon}^r$. We can now write the tangent operator as

$$\Delta\delta W = \int_L \left(\boldsymbol{D}\boldsymbol{\Psi}\boldsymbol{\Upsilon}\Delta\boldsymbol{d} \cdot \boldsymbol{\Psi}\boldsymbol{\Upsilon}\delta\boldsymbol{d} + \boldsymbol{\Lambda}\boldsymbol{\Upsilon}\Delta\boldsymbol{d} \cdot \boldsymbol{\Upsilon}\delta\boldsymbol{d} - \boldsymbol{L}\Delta\boldsymbol{d} \cdot \delta\boldsymbol{d} \right) dL. \tag{60}$$

Operator $\boldsymbol{D}$ represents the constitutive effects of the internal forces and with it, in case of a linear elastic material, we can directly obtain $\boldsymbol{\sigma}^r = \boldsymbol{D}\boldsymbol{\varepsilon}^r$. Observe that if $\boldsymbol{D}$ is symmetric and the external loading is conservative, the tangent operator will also be symmetric. Operator $\boldsymbol{\Lambda}$ is a representation of the geometric effects of the internal forces, and $\boldsymbol{L}$

of the geometric effects of the external loading on the tangent operator. For a detailed deduction and description of these operators, we refer to Pimenta and Yojo (1993b) and Tiago (2007).

3 Rod constitutive models

3.1 Constitutive laws

In the general case, a physical description of phenomena concerning a continous medium requires, besides kinematics and equilibrium relations, that we be able to relate the history of the motion to the internal state of the material, and do so while distinguishing between different materials. To achieve this, we formulate constitutive laws to describe the behavior of the materials considered in the analysis.

The kinematics and equilibrium presented in the previous chapter depend only on general physical laws and mathematical models and can receive a rather intuitionistic algebraic and geometric treatment. They are fully applicable to any material whose stresses can be described with the symmetric Cauchy stress tensor in the framework of continuum mechanics, thus ruling out couple stresses and microstructure size-dependency. To apply these relations to specific materials we must provide a relationship between the Cauchy stress tensor and the history of the motion of the bodies. This relationship is mathematically encoded in a constitutive equation along with a set of material parameters determined empirically.

Most generally, a constitutive equation is a relation between two physical quantities describing the behavior of an idealized material with respect to these quantities. It assigns a function to the stress tensor choosing from a wide set of admissible functions (see Truesdell and Noll, 2004, with first edition in 1965). The functions are those that fulfill a number of principles or assumptions as stated, for example, in Bertram (2012, p. 153): *principle of determinism*: "The stresses in a material point at an instant of time are determined by the current and the past (but not the future) motion of the body.", *principle of local action*: "The stresses at a material point depend on the motion of only a finite neighbourhood of that point.", *principle of material objectivity*: "The stress power is objective (and thus also invariant) under Euclidean transformations.", *principle of invariance under superposed rigid body motions*: "If $\boldsymbol{T}$ are the Cauchy stresses after a motion, then the stresses after superposing a rigid body motion $\boldsymbol{Q}$ are $\boldsymbol{QTQ}^T$". This last one can be ragarded as the active version of the *principle of material objectivity*, which is also often called *principle of Euclidean invariance* or *principle of frame invariance*. Recalling that Euclidean tranforma-

tions are operations on vectors that are bijective and distance-preserving for different observers and for simultaneous events (Bertram, 2012, p. 132), for these principles, the *objectivity* of a tensor is defined as translation-invariance under Euclidean transformations $\boldsymbol{Q}$, thus being only rotated in $\boldsymbol{T}^* = \boldsymbol{Q} \star \boldsymbol{T}$, where $\star$ is the Rayleigh product defined for tensors of order n as $\boldsymbol{Q} \star T_{i_1 i_2 \ldots i_n}(\boldsymbol{e}_{i_1} \otimes \boldsymbol{e}_{i_2} \otimes \cdots \otimes \boldsymbol{e}_{i_n}) = T_{i_1 i_2 \ldots i_n}\Big(\boldsymbol{Q}\boldsymbol{e}_{i_1} \otimes \boldsymbol{Q}\boldsymbol{e}_{i_2} \otimes \cdots \otimes \boldsymbol{Q}\boldsymbol{e}_{i_n}\Big)$.

The *principle of material objectivity* together with the *principle of invariance under superposed rigid body motions* imply another one called *principle of form invariance*: "The material functions are invariant under change of observer." (Bertram, 2012, p. 158). It is also named by Noll (2005a) *principle of material frame-indifference*, and stated as: "The constitutive laws governing the internal interactions between the parts of the system should not depend on whatever external frame of reference is used to describe them."

For certain materials, the *principle of invariance under superposed rigid body motions* is sometimes chellenged with counterexamples from electrodynamics, thermo-mechanics of rarified gases and other fields which show that this principle is not a general natural law, see, e.g., Murdoch (2003), Noll (2005b) and Bertram, (2012, p. 157). But, as said by Noll (2005a), the interactions in some of these systems cannot be fully described as pure surface interactions in the conceptual framework of continuum mechanics.

Under these principles, a material model is an ideal representation of certain aspects of a natural material. In structural theories, for example, we are mostly interested in material responses related to gravitational, elastic, plastic and damage phenomena from a macroscopic point of view, most of the time, but not always, neglecting thermal, electromagnetic and chemical properties, effects and interactions. This representation may be characterized by a response functional $\mathfrak{M}(\boldsymbol{\varphi})$ that is a function of the transformation $\boldsymbol{\varphi}$ of the body and yields a stress tensor at the end of the transformation. Therefore, $\boldsymbol{T}(t) = \mathfrak{M}(\boldsymbol{\varphi})$ is the general form of a constitutive equation with time variable t (Truesdell and Noll, 2004, p. 57).

If we can approximate $\boldsymbol{\varphi}$ in an arbitrarily small neighborhood of a material point by the history of the gradient of the transformation at that point, we can reduce the constitutive equation to $\boldsymbol{T}(t) = \mathfrak{N}(\nabla\boldsymbol{\varphi}(t))$. Materials characterized by this kind of functionals are called *simple materials* by Truesdell and Noll (2004) and, with a few exceptions, constitute the material models dealt with in solid mechanics and structural theories.

The choice of constitutive equation and material model depends on which phenomena we wish to consider in our analysis. When a material behaves as solid or fluid depending on some internal state, it is the object of study of rheology. Rheology, as a discipline, is motivated by the complex behavior of certain polymers and organic materials, but is also applicable to metals and granular materials, e.g., concrete, used in structural engineering. It is a common and useful framework for the study of solids that exibit viscous elastic or plastic deformations and to fluids that undergo variations in viscosity when stressed, e.g., non-Newtonian fluids. It often makes use of one-dimensional models to describe the idealized behavior in a simple, intuitive way.

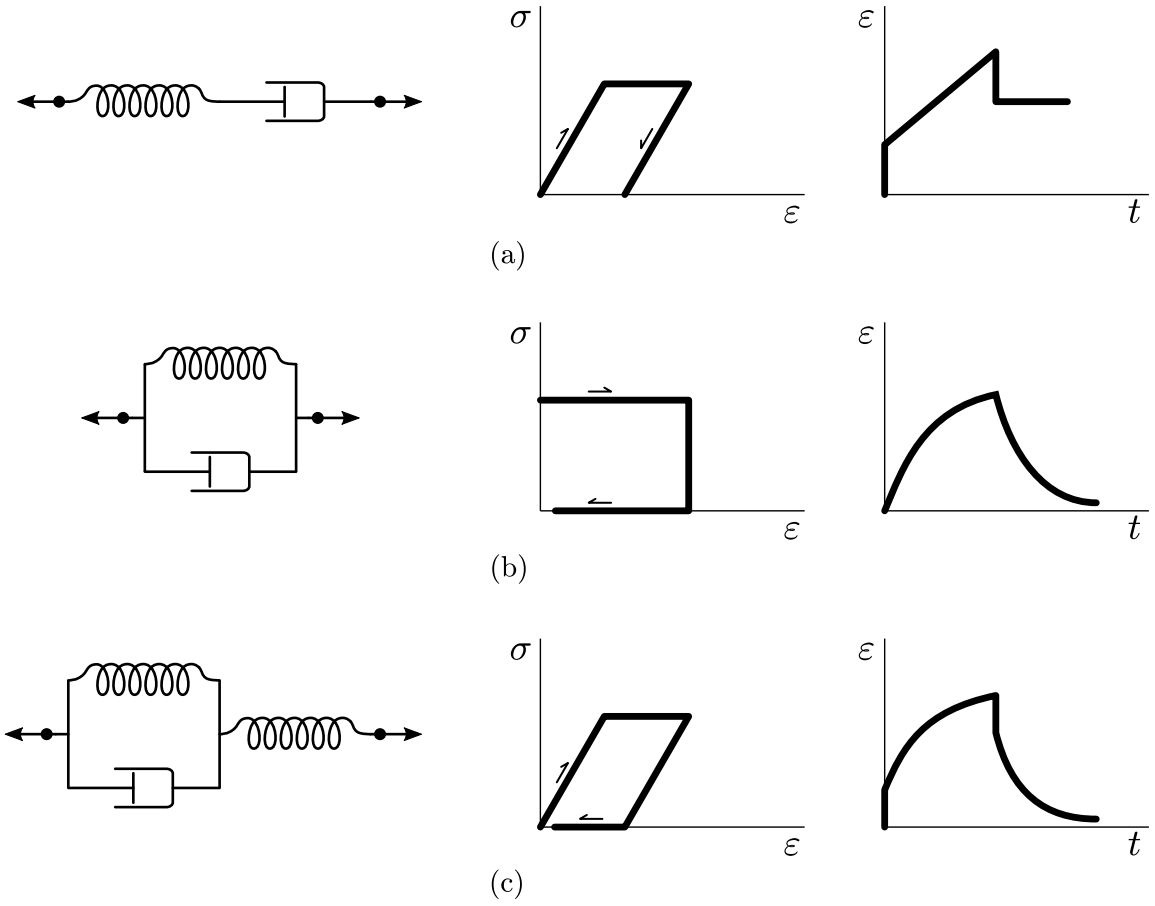

Figure 3: Common rheological models for viscoelastic materials and their responses to imposed sudden constant stress that is instantaneously released: (a) Maxwell material, (b) Kelvin-Voigt material, (c) Standard linear solid material. Source: the author.

These one-dimensional rheological models are composed of elementary devices to represent certain aspects of the material response in stress and strain: a spring (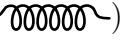) is used to model a response with instantaneous deformation, stiffness and recovery when the stress imposition ceases; a dashpot (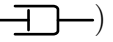) is used for the delayed or rate-dependent strain response to applied stress; and a friction device (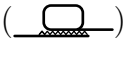) for irreversible strain

response to stress, which may also capture the idea of a stress threshold before which no deformation takes place. Besides their elementary behavior, specific compositions can be used to adequately model different phenomena such as creep and relaxation as in the models seen in Figure 3. For details on this approach the reader can refer to many excelent works and courses on rheology and mechanics of materials such as, e.g., the in-depth work of Dowling (2013).

Analyses regarding stresses in three dimensions or complex materials such as those sensitive to shearing or with some form of anisotropy require advanced models that don't have a direct one-dimensional representation. For three-dimensional plasticity in particular, of interest for the models derived in this work, it is conventional to resort to functions in stress space, also called Haigh-Westergaard space (see, e.g., Chen and Han, 1988, p. 66 and Puzrin, 2012, p. 171), to define yield surfaces interfacing elastic and plastic domains, giving a geometric intuition to the material behavior. In this way, the deformation regime of material points can be derived from its stress state relative to this yield surface.

Structural steel, the material of interest in this work, is a ductile metal alloy composed of iron, carbon and a variety of other elements like manganese, phosphorus, sulfur, silicon, copper, etc. It presents a number of metalurgical microstructures dependent on the heat treatments underwent in its manufacturing. It is divided in two broad categories for carbon steels and high strength low alloy steels with many types standardized for different applications and requirements of material properties. Low carbon steels in particular suffer from yield point runout, presenting two yield points in its stress-strain curve. After the first, upper yield point, is reached, resistance drops abruptly to the lower yield point until the instabilities associated with dynamic strain aging of the material develop completely and the strain hardening phase starts (Mesarovic, 1995). During this phase, the stress-strain curve of the material presents a plateau that is practically flat.

To model structural steel behavior for macro structural purposes, it is often adequate to consider it an isotropic and homogeneous material with symmetric response to applied stress and instantaneous deformation in one of two regimes, elastic or plastic. Given that the upper yield point has neglectable effects in structural applications, being more relevant in other contexts, e.g., manufacturing, the yield point for low carbon steel is considered to be the lower yield point as conventionally established in many structural engineering

standards.

In the following sections, we formulate a constitutive equation for the elastic regime and then build on it to define our elastoplastic material model.

3.2 Elastic material

When the stress state at each point of a material does not depend on the history of the motion, i.e., when it can be fully determined from a reference configuration and the current one at time t, it is called a Cauchy elastic material (Ogden, 1997, p. 175). Its stress state is independent of the rate of deformation, independent of the time frame taken and also independent of the path between the reference and deformed configurations (Ogden, loc. cit.). Nevertheless, the work done by the stress is, in general, dependent on the path taken and, therefore, a Cauchy elastic material has a non-conservative structure with respect to the strain energy of the body.

Given that the stress power per unit volume can be expressed as $\mathrm{tr}(\boldsymbol{P}\dot{\boldsymbol{F}})$ (Ogden, 1997, p. 156), a particular case of the Cauchy elastic material is that of a material for which there exists a function $W(\boldsymbol{F})$ such that $\dot{W} = \mathrm{tr}(\boldsymbol{P}\dot{\boldsymbol{F}})$. Defined from this relationship with the stress power, W is refered to as the strain energy density function of the material. From this definiton we can derive the classic relation for the second Piola-Kirchhoff stress tensor $\boldsymbol{S} = \partial W/\partial \boldsymbol{E}$. These materials are called hyperelastic materials or Green elastic materials. Not every Cauchy elastic material is hyperelastic because $\mathrm{tr}(\boldsymbol{P}d\boldsymbol{F})$ is not, in general, an exact differential (see Ogden, 1997, p. 205).

An important use of this function is in establishing criteria to ensure the existence of a solution to the boundary value problem of nonlinear elastic equilibrium. Crucial research results on this issue with regard to continuum mechanics date to the 1980s and are mostly due to Ball (1977), Ciarlet (1988), Knops and Stuart (1984), Ogden (1997, with first edition in 1984), Raoult (1986) and, in a more general mathematical setting, to many others as referenced by Ciarlet (1988). As observed by Antman (1970 apud Ciarlet, 1988, p. 170 and 174), strictly convex strain energy density functions are inconsistent with physical observations. The alternative weaker condition of polyconvexity as formulated by Ball (1977) can be used to determine a class of functions for which a solution to the problem of nonlinear elasticity is proved to exist. Its general nonuniqueness is also

consistent with general physical observations, mostly on problems with multiple stable equilibrium states.

Many material models fulfilling Ball's polyconvexity criterion have been formulated for both compressible and incompressible materials such as, for example, Ciarlet's material model with $W = (\lambda/4)(\det \boldsymbol{B} - 1) - (\lambda/4 + \mu/2)\ln(\det \boldsymbol{B}) + (\mu/2)(\mathrm{tr}(\boldsymbol{B}) - 3)$ and Ogden's materials with $W = \sum_{i=1}^{N} (\beta_i/\alpha_i)\ \mathrm{tr}(\boldsymbol{B}^{\alpha_i} - \boldsymbol{I})$ for which $\boldsymbol{B} = \boldsymbol{F}\boldsymbol{F}^T$ and λ, μ, α_i and β_i are material paramaters (Bertram, 2012, p. 226). As can be seen in Ogden's material, consistent polyconvex material models sometimes require many different parameters determined by empirical measurements. Moreover, even when the parameters are minimal, algebraically expensive operations are required, as the inversions of the deformation gradient implied for constitutive equations with Ciarlet's material.

The material model that is most widely used in structural engineering along with the finite element method, proposed independently by St. Venant in 1844 and Kirchhoff in 1852 (cf. Ciarlet, 1988), the St. Venant-Kirchhoff material is sometimes refered to as the neo-Hookean material, due to its resemblance to a generalization of Hooke's law for three dimensions. Conversely to the previous examples, it is not polyconvex (Raoult, 1986), therefore the existence of a solution to the boudary value problem cannot be fully asserted. Besides this, it presents other difficulties which restrict its applicability to basically the simple, but fortunately common, problems encountered in engineering structures.

The St. Venant-Kirchhoff material is a simple material characterized by the strain energy density $W = (\lambda/2)(\mathrm{tr}\,\boldsymbol{E})^2 + \mu\,\mathrm{tr}\,\boldsymbol{E}^2$ where $\boldsymbol{E} = (1/2)(\boldsymbol{F}^T\boldsymbol{F} - \boldsymbol{I})$ is the Green-Lagrange strain tensor. It implies a linear stress response with respect to the strains in the constitutive equation. However, in certain physical systems, large strains are possible even for small stresses, a response precluded by this linearity (Antman, 1979; Ciarlet, 1988). It also lacks implied restrictions for the cases when $\det(\nabla\boldsymbol{\varphi})$ approaches zero or negative values, leading to physical inconsistencies and numerical difficulties, requiring additional care in computational implementations and analysis (Ciarlet, 1988, p. 132).

Nevertheless, the St. Venant-Kirchhoff material is well suited for the problems to which it is applicable. As showed by Ciarlet (1988, p. 120), for bodies of homogeneous, isotropic, elastic materials whose deformed configuration is *near the reference configuration*, any

constitutive equation can be expressed in the form

$$\boldsymbol{S} = \lambda \operatorname{tr}(\boldsymbol{E})\boldsymbol{I} + 2\mu\boldsymbol{E} + o(\boldsymbol{E}) \tag{61}$$

in which $\boldsymbol{S}$ is the second Piola-Kirchhoff stress tensor and, in this case, λ and μ are Lamé parameters and $o(\bullet)$ is the Little-O notation: $o(g(n)) = \{f(n) : \forall c > 0,\ \exists N > 0$ such that $0 \leq f(n) < cg(n)\ \forall n \geq N$ with $c, n, N \in \mathbb{R}\}$ (Cormen et al., 2001, p. 47). We can see that the St. Venant-Kirchhoff material, with constitutive equation

$$\boldsymbol{S} = \frac{\partial W}{\partial \boldsymbol{E}} = \lambda \operatorname{tr}(\boldsymbol{E})\boldsymbol{I} + 2\mu\boldsymbol{E}, \tag{62}$$

is the simplest material compatible with equation (61), and performs better than linearizations of other material models (Ciarlet, 1988, p. 132).

3.3 Elastic constitutive equation for the rod model

As seen in equation (42), we need the linearization of $\boldsymbol{S}$ to obtain $\Delta\boldsymbol{P}^r$. Taking the Fréchet derivative of the simple expression above, it is written as

$$\begin{aligned}\Delta\boldsymbol{S} &= (\lambda/2)\operatorname{tr}(\Delta\boldsymbol{F}^T\boldsymbol{F} + \boldsymbol{F}^T\Delta\boldsymbol{F})\boldsymbol{I} + \mu(\Delta\boldsymbol{F}^T\boldsymbol{F} + \boldsymbol{F}^T\Delta\boldsymbol{F}) \\ &= (\lambda/2)\operatorname{tr}(\Delta\boldsymbol{C})\boldsymbol{I} + \mu\Delta\boldsymbol{C}\end{aligned} \tag{63}$$

where $\boldsymbol{C} = \boldsymbol{F}^T\boldsymbol{F} = \boldsymbol{F}^{rT}\boldsymbol{F}^r$ is the right Cauchy-Green strain tensor. As seen in, e.g., Gaussmann, (1951), for homogeneous, isotropic materials, the Lamé parameters, can be written in terms of the elastic modulus E and shear modulus G as

$$\mu = G \qquad \text{and} \qquad \lambda = \frac{G(E - 2G)}{3G - E}. \tag{64}$$

In the rod theory of chapter 2, it can be shown that, up to the first order in the strains, we have $\boldsymbol{P}^r \approx \boldsymbol{S}$. This approximation allows us a simple expression for the back-rotated stress vectors $\boldsymbol{\tau}_i^r$. We start with the Green-Lagrange strain tensor $\boldsymbol{E}$, energetically conjugated to $\boldsymbol{S}$, that is

$$\boldsymbol{E} = \frac{1}{2}(\boldsymbol{F}^T\boldsymbol{F} - \boldsymbol{I}) = \frac{1}{2}(\boldsymbol{F}^{r\,T}\boldsymbol{F}^r - \boldsymbol{I}). \tag{65}$$

Replacing $\boldsymbol{F}^r$ as defined in equation (26), and by using a component-wise form of that expression, we get

$$\boldsymbol{E} = \frac{1}{2}\left(\begin{bmatrix} 1 & 0 & \gamma_{13}^r \\ 0 & 1 & \gamma_{23}^r \\ \gamma_{31}^r & \gamma_{32}^r & 1+\gamma_{33}^r \end{bmatrix} \begin{bmatrix} 1 & 0 & \gamma_{31}^r \\ 0 & 1 & \gamma_{32}^r \\ \gamma_{13}^r & \gamma_{23}^r & 1+\gamma_{33}^r \end{bmatrix} - \boldsymbol{I} \right), \tag{66}$$

wherein $\gamma_{\alpha i}^r$ and γ_{3i}^r $(i = 1, 2, 3)$ are the components are the components of vectors $\boldsymbol{\gamma}_\alpha^r$ and $\boldsymbol{\gamma}_3^r$ respectively. Keeping only the terms up to the first order in $\boldsymbol{\eta}^r$, $\boldsymbol{\kappa}^r$ and p in this equation yields

$$\boldsymbol{E} = \frac{1}{2}\begin{bmatrix} 0 & 0 & \gamma_{31}^r + \gamma_{13}^r \\ 0 & 0 & \gamma_{32}^r + \gamma_{23}^r \\ \gamma_{13}^r + \gamma_{31}^r & \gamma_{23}^r + \gamma_{32}^r & 2\gamma_{33}^r \end{bmatrix}. \tag{67}$$

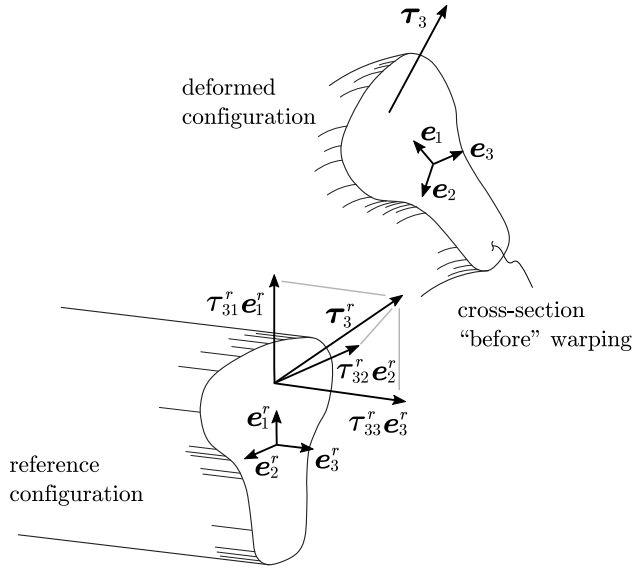

Figure 4: Stress vectors $\boldsymbol{\tau}_3$ and $\boldsymbol{\tau}_3^r$. Source: the author.

By replacing equations (67) and (64) in equation (62), we obtain the classic linear elastic relations for all stresses in $\boldsymbol{P}^r \approx \boldsymbol{S}$, which reads as

$$\tau^r_{3\alpha} = \tau^r_{\alpha 3} = G(\gamma^r_{3\alpha} + \gamma^r_{\alpha 3}) \tag{68}$$

$$\tau^r_{\alpha\alpha} = \lambda\gamma^r_{33} \tag{69}$$

$$\tau^r_{33} = (\lambda + 2\mu)\gamma^r_{33} \approx E\gamma^r_{33} \tag{70}$$

where $\tau^r_{3\alpha}$ and τ^r_{33} are the components of $\boldsymbol{\tau}^r_3$, i.e., the components of the stress vector of points of the rod's section, therby corresponding to the cross sectional shear and normal stresses respectively. Components $\tau^r_{\alpha\alpha}$ do not do any work, but will be needed for the plastic flow tensor. The remaining components of $\boldsymbol{S}$ are zero. Vector $\boldsymbol{\tau}^r_3$ is illustrated in Figure 4. The approximation to the first order in the strains in equation (67) in practice reduces the Green strain tensor to the infinitesimal strain tensor. We ask the reader to forgive the abuse of notation, since we will continue to use $\boldsymbol{E}$ and $\boldsymbol{S}$ for the strain and stress tensors throughout this work. We will make notice of any development step where this is relevant and would be otherwise impacted had these approximations not been made.

Observe that, for materials with $E = 2G$, equation (70) and the relation $\lambda + 2\mu = E$ are exact. A material with $E = 3G$ would have Poisson's ratio $\nu = 1/2$, a bulk modulus approaching infinity and would be perfectly incompressible. The approximation $\lambda + 2\mu \approx E$ in equation (70) is consistent with the rod's kinematical hypothesis of non-deformability of the cross section in the projecton of its plane. Notice that $\lambda + 2\mu = E(1-\nu)\Big/\Big((1+\nu)(1-2\nu)\Big) = E\Big(1 + 2\nu^2 + O(\nu^3)\Big)$, which means that $\nu \to 0$ is indirectly assumed in the theory. Considering both $\nu \neq 0$ and this hypothesis would mean an excessive stiffening of the rod, as indeed was observed in some of our numerical tests.

If we choose to adopt the alternative formulation of the internal virtual work as seen in section 2.4, we can insert equations (68) and (70) into the definitions of $\boldsymbol{n}^r$, $\boldsymbol{m}^r$, Q and B given in equations (51) through (54) to obtain the tangent matrix $\boldsymbol{D} = \partial\boldsymbol{\sigma}^r/\partial\boldsymbol{\varepsilon}^r$ of constitutive effects. By differentiating these equations with respect to $\boldsymbol{\varepsilon}^r$, neglecting terms of higher order in the strain variables and performing analytical integration, we obtain

$$\boldsymbol{D} = \frac{\partial \boldsymbol{\sigma}^r}{\partial \boldsymbol{\varepsilon}^r} \approx \begin{bmatrix} GA & 0 & 0 & 0 & 0 & -GS_1 & -GS_1^* & 0 \\ 0 & GA & 0 & 0 & 0 & -GS_2 & -GS_2^* & 0 \\ 0 & 0 & EA & ES_1 & ES_2 & 0 & 0 & 0 \\ 0 & 0 & ES_1 & EJ_{11} & EJ_{12} & 0 & 0 & 0 \\ 0 & 0 & ES_2 & EJ_{21} & EJ_{22} & 0 & 0 & 0 \\ -GS_1 & -GS_2 & 0 & 0 & 0 & GJ_P & GJ_T^* & 0 \\ -GS_1^* & -GS_2^* & 0 & 0 & 0 & GJ_T^* & GJ_P^* & 0 \\ 0 & 0 & 0 & 0 & 0 & 0 & 0 & EJ_\psi \end{bmatrix}, \tag{71}$$

in which

$$A = \int_A dA \tag{72}$$

$$S_\alpha = R_{\alpha\beta} \int_A x_\beta \, dA \tag{73}$$

$$J_{\alpha\beta} = R_{\alpha\gamma} R_{\beta\delta} \int_A x_\gamma x_\delta \, dA \tag{74}$$

$$J_P = \int_A x_\alpha x_\alpha \, dA \tag{75}$$

$$S_\alpha^* = \int_A \psi_{,\alpha} \, dA \tag{76}$$

$$J_T^* = R_{\alpha\beta} \int_A x_\alpha \psi_{,\beta} \, dA \tag{77}$$

$$J_P^* = \int_A \psi_{,\alpha} \psi_{,\alpha} \, dA \tag{78}$$

$$J_\psi = \int_A \psi^2 \, dA. \tag{79}$$

In the above, $R_{\alpha\beta}$ are the components of the same matrix $\boldsymbol{R} = \left[\begin{smallmatrix} 0 & 1 \\ -1 & 0 \end{smallmatrix}\right]$ as defined in section 2.1, where we also established the steps to obtain the cross sectional warping function ψ seen here. For more details on this formulation we refer the reader to Campello (2000, chapter 5) and Campello and Pimenta (2001). In addition, for full consideration of higher order terms in the components of $\boldsymbol{D}$, see Campello and Lago (2014).

3.4 Three-dimensional elastoplastic model

The elastoplastic materials described in this section and the next are extensions of the elastic model presented above to consider plastic deformations. They consist of a yield criterion that establishes the admissible stress states and determines the onset of plastification, a plastic flow law that governs the evolution of plastic strains, a hardening law, in our case accounting for strain-hardening phenomena due to internal properties of the material, and an integration algorithm with return mapping of stresses, strains and internal variables. Due to the characteristics of structural steel presented earlier and of the external loadings which are of interest in this work, it suffices to consider rate-independent plasticity. Detailed descriptions of these models, most of the times applied to shells and solids in general, and variations thereof, can be found in many works about classic computational plasticity, e.g., Simo and Hughes (1998).

The materials proposed are simple elastoplastic models valid for large displacements and rotations but small strains. The restriction to small strains is consistent with the hypothesis of no in-plane deformations of the rod's section, and may be regarded as acceptable for a wide-range of structural engineering applications wherein small strains are often observed but large displacements and rotations may occur. It allows us to compound the elastic and plastic strains additively. Accordingly, the total strain given by the Green-Lagrange strain tensor $\boldsymbol{E}$ from equation (67) is split into elastic and plastic parts such that $\boldsymbol{E} = \boldsymbol{E}^e + \boldsymbol{E}^p$, using superscripts e and p for the elastic and plastic parts respectively.

Structural steel is a near-incompressible material. This characteristic is reflected in the conventional values of the elastic and shear moduli, adopted as $E = 200$ GPa and $G = 77$ GPa respectively in the ABNT NBR 8800:2008 standard and the same E and $G = 77.2$ GPa in ANSI/AISC 360-16 standard for example. Its Poisson's ratio is about 0.3 and quickly approaches 0.5 after yield under compressive stress (Park et al., 1983). These properties make it suitable for analysis with the von Mises yield criterion, which is independent of hydrostatic pressure and related to the quadratic mean of the principal shear stresses (Chen and Han, 1988, p. 63) and best suited for ductile materials.

In the rod kinematical model adopted in this work, first order strains due to cross sectional shear stresses arising from bending are accounted for by assuming a kinematical hypothesis

as that of Timoshenko for the cross sections, i.e., they are not necessarily orthogonal to the rod axis after deformation.

One way to express the classic von Mises yield criterion is to state that the material yields when the the second invariant J_2 of the deviatoric part of the stress tensor $\boldsymbol{\Sigma} = \text{dev}(\boldsymbol{S})$ reaches a critical value k^2. Here, under the assumption of small strains mentioned in the previous section, note that $\boldsymbol{S}$ is the stress tensor that is energy conjugate to the small strains tensor $\boldsymbol{E}$. The von Mises yield criterion is written as

$$\mathcal{F} = \sqrt{J_2} - k \leq 0. \tag{80}$$

Recalling that $J_2 = (1/6)\Big((\sigma_1 - \sigma_2)^2 + (\sigma_2 - \sigma_3)^2 + (\sigma_3 - \sigma_1)^2\Big)$ where σ_i are the principal stresses, we can rewrite equation (80) as

$$\mathcal{F} = (\sigma_1 - \sigma_2)^2 + (\sigma_2 - \sigma_3)^2 + (\sigma_3 - \sigma_1)^2 - 6k^2 \leq 0, \tag{81}$$

from which we can see that k is the yield stress in pure shear. It is usually determined by uniaxial tensile tests where the yield stress in simple tension Y can be determined. In simple tension we have $\sigma_1 = Y$ and $\sigma_2 = \sigma_3 = 0$. Replacing these values in equation (81) we obtain $k = Y/\sqrt{3}$ with which we can rewrite equation (80) again as

$$\mathcal{F} = \sqrt{3J_2} - Y \leq 0. \tag{82}$$

We will now use $\|\bullet\| = \sqrt{\bullet : \bullet}$ to denote the Frobenius norm of a tensor. By recalling that the deviatoric part of the stress tensor is $\boldsymbol{\Sigma} = \boldsymbol{S} - (\text{tr}(\boldsymbol{S})/3)\boldsymbol{I}$, we have that its Forbenius norm is $\|\boldsymbol{\Sigma}\| = \sqrt{(1/3)\Big((\sigma_1 - \sigma_2)^2 + (\sigma_2 - \sigma_3)^2 + (\sigma_3 - \sigma_1)^2\Big)}$. We can then relate it to the J_2 invariant and obtain $\|\boldsymbol{\Sigma}\| = \sqrt{2J_2}$, with which we can rewrite equation (82) as

$$\mathcal{F} = \|\boldsymbol{\Sigma}\| - \sqrt{\frac{2}{3}}Y \leq 0. \tag{83}$$

This yield criterion can be expressed in many other ways, which are presented in basic works on yield criteria. For a concise presentation of a few of them, we refer the reader to Chaves (2013, p. 474).

The *current* yield stress of the material, $Y = Y(f_y, \alpha, k_n)$, is a function of the initial yield

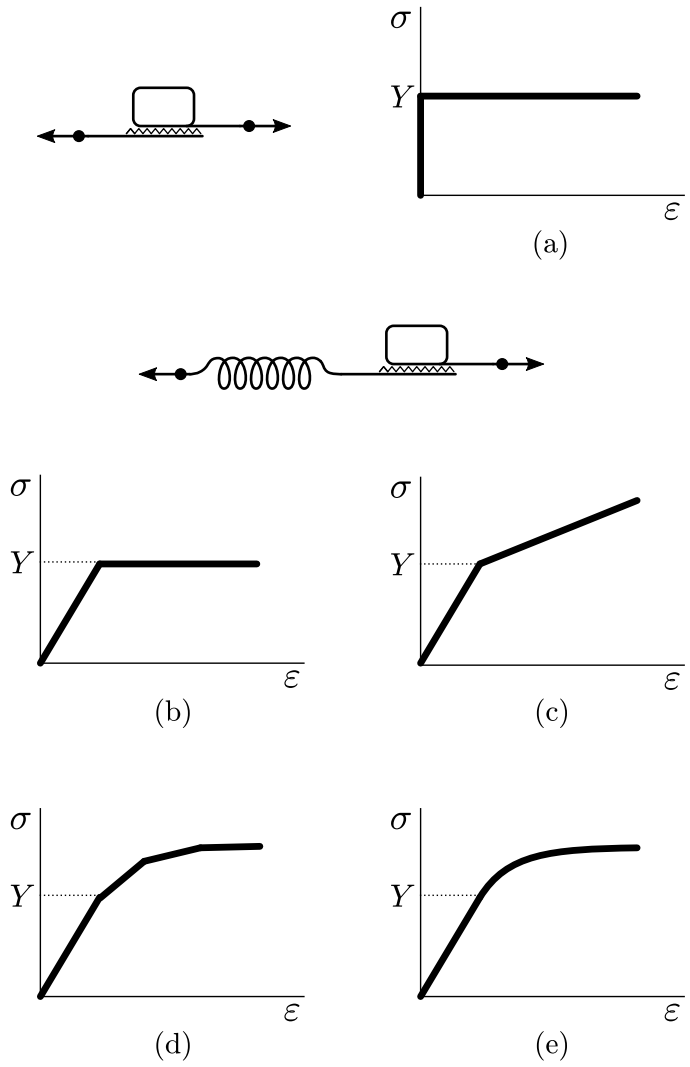

Figure 5: Unidimensional rheological models and stress-strain curves for rigid-plastic material (a) and elastoplastic material with perfect plasticity (b), linear hardening (c), piecewise linear (d) and nonlinear hardening (e). Source: the author.

stress f_y, the internal hardening variable α and a number of material plasticity parameters k_n. It can be defined in different ways depending on the number of material parameters available and the kind of approximation of the stress-strain curve we wish to consider, as illustrated in Figure 5. The rigid-plastic material seen in Figure 5a is a simpler variant that precludes any elastic deformation prior to plastification. For elastoplastic materials, the simplest choice is to consider Y constant as in $Y = f_y$, seen in Figure 5b. This behavior is refered to as *perfect* or *ideal* plasticity. Since no real material is perfectly plastic, their utility lies in modeling a small strain range of certain materials such as, e.g., the yield plateau in low-carbon steel, seen in Figure 6a. Linear hardening, usually given by $Y = f_y + k\alpha$, seen in Figure 5c, is useful when modeling the behavior of materials within the strain range of a sloped yield plateau as shown by Sadowski et al. (2017), or

of materials that present a plastic strain range that is reasonably well approximated by linear hardening, as seen in Figure 6b for some carbon steels. Nonlinear hardening (Fig-

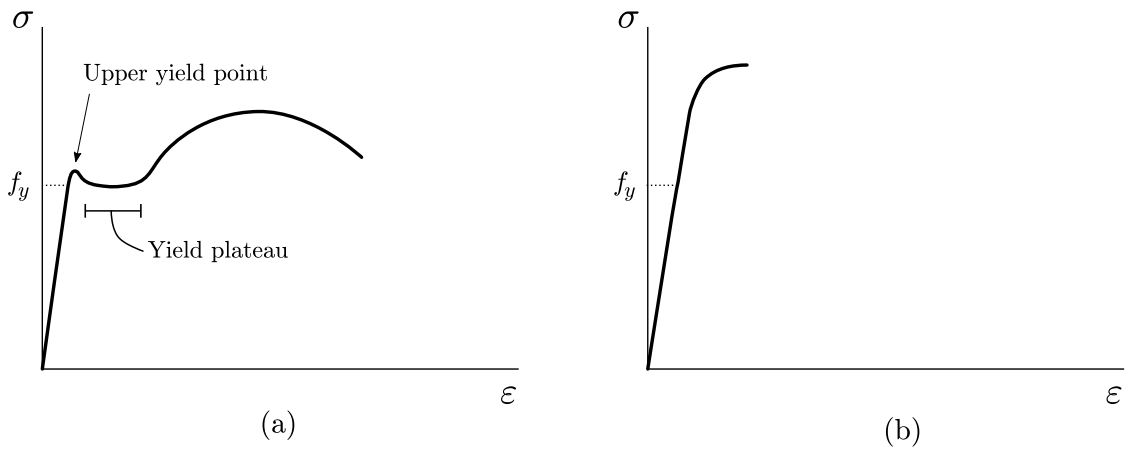

Figure 6: Typical qualitative stress-strain curves for (a) low-carbon steel, wherein a yield plateau is well defined and (b) high-strength, carbon steel. Source: the author.

ure 5e) can be used as either interpolation of experimental mesurements with some, often polynomial, curve or when considering *a priori* a nonlinear hardening law such as, e.g., Ramberg-Osgood or Ludwik's hardening laws, commonly used to model stainless steels or high-strength carbon steels (Figure 6b). Depending on the availability of measurements, the stress-strain curve can also be approximated by interpolating a piecewise linear curve as seen in figure 5d or some higher degree spline. For the purposes of this work, modeling of structural steel rods undergoing small strains, it suffices to implement constant and linear functions for perfect plasticity and linear hardening, matching the initial plastic strain region of the stress strain curve in figure 6a reasonably well.

For functions Y with $dY/d\alpha > 0$, it can be shown that the solution to the initial boundary value problem of elastoplasticity is unique even when considering kinematic hardening of the material (Simo and Hughes, 1998, p. 29). As we are dealing only with quasi-static problems in this work, we assume that the material undergoes only isotropic hardening, but its extension to consider kinematic hardening is possible based on Ziegler's hardening law, which considers internal variables of back stress.

We adopt an associative plastic flow law as follows:

$$\dot{\boldsymbol{E}}^p = \dot{\alpha}\nabla\mathcal{F} = \dot{\alpha}\,\frac{\partial\mathcal{F}}{\partial\boldsymbol{\Sigma}} = \dot{\alpha}\hat{\boldsymbol{N}} \qquad \text{where} \qquad \hat{\boldsymbol{N}} = \frac{\boldsymbol{\Sigma}}{\|\boldsymbol{\Sigma}\|} \tag{84}$$

Tensor $\hat{\boldsymbol{N}}$ is called plastic flow tensor and determines the flow direction of the stress

relative to the yield surface. Note that its Froebenius norm $\|\hat{\boldsymbol{N}}\| = 1$ and it must be determined from the full tensor $\boldsymbol{S}$, including components $\tau^r_{\alpha\alpha}$ from equation (69). The Kuhn-Tucker loading/unloading conditions and the consistency condition are expressed in a standard way as

$$\mathcal{F} \leq 0, \qquad \dot{\alpha} \geq 0, \qquad \dot{\alpha}\mathcal{F} = 0 \qquad \text{and} \qquad \dot{\alpha}\dot{\mathcal{F}} = 0. \tag{85}$$

With these conditions, it is possible to characterize the material behavior in the elastic and plastic states when subject to either loading or unloading:

$$\text{elastic state:} \quad \begin{cases} \text{loading:} & \mathcal{F} < 0, \quad \dot{\mathcal{F}} > 0, \quad \dot{\alpha} = 0 \\ \text{unloading:} & \mathcal{F} < 0, \quad \dot{\mathcal{F}} < 0, \quad \dot{\alpha} = 0 \end{cases} \tag{86}$$

$$\text{plastic state:} \quad \begin{cases} \text{loading:} & \mathcal{F} = 0, \quad \dot{\mathcal{F}} = 0, \quad \dot{\alpha} > 0 \\ \text{unloading:} & \mathcal{F} = 0, \quad \dot{\mathcal{F}} < 0, \quad \dot{\alpha} = 0 \end{cases} \tag{87}$$

To write the expressions for the plastic consistency parameter and the elastoplastic tangent modulus we must first recover the linear elastic constitutive relation from equation (62) and extract the fourth order constitutive tensor $\mathbb{C} = \lambda \boldsymbol{I} \otimes \boldsymbol{I} + 2\mu\mathbb{I}$ where $\mathbb{I} = (1/2)(\delta_{ik}\delta_{jl} + \delta_{il}\delta_{jk})\, \boldsymbol{e}_i \otimes \boldsymbol{e}_j \otimes \boldsymbol{e}_k \otimes \boldsymbol{e}_l$ is the symmetric fourth order identity tensor, written with the aid of the Kronecker delta function δ_{ij}. The associative plastic flow, at least with perfect plasticity, is consistent with the hypothesis that $\nabla\mathcal{F} : \mathbb{C} : \nabla\mathcal{F} > 0$. With this assumption, it is possible to obtain expressions for the plastic consistency parameter $\dot{\alpha}$ and the consistent elastoplastic stiffness tensor. The full procedures will be omitted here due to its length and since these results are common knowledge in the field of computational plasticity. We refer the reader to one of several works that present the proofs in full such as, e.g., Simo and Hughes (1998, p. 79-91), Chaves (2013, p. 505-514), Chen and Han (1988, p. 207-215). The formulation presented here, however, does not hold the hypothesis of volume conservation of the rod. The plastic consistency parameter is written as

$$\dot{\alpha} = \frac{\nabla\mathcal{F} : \mathbb{C} : \dot{\boldsymbol{E}}}{\nabla\mathcal{F} : \mathbb{C} : \nabla\mathcal{F}} = \frac{\hat{\boldsymbol{N}} : \dot{\boldsymbol{E}}}{1 + \dfrac{dY/d\alpha}{3\mu}}. \tag{88}$$

The fourth order consistent elastoplastic tangent tensor can then be expressed as follows:

$$\mathbb{C}^p = \lambda \boldsymbol{I} \otimes \boldsymbol{I} + 2\mu \mathbb{I} - 2\mu \frac{\hat{\boldsymbol{N}} : \dot{\boldsymbol{E}}}{1 + \dfrac{dY/d\alpha}{3\mu}} \tag{89}$$

We can then use it to obtain the rate of change of stress with respect to the total strain rate in elastic and plastic states:

$$\dot{\boldsymbol{S}} = \begin{cases} \mathbb{C}\dot{\boldsymbol{E}} & \text{if} \quad \dot{\mathcal{F}} < 0, \\ \mathbb{C}^p \dot{\boldsymbol{E}} & \text{if} \quad \dot{\mathcal{F}} = 0. \end{cases} \tag{90}$$

3.5 Simple one-dimensional elastoplastic model

In this model, we assume that the strain on the cross sectional normal direction dominates the behavior of the rod, such that plastic deformations are considered to occur only for this component of strain, i.e., only for component E_{33} of tensor $\boldsymbol{E}$. From equation (67) and the additive split of the total strains mentioned earlier, it follows that $E_{33} = \gamma^r_{33} = \gamma^{r|p}_{33} + \gamma^{r|p}_{33}$. This allows us to work under a simple uniaxial framework for the plastic deformations. With these assumptions and considering the linear elastic relation of the St. Venant-Kirchhoff material, we write the elastic part of the stress-strain relationship by rewriting equation (70) as follows:

$$\tau^r_{33} = E\gamma^{r|e}_{33} = E(\gamma^r_{33} - \gamma^{r|p}_{33}). \tag{91}$$

Furthermore, we also assume that plastic strains occur due only to the cross sectional normal stress $S_{33} = \tau^r_{33}$, which implies that $\sigma_1 = S_{33} = \tau^r_{33}$, $\sigma_2 \to 0$ and $\sigma_3 \to 0$. Rewriting equation (83) for the yield criterion with these assumptions, we obtain

$$\mathcal{F} = \sqrt{\frac{2}{3}(\sigma_1)^2} - \sqrt{\frac{2}{3}}\, Y \leq 0, \tag{92}$$

which simplifies to

$$\mathcal{F} = |\tau^r_{33}| - Y \leq 0. \tag{93}$$

Because the developments of the expressions for the plastic consistency parameter, the evolutionary equation of material hardening and the consistent elastoplastic tangent modulus in one-dimensional plasticity are very concise, we will include it here. In this uniaxial framework, the associative plastic flow law has a very simple expression as follows:

$$\dot{\gamma}_{33}^{r|p} = \dot{\alpha}\hat{n}, \tag{94}$$

where $\hat{n} = \partial\mathcal{F}/\partial\tau_{33}^{r}$ is the unit normal to the yield surface in stress space. The evolutionary equation for the hardening variable as equivalent plastic strain is given by

$$\dot{\alpha} = |\dot{\gamma}_{33}^{r|p}|. \tag{95}$$

With function Y and the conditions seen in equations (85) above, we can obtain the elastoplastic tangent modulus for the plastic state of the material. While the material is incurring loading in plastic state, from equation (93) and relations (87) we have

$$\dot{\mathcal{F}} = \frac{d\mathcal{F}}{d\tau_{33}^{r}}\,\dot{\tau}_{33}^{r} + \frac{d\mathcal{F}}{dY}\,\dot{Y} \tag{96}$$

$$= \frac{\tau_{33}^{r}}{|\tau_{33}^{r}|}\,\dot{\tau}_{33}^{r} - \frac{dY}{d\alpha}\dot{\alpha} = 0. \tag{97}$$

With the aid of equations (91) and (94) into equation (97) and by solving the resulting expression for $\dot{\alpha}$, we have

$$\frac{\tau_{33}^{r}}{|\tau_{33}^{r}|}\,E(\dot{\gamma}_{33}^{r} - \dot{\gamma}_{33}^{r|p}) - \frac{dY}{d\alpha}\dot{\alpha} = 0 \tag{98}$$

$$\frac{\tau_{33}^{r}}{|\tau_{33}^{r}|}\,E\,\dot{\gamma}_{33}^{r} - \frac{\tau_{33}^{r}}{|\tau_{33}^{r}|}\,E\,\dot{\gamma}_{33}^{r|p} - \frac{dY}{d\alpha}\dot{\alpha} = 0 \tag{99}$$

$$\frac{\tau_{33}^{r}}{|\tau_{33}^{r}|}\,E\,\dot{\gamma}_{33}^{r} - \frac{\tau_{33}^{r}}{|\tau_{33}^{r}|}\,E\,\dot{\alpha}\frac{\tau_{33}^{r}}{|\tau_{33}^{r}|} - \frac{dY}{d\alpha}\dot{\alpha} = 0 \tag{100}$$

$$\frac{\tau_{33}^{r}}{|\tau_{33}^{r}|}\,E\,\dot{\gamma}_{33}^{r} - E\,\dot{\alpha} - \frac{dY}{d\alpha}\dot{\alpha} = 0 \tag{101}$$

$$\dot{\alpha} = \frac{(\tau_{33}^{r}/|\tau_{33}^{r}|)\,E\,\dot{\gamma}_{33}^{r}}{E + dY/d\alpha}. \tag{102}$$

With $\dot{\alpha}$ back in equation (94), we find that

$$\dot{\gamma}_{33}^{r|p} = \frac{\tau_{33}^r}{|\tau_{33}^r|} \frac{E\,\dot{\gamma}_{33}^r}{E + dY/d\alpha} \frac{\tau_{33}^r}{|\tau_{33}^r|} = \frac{E\,\dot{\gamma}_{33}^r}{E + dY/d\alpha} \tag{103}$$

The elastoplastic stress-strain relation can then be obtained from equation (91), written as

$$\dot{\tau}_{33}^r = E(\dot{\gamma}_{33}^r - \dot{\gamma}_{33}^{r|p}) = E\left(\dot{\gamma}_{33}^r - \frac{E\,\dot{\gamma}_{33}^r}{E + dY/d\alpha}\right) = \left(\frac{E\,(dY/d\alpha)}{E + dY/d\alpha}\right)\dot{\gamma}_{33}^r \tag{104}$$

As before, we can use it to obtain the rate of change of stress with respect to the total strain rate in elastic and plastic states as follows:

$$\dot{\tau}_{33}^r = \begin{cases} E\dot{\gamma}_{33}^r & \text{if} \quad \dot{\mathcal{F}} < 0, \\ \left(\dfrac{E\,(dY/d\alpha)}{E + dY/d\alpha}\right)\dot{\gamma}_{33}^r & \text{if} \quad \dot{\mathcal{F}} = 0. \end{cases} \tag{105}$$

In rate-independent elastoplasticity, the above relation is integrated over time using a class of algorithms commonly called *return mapping algorithms* that work with a time variable discretized in finite increments. They also handle the update of the internal variables and other physical quantities involved (cf. Simo and Hughes, 1998, p. 39).

3.6 Return mapping algorithm

As mentioned by Simo and Hughes (1998, p. 116), the continuum problem of elastoplasticity presented in the previous sections can be transformed into a discrete, constrained optimization problem by applying an implicit backward-Euler difference scheme. This turns the procedure into an iterative problem of finding the closest distance of the point of state in stress space to the convex yield surface that bounds the elastic domain. To implement the stress integration algorithm, specifically the well-known radial return mapping algorithm proposed by Wilkins (1964 apud Simo and Hughes, 1998, p. 120) for both three-dimensional and one-dimensional elastoplastic models, we replace the stress, strain and hardening rates by finite increments. This allows us to perform the analysis using a simple incremental loading scheme.

Central to this algorithm is the definition of a two-step-solution: an elastic *trial* predictor,

and a plastic corrector that projects the trial stress state onto the yield surface (Simo and Hughes, 1998, p. 139). As the name implies, the elastic predictor is computed as if the problem were purely elastic, and from it we obtain an intermediate state refered to as *trial stress*. This trial stress is then verified for admissibility with the yield criterion and, if failed, a plastic corrector is added to it. This plastic corrector is determined from the solution of a closest point projection problem, which takes the trial stress as inital condition. Figure 7 shows an illustration of this procedure. For the yield criteria and hardening functions considered in this work, it suffices to use a simple radial return procedure that projects the trial stress onto the yield surface directly.

At the start of the analysis, variables for the hardening and plastic strains are initialized and have their history stored to be used in later steps. We solve the weak form of equilibrium presented in section 2.3 by the finite element method and compute the elastic trial stress $\boldsymbol{S}_{n+1}^{\text{trial}}$ from equation (62). We then compute $\mathcal{F}$ and verify the compliance with the yield criterion. Here, the known hardening variable and plastic strain of the current step n are used:

$$\boldsymbol{S}_{n+1}^{\text{trial}} = \lambda \,\text{tr}(\boldsymbol{E}_{n+1} - \boldsymbol{E}^{p}{}_{n})\boldsymbol{I} + 2\mu(\boldsymbol{E}_{n+1} - \boldsymbol{E}^{p}{}_{n}) \tag{106}$$

$$\mathcal{F}_{n+1}^{\text{trial}} = \|\boldsymbol{\Sigma}_{n+1}^{\text{trial}}\| - \sqrt{\frac{2}{3}}\, Y_n \tag{107}$$

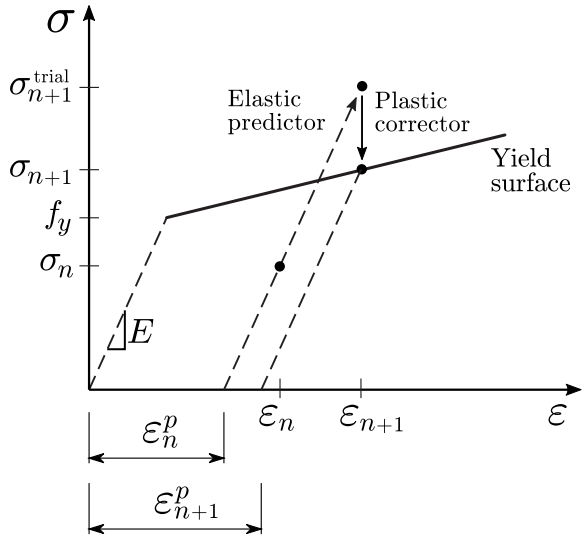

Figure 7: Return mapping algorithm. Source: the author.

If $\mathcal{F}_{n+1}^{\text{trial}} \leq 0$, the model is either in elastic state or in neutral loading, and the stress and strain are effectively the trials computed. In this case, the hardening and plastic strain variables do not change. If, however, the yield criterion is not met, the trial stress is projected onto the yield surface and the plastic strain and hardening variables are incremented:

$$\Delta\alpha = \frac{1}{2\mu}\frac{\mathcal{F}_{n+1}^{\text{trial}}}{1+\dfrac{dY/d\alpha}{3\mu}} \quad \text{if} \quad \mathcal{F}_{n+1}^{\text{trial}} > 0, \quad \text{else} \quad \Delta\alpha = 0, \tag{108}$$

$$\boldsymbol{E}^{p}{}_{n+1} = \boldsymbol{E}^{p}{}_{n} + \Delta\alpha\hat{\boldsymbol{N}} \quad \text{with} \quad \hat{\boldsymbol{N}} = \frac{\boldsymbol{\Sigma}_{n+1}^{\text{trial}}}{\|\boldsymbol{\Sigma}_{n+1}^{\text{trial}}\|}, \tag{109}$$

$$\alpha_{n+1} = \alpha_n + \sqrt{\frac{2}{3}}\Delta\alpha, \tag{110}$$

$$\boldsymbol{S}_{n+1} = \mathbb{C}(\boldsymbol{E}_{n+1} - \boldsymbol{E}^{p}{}_{n+1}). \tag{111}$$

Because, for the one-dimensional model, the yield stress is the same as the yield stress under pure tension, we do not need to scale the the hardening evolution by $\sqrt{2/3}$ and the shear modulus $\mu = G$ plays no role in the plasticity process. For one-dimensional plasticity, the expressions are:

$$\tau_{33\,n+1}^{r\ \text{trial}} = E(\gamma_{33\,n+1}^{r} - \gamma_{33\ n}^{r|p}), \tag{112}$$

$$\mathcal{F}_{n+1}^{\text{trial}} = |\tau_{33\,n+1}^{r\ \text{trial}}| - Y, \tag{113}$$

$$\Delta\alpha = \frac{\mathcal{F}_{n+1}^{\text{trial}}}{E + dY/d\alpha} \quad \text{if} \quad \mathcal{F}_{n+1}^{\text{trial}} > 0, \quad \text{else} \quad \Delta\alpha = 0, \tag{114}$$

$$\gamma_{33\ n+1}^{r|p} = \gamma_{33\ n}^{r|p} + \hat{n}\Delta\alpha \quad \text{with} \quad \hat{n} = \frac{\tau_{33\,n+1}^{r\ \text{trial}}}{|\tau_{33\,n+1}^{r\ \text{trial}}|}, \tag{115}$$

$$\alpha_{n+1} = \alpha_n + \Delta\alpha, \tag{116}$$

$$\tau_{33\,n+1}^{r} = E(\gamma_{33\,n+1}^{r} - \gamma_{33\ n+1}^{r|p}). \tag{117}$$

Notice that instead of obtaining the corrected stress ($\boldsymbol{S}_{n+1}$ or $\tau_{33\,n+1}^{r}$) through equations (111) or (117), we could have used the consistent elastoplastic tangent moduli defined in the previous sections. However, these moduli are better suited to large strains plasticity, and impose an unecessary computational cost for these small strains models, especially for the one-dimensional one.

4 Computational implementation and numerical examples

The formulations presented in the previous chapters were implemented in a computer program using the finite element method. The rod elements used were standard Lagrangian polynomial elements of second degree, i.e., three-node finite elements. The meshes for all numerical examples were defined as close as possible to the ones used in the comparision works, especially when these works use different polynomial degrees for their finite elements than the ones used here and when other special methods are employed.

For the boundary conditions, whenever a rod end is clamped, the corresponding node is fully restricted, including the parameter for the warping magnitude. When the end is articulated, on the other hand, the rotational degrees of freedom are treated accordingly, and the degree of freedom of warping magnitude is left unrestricted. The rod axis is always positioned at the centroid of the cross sections, where all external loads are applied, although other positions could have been used, as the theory allows. The loads are typically applied in an incremental form, wherein the increment size is kept constant throughout the whole analysis for the sake of simplicity. Its value is presented for each example.

To compute the internal virtual work δW_{int} in equation (31), first we break down the volume integral of equation (31) into a cross sectional integration and a length integration. The cross sectional integration is, then, performed using a numerical integration scheme. In this scheme, we must provide the values of coordinates of points on the cross section $\boldsymbol{a}^r = x_\alpha \boldsymbol{e}^r_\alpha$ and of ψ and its derivatives $\psi_{,\alpha}$, as seen in equations (16) and (17) for $\boldsymbol{\gamma}^r_\alpha$ and $\boldsymbol{\gamma}^r_3$. The basic structure of the plastic zone method proposed here is to compute ψ and $\psi_{,\alpha}$ prior to the solution of the rod deformation problem and store their values for each evaluation point of the discretized section. We then use these values when performing the cross sectional integration that determines δW_{int}. Accordingly, considering integration over the volume Ω of the rod, we have

$$\int_\Omega (\bullet)\, d\Omega = \int_L \int_A (\bullet)\, dA\, dL \approx \int_L \sum_{i=1}^{N} (\bullet_i) s_i\, dL, \tag{118}$$

where N is the number of evaluation points on the discretized mesh and s_i are the weights corresponding to those points to complete the numerical integration scheme. Whenever an elastoplastic constitutive model is used, values for the plastic strains and hardening

variables are also stored for each evaluation point, thus allowing simulation of partial plastification of the cross section. The last integral in equation (118) is the one that is used in the assembly phase of the finite element method with the rod mesh, where the integration along the rod axis is also performed numerically via a standard Gaussian scheme.

The cross sectional integration is performed numerically via a triangular unstructured mesh scheme. In practice, any two-dimensional mesh over which we can define a numerical integration scheme with evaluation points and weighting functions will suffice. Example meshes can be seen in Figure 8. The level of refinement established was the least refinement that presents at least two rows of cells on the thickness direction of each part of the cross section. This is consistent with the discretizations used in the referenced works that also employ a variant of the plastic zone method.

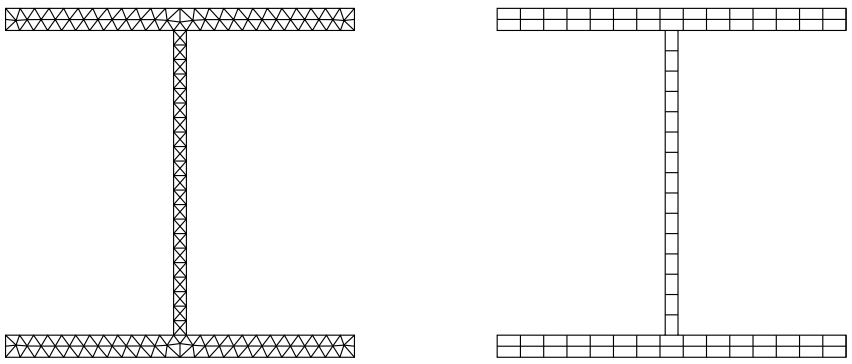

Figure 8: Discretized I-shaped setions into (a) 286 unstructured triangular cells and (b) 75 structured rectangular cells.

All integration procedures implemented on the triangle mesh are of classic quadrature scheme, see, e.g., Hammer et al. (1956) and Douvant (1985). When the material is elastic, we have the opportunity to perform this integration prior to the finite element analysis, and thus use the alternative formulation presented in section 2.4. A discussion about the order of integration is made in section 4.2 ahead.

In what follows, the first examples in this chapter are validation tests to show agreement of the theory and its implementation with results from simple problems involving only one rod under geometric linearity. The later examples compare results from the present work to those from the literature on more elaborate problems, involving geometric nonlinearity or material nonlinearity. In all examples, it was observed that, even in the region of the

structural system with the largest plastic strains, their values are still small, which is consistent with the rod kinematical and constitutive hypotheses of this work.

4.1 Simple cantilever beam

This cantilever beam, whose data are presented in Figure 9, is a simple example that was used to attest the validity of the initial implementation of the rod kinematics and the elastic constitutive model. Therefore, no plasticity takes place and we remain in linear material conditions and nearly linear geometric conditions due to small displacements and rotations. It was analyzed by Campello (2000) with the same kinematics and elastic constitutive equation used here. The results of the analysis show a very good match with the work of Campello (2000), as can be seen in Tables 1 and 2.

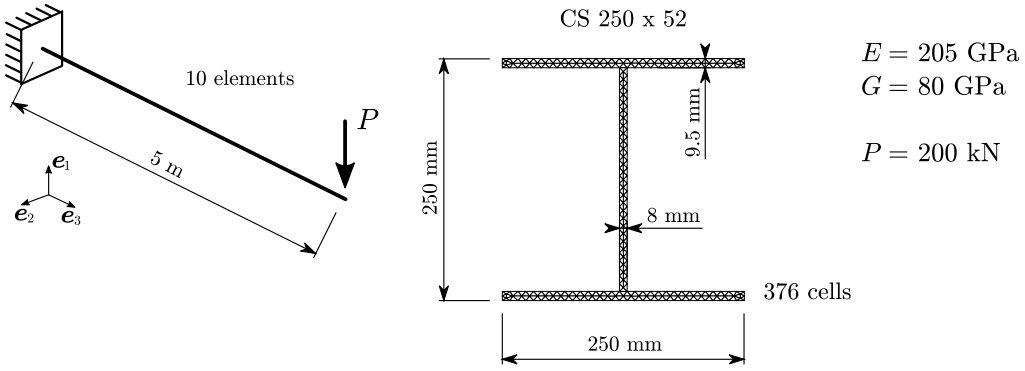

Figure 9: Problem data for simple cantilever beam example. Source: the author.

The work of Campello (2000) performs analytical integration over the cross section to obtain geometric properties used in the constitutive matrix, uses the kinematics as presented in section 2.4. In this example, we use numerical integration of order 2 over the triangle mesh of the cross section. The small differences seen below can be attributed to these differences in implementation. Notice that, in the work of Campello (2000), different elastic materials are presented, including the linear elastic material, a quadratic material of St. Venant-Kirchhoff, and a quadratic material of Simo. We compare our results only with those of the linear elastic material, that makes the same approximation of the constitutive equation as we do in this work.

	Campello (2000)	Present work
u_1 (m)	-5.2300e-1	-5.2307e-1
u_2 (m)	0.0	0.0
u_3 (m)	-3.279e-2	-3.287e-2
θ_1 (rad)	0.0	0.0
θ_2 (rad)	-1.571e-1	-1.571e-1
θ_3 (rad)	0.0	0.0
p (m^{-1})	0.0	0.0

Table 1: Values for the degrees of freedom of the vertex at the free end of the beam.

	Campello (2000)	Present work
V_1 (N)	-1.9756e5	-1.9756e5
V_2 (N)	0.0	0.0
N (N)	3.113e4	3.114e4
M_1 (N·m)	0.0	0.0
M_2 (N·m)	-4.93888e4	-4.93886e4
T (N·m)	0.0	0.0
Q (N·m)	0.0	0.0
B ($N \cdot m^2$)	0.0	0.0

Table 2: Values for the resultant forces, moments, bi-shear (Q) and bi-moment (B) on the rod finite element at the free end of the beam.

4.2 Rod under pure torsion

In this example, we can observe the behavior or the formulation and implementation of the kinematics presented in this work with respect to the degrees of freedom of rotation about the rod axis, θ_3, and warping magnitude along the axis, p. The configuration and data for the problem can be found in Figure 10. Function ψ over the cross section, obtained through the procedure presented in section 2.1, is shown in Figure (11). Due to the relevance of sectional warping in this problem, we have used it to test different levels of refinement and orders of numerical integration over the cross section.

Four combinations of integration order and mesh refinement were benchmarked in this example: (1) with the cross section mesh presented in Figure 10 and numerical integration of order 1, i.e., one evaluation point and cell areas as weights for all functions, (2) that same mesh with integration order 2 for terms of δW_{int} that depend on function ψ and its derivatives $\psi_{,\alpha}$ and integration of order 1 for terms that depend on $\boldsymbol{a}^r$, (3) integration of

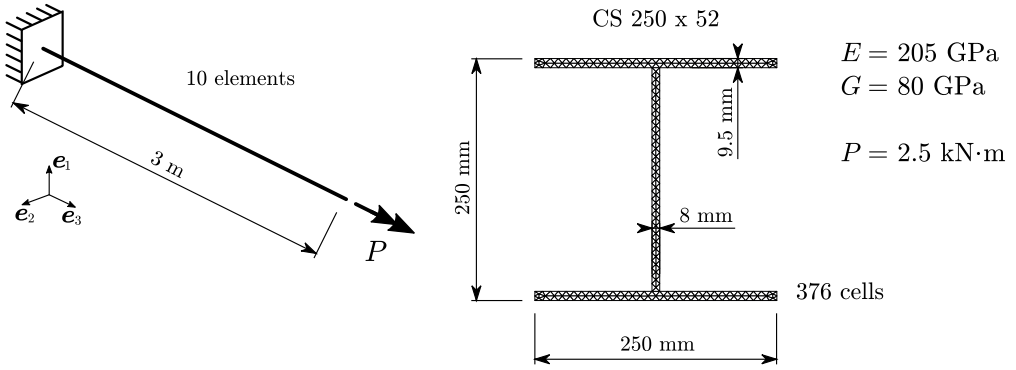

Figure 10: Problem data for cantilever beam under pure torsion example. Source: the author.

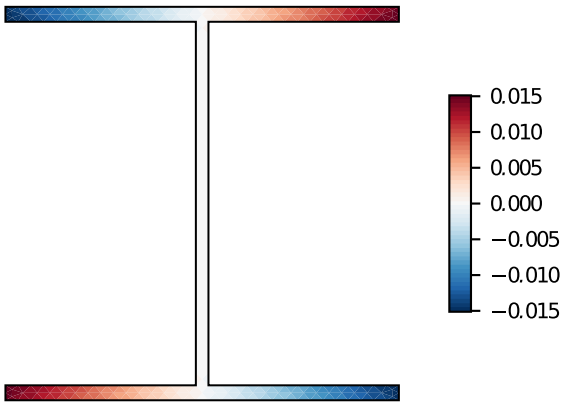

Figure 11: Function ψ for the cross section of a CS 250 x 52 profile. Source: the author.

order 1 for all terms of δW_{int} but with a more refined mesh, and (4) by using the initial mesh but performing integration of order 2 for all terms of δW_{int}. The refined mesh of case (3) is obtained by taking the initial mesh of Figure 10 and connecting the midpoints of all edges, dividing each cell into four smaller ones as seen in Figure 12.

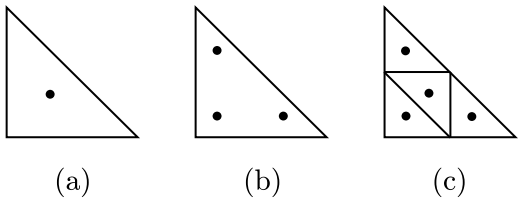

Figure 12: Evaluation points for numerical integration of (a) order 1, (b) order 2, (c) order 1 with refined mesh. Source: the author.

Results for θ_3 and p of the vertex at the free end of the rod are shown in Figures 13 and 14 respectively comparing all cases described. We also compared the present work with the results obtained with the same formulation and implementation used to obtain the

results of the works of Campello(2000) and Campello and Pimenta (2001). The relative errors in θ_3 with respect to the PEFSYS results for each case are: 7.7% case (1), 6.1% case (2), 2.0% case (3), and 0.08% in case (4).

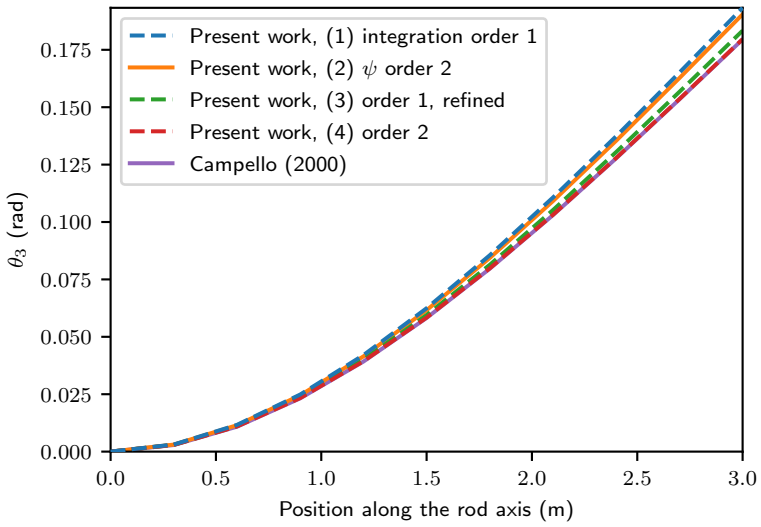

Figure 13: Values of θ_3 along the rod axis comparing different orders of numerical integration over the cross section. Source: the author.

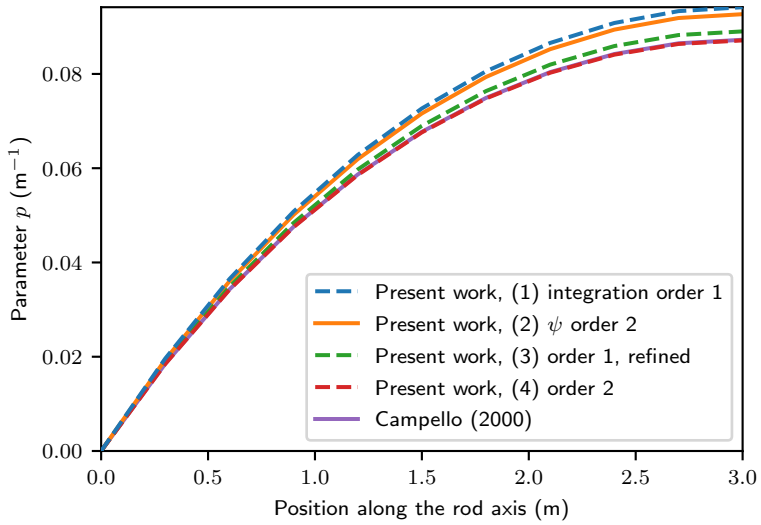

Figure 14: Values of p along the rod axis comparing different orders of numerical integration over the cross section. Source: the author.

The integrals in equations (72) through (79) hint at the relevance of the order of integration, because in many of the expressions integrated there, we have second degree polynomials. Besides, since we have found the order of integration important in the process of obtaining an approximation for ψ, we expect these values to be more relevant on problems that are dominated by sectional shear stresses and especially those under torsion

and warping. When under flexural or normal stress, on the other hand, the relevance of the area function of the cross section, seen in equation (72), becomes more relevant and, because it can be integrated numerically exactly with order 1, it mitigates the loss to approximation. Therefore, we have used integration of order 1 whenever we found that the order of integration does not make a pronounced difference in the results.

4.3 Simply supported elastoplastic beam

This example analyses the elastoplastic behavior of a simply supported beam with consideration of geometric nonlinearities and distributed plasticity when compared to the behavior expected from analysis of strength of materials. There have been innumerous works published concerning these classic methods of structural and stress analysis. For a direct reference, we can cite, e.g., the comprehensive work of Megson (2014).

The configuration and problem data for the example can be found in Figure 15, where I is the second moment of area, or moment of inertia, about the major axis of the cross section, W is the elastic section modulus and Z is the plastic section modulus. The beam is also fully restricted against lateral, out-of-plane, displacements. Force P applied at the midpoint of the rod axis is defined so that, under this load, the moment at that point is $PL/4 = Wf_y = M_y$, the moment of initial yielding of the beam. We can also calculate the factor that multiplies P to reach the plastic moment $M_p = Zf_y = 1.106PL/4$. The deflection u_3 of the beam for comparison with the results of the present work is obtained from $u_3 = PL^3/48EI$.

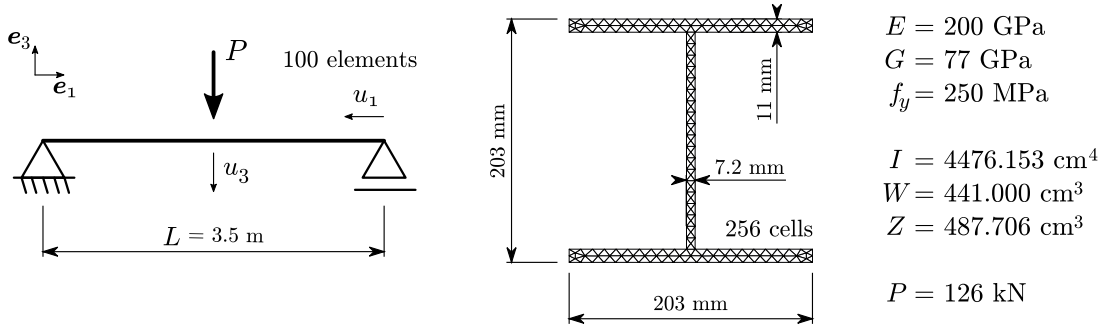

Figure 15: Configuration and problem data for simply supported elastoplastic beam. Source: the author.

For this analysis, we used incremental loading with increment size for the load factor equal to 0.005. We analyzed the beam with both the three-dimensional and one-dimensional

elastoplastic models of sections 3.4 and 3.5. In this case, we considered the material perfectly plastic.

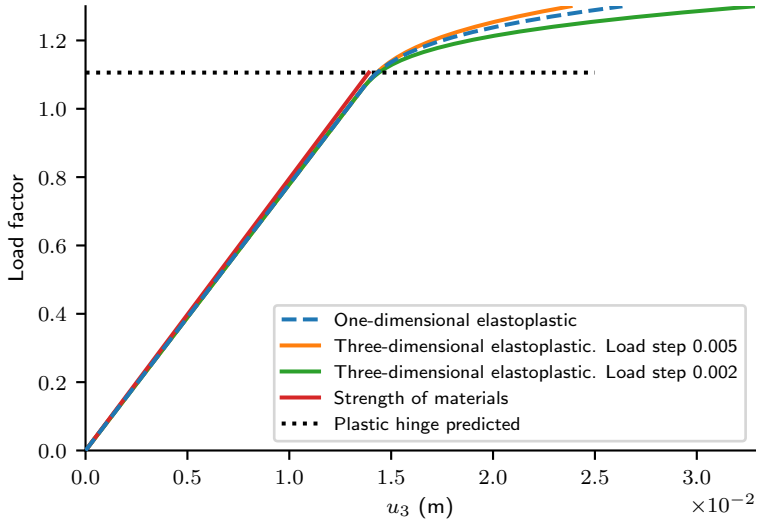

Figure 16: Displacement u_3 at the midpoint of the beam axis. Source: the author.

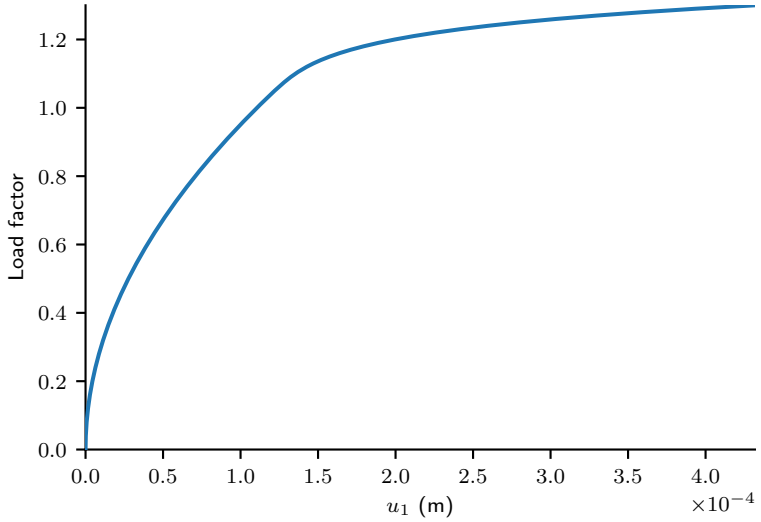

Figure 17: Displacement u_1 at the rolling end of the beam. Source: the author.

We can observe the results for the deflection of the beam in Figure 16. We can see that the system has a nearly linear behavior up until the load level in which M_p is reached. The results for the one-dimensional and three-dimensional constitutive models match very closely. The degree of freedom of displacement u_1, at the roller end of the beam, on the other hand, exibits a noticeably nonlinear behavior, as seen in Figure 17. It is, however, too small to influence the whole system, even near the load level of M_p, although growing rapidly.

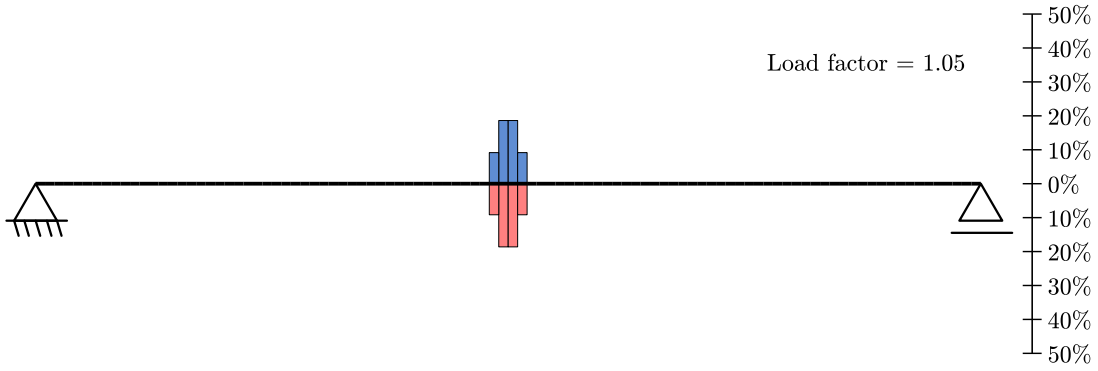

Figure 18: Ratio of plastified section area of rod finite elements of the beam midspan that yield at load factor 1.05. Each bin corresponds to a finite element that has 1% of the beam's length. Source: the author.

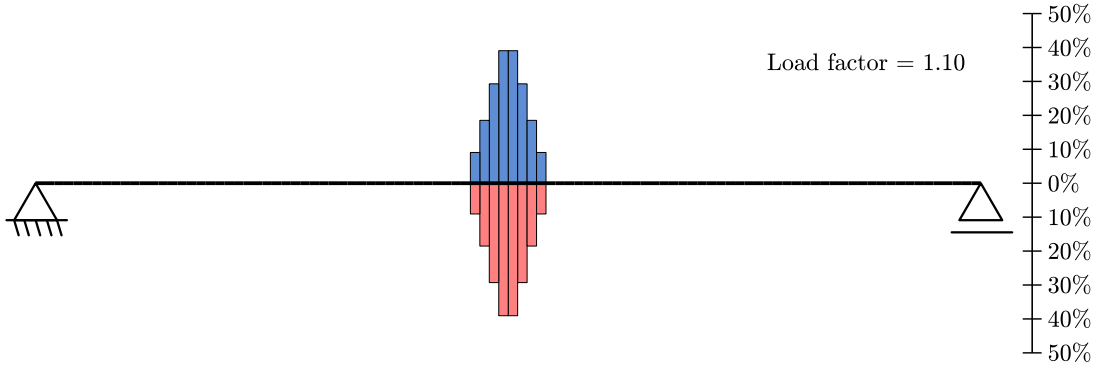

Figure 19: Ratio of plastified section area of rod finite elements of the beam midspan that yield at load factor 1.10. Each bin corresponds to a finite element that has 1% of the beam's length. Source: the author.

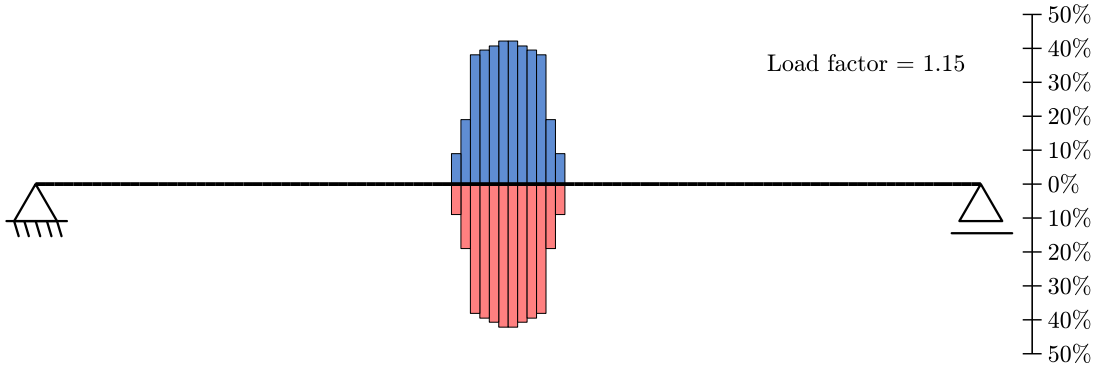

Figure 20: Ratio of plastified section area of rod finite elements of the beam midspan that yield at load factor 1.15. Each bin corresponds to a finite element that has 1% of the beam's length. Source: the author.

Due to the path-dependent nature of plasticity, the elastoplastic behavior of the beam *after initial yield* is tied to the load increment size, which, in case of perfect plasticity, means that the post-yield curve becomes asymptotically flatter the smaller the load increment. To demostrate this behavior, we also analyzed the beam with the three-dimensional elastoplastic constitutive model with a smaller load step size of 0.002, as shown in Figure 16. The behavior of the beam regarding u_3 between the load levels of initial yielding and ultimate moment resistance capacity is still nearly linear. It does, however, presents

a small decrease in stiffness, signaling the spread of stiffness degradtation due to redistribution of stresses to neighboring cross sections near the midspan of the beam.

The spread of plasticity along the rod's length can be seen in Figures 18, 19 and 20. The predicted length of the plastic region is $L(1 - M_y/M_p)$ (Megson, 2014, p. 622), which in this case is $9.6\%L$. In Figure 19, for load factor 1.10, we can see that this matches the results obtained, showing $8\%L$ of plastic region at a loading close to the predicted factor of 1.106 for M_p.

Initial yielding of the middle elements of the beam happens at load factor 1.025, 2.5% above the expected value. We expect this value to diminish with greater refinement of rod and cross section meshes as well as smaller load increments, although further convergence tests are needed in these three variables to find optimum values.

Distributed plasticity over the cross sections can be seen in Figure 21 for the finite elements in the middle of the beam under different load factors and in Figure 22 for the plastified region of the beam midspan under the load of $1.1P$. Differences in the spread of plasticity between the three-dimensional and one-dimensional elastoplastic models oscillates below 2% in area ratio among the load steps.

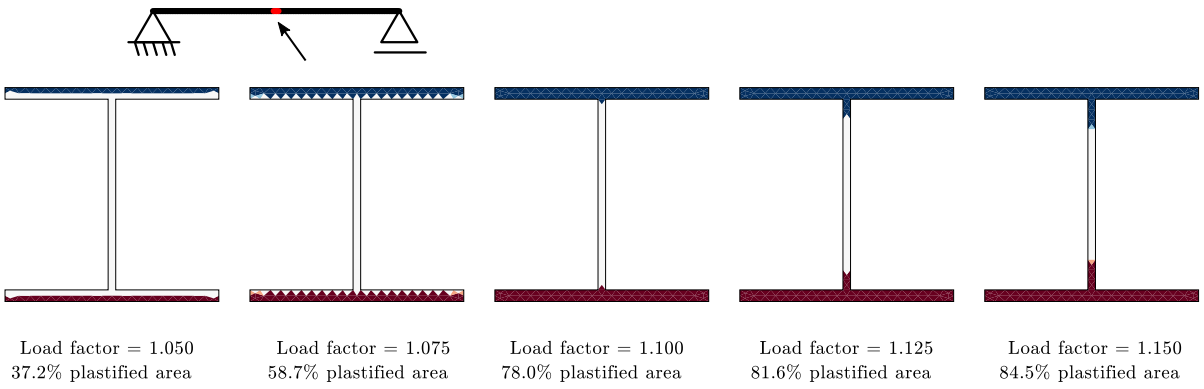

Figure 21: Distributed plasticity over the cross sections of the two rod finite elements connected to the middle vertex of the rod axis. Source: the author.

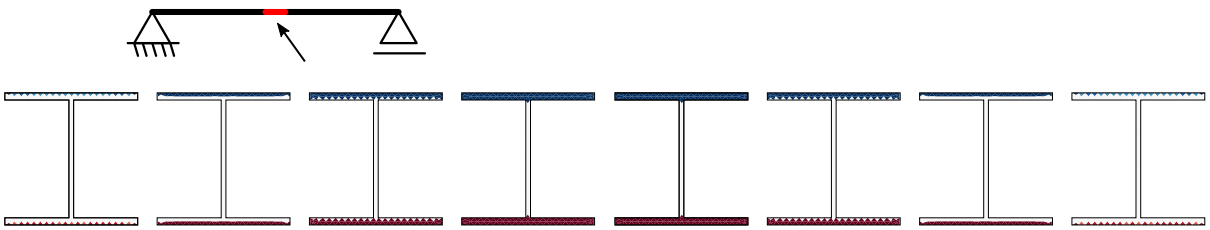

Figure 22: Distributed plasticity over the cross sections of the eight rod finite elements of the beam midspan that yield at the load level of 1.1. Source: the author.

4.4 Lateral torsional buckling of cantilever beams

This example analyzes cantilever beams with three different cross sections, I, C and rectangular, shown in Figure 23 along with the problem data. This example was analyzed before by Yojo (1993) and Campello (2000). For the beams with symmetric sections, I and rectangular, a small lateral force of $10^{-5}P$ was applied at the free end to bypass the bifurcation point. Warping functions ψ for each cross section can be seen in Figure 24.

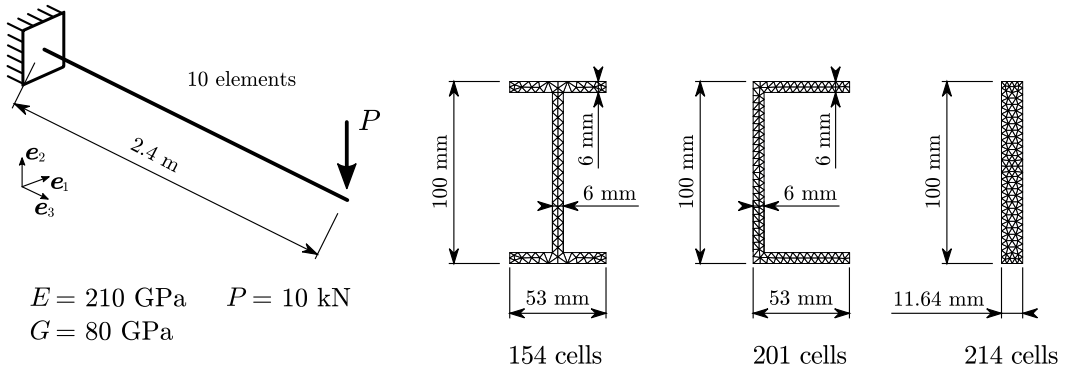

Figure 23: Problem data. Source: the author.

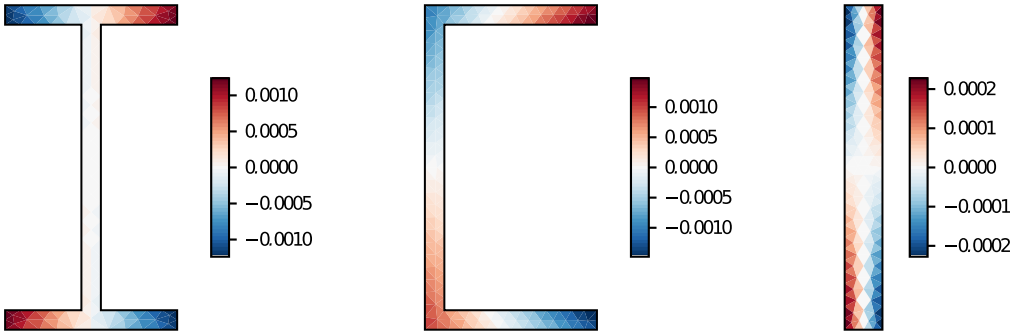

Figure 24: Warping functions ψ for cross sections I, C and rectangular. Source: the author.

As seen in Figure 25, the results for u_1 match very closely those of Campello (2000) for sections I and C. The difference in post-critical path for the beam with rectangular cross section is again due to differces in implementation. The work of Campello (2000) uses Vlasov's sectorial area for the warping function which, for the rectangular section, yields a warping constant $\int_A \psi^2 \, dA = J_\psi = 0$. In the present work, however, a higher order approximation of ψ is possible, and we have found that, for that section, $J_\psi = 10.32$ cm^6, which is very small, but is enough to make a noticeable difference in the post-critical behavior of the rod.

Warping magnitude at the free end for each beam is presented in Figures 26, 27, and 28. The warping of the beam with rectangular cross section is of much lower magnitude,

matching its geometry, and does not suffer inversion as do the other two, but has an inflection matching the curve in Figure 25 where the lateral displacement starts to decrease.

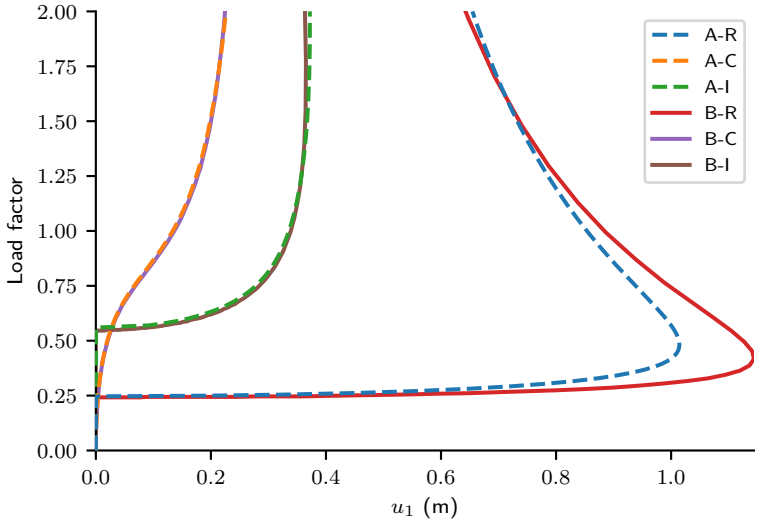

Figure 25: Lateral displacement u_1 for beams by their cross section: A-R, A-C and A-I are for the present work, rectangular, C, and I sections respectively, B-R, B-C and B-I are the results of Campello (2000) for rectangular, C, and I sections respectively. Source: the author.

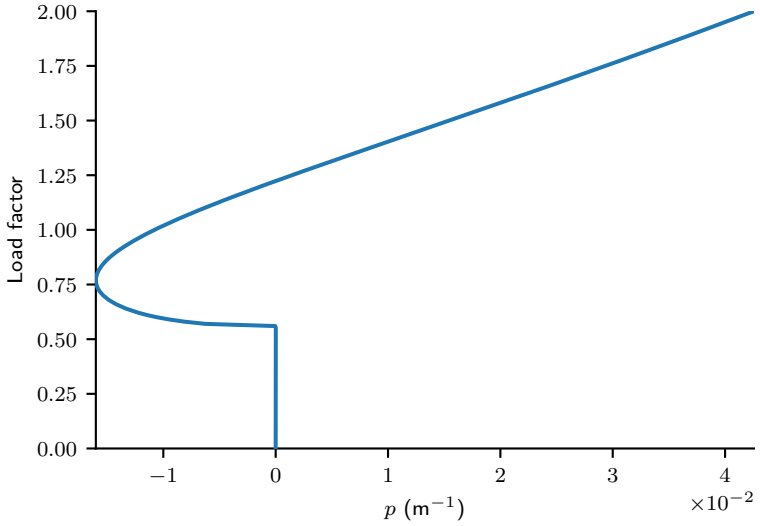

Figure 26: Warping magnitude p at the free end of cantilever beam with section I. Source: the author.

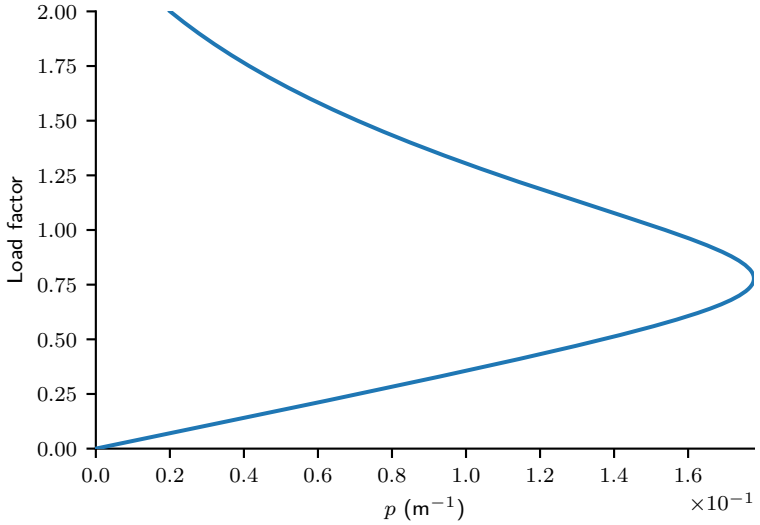

Figure 27: Warping magnitude p at the free end of cantilever beam with section C. Source: the author.

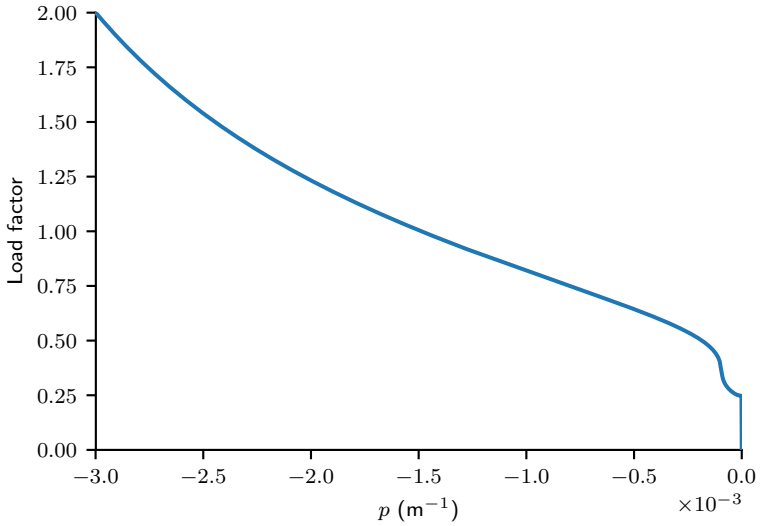

Figure 28: Warping magnitude p at the free end of cantilever beam with rectangular cross section. Source: the author.

4.5 Vogel's portal frame

The frame shown in Figure 29 was first analyzed by Vogel (1985) as part of a set of proposed "calibrating" frames against which computational implementations and simplified or approximated mechanical models can be compared. Since then it has been analyzed by many authors like Chen et at. (1996), Barsan and Chiorean (1999), Avery and Mahendran (2000), Kim and Lee (2002), Lavall et al. (2013) and Rigobello et al. (2013), to mention just a few. The frame is a plane rectangular unbraced portal with fixed column bases.

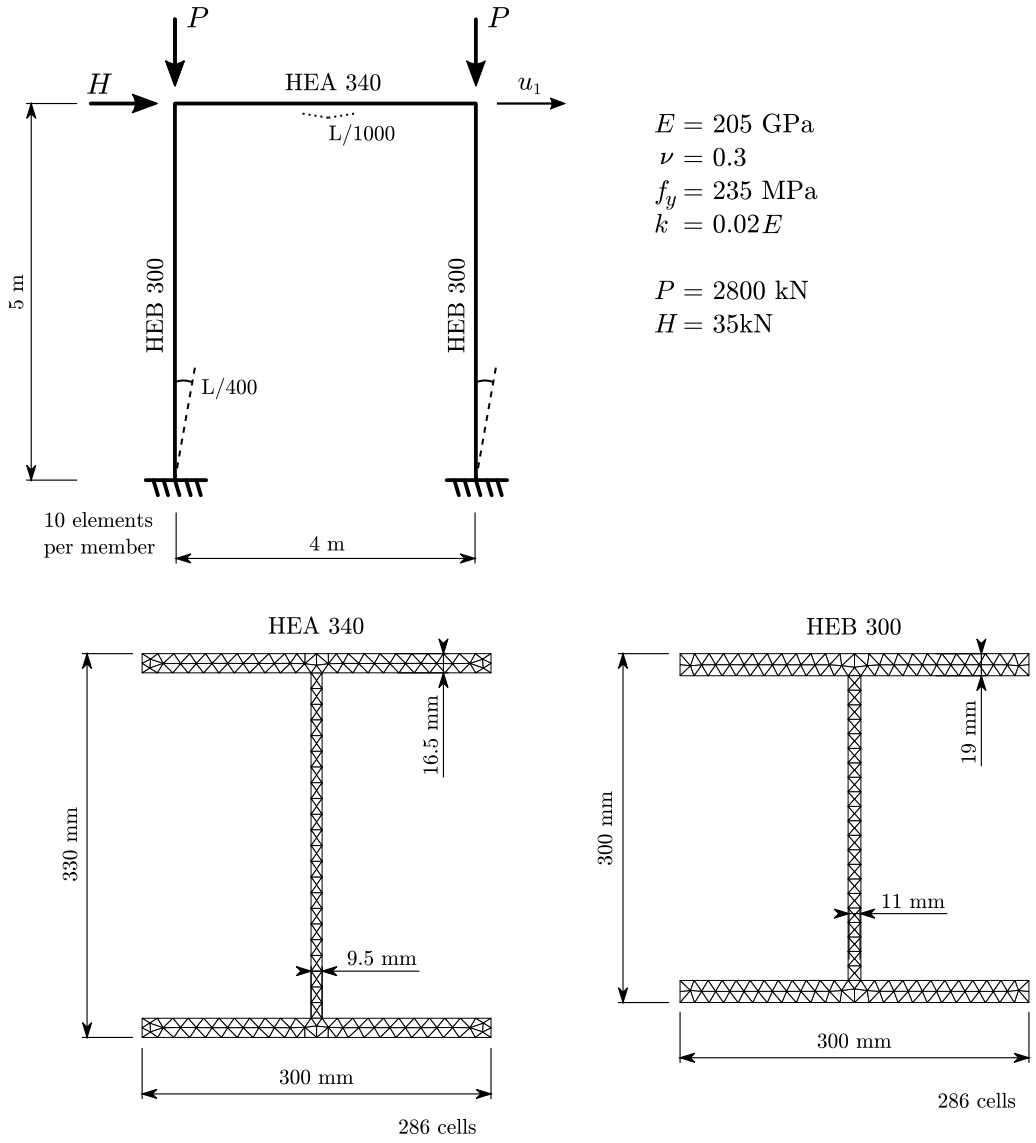

Figure 29: Configuration and problem data for analysis of Vogel's portal frame. Source: the author.

All members are oriented with their webs in the plane of the frame. Each column is subject to a 2800 kN compression force, whereas a horizontal force of 35 kN is applied to the top

of the left column. Each member is discretized here in 10 rod finite elements. Geometric imperfections are modeled directly in the rod mesh with a $L/400$ out-of-plumbness at the top of the columns, and a $L/1000$ out-of-straightness at the midpoint of the beam. The stress-strain curve considered in the analysis, shown in Figure 30, is the same as that of Vogel (1985). Throughout the analysis, no element has reached the strain-hardening phase, thus only perfect plasticity was observed. We used a constant increment size to the load factor of 0.001.

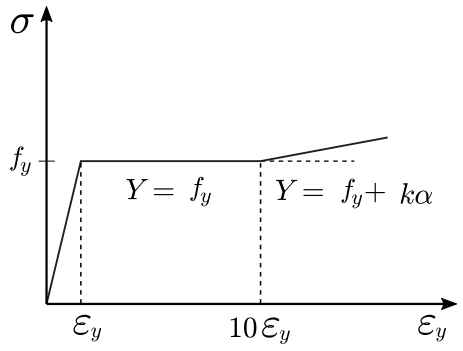

Figure 30: Stress-strain curve for Vogel's portal frame. Source: the author.

The sections of the members are discretized in 286 cells, holding residual stress values. The residual stress considered, $\sigma_r = \hat{\sigma}_r f_y$, is distributed according to the pattern established in ECCS publication 33 (1984), seen in Figure 31. The distribution over the discretized sections is made using a simple surface equation $\hat{\sigma}_r = c\,(2||\bar{x}_1| - |\bar{x}_2|| - 1)$, where the base factor is $c = 0.5$ if $d/b_f \leq 1.2$ or $c = 0.3$ if $d/b_f > 1.2$. Here, $\bar{x}_1 = (x_1 - g_1)/(b_f/2)$ and $\bar{x}_2 = (x_2 - g_2)/(d/2)$ are normalized coordinates relative to the centroid of the section, ranging from -1 to 1, with g_α as the coordinates of the centroid. The resulting values of $\hat{\sigma}_r$ for the sections of the columns and beam can be seen in Figure 32.

The frame is restricted against out of plane displacements and it is assumed that its cross sections do not suffer local distortions. The frame was analyzed with consideration of sectional warping, for which the ψ function for the column sections and beam sections can be seen in figure 33. Due to the lateral restrictions and the specific sections used, however, the magnitude of the sectional warping resulted to be very small throughout the whole analysis, as expected.

The horizontal displacement u_1 obtained at the top of the right column is plotted in

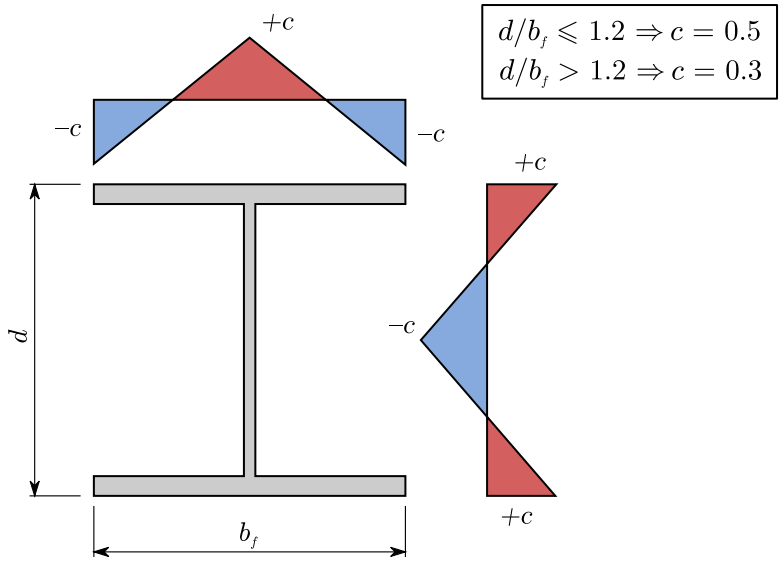

Figure 31: Residual stress distribution according to ECCS publication 33 (1984). Source: the author.

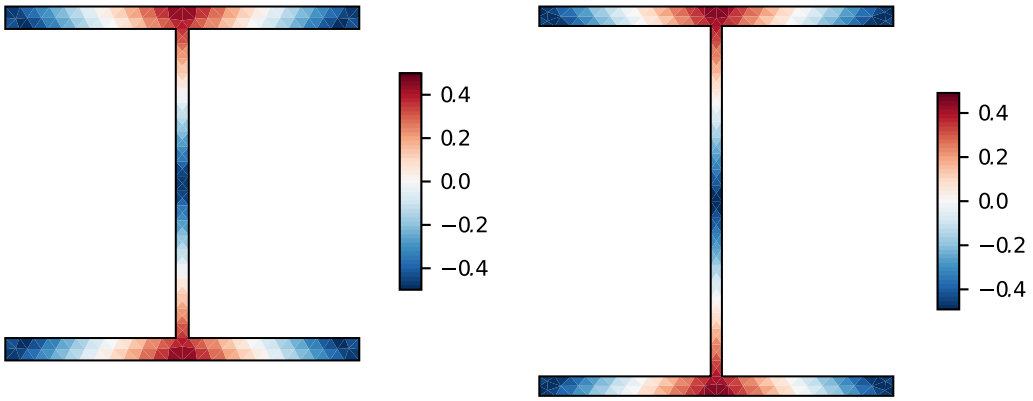

Figure 32: Residual stress factors $\hat{\sigma}_r$ for the sections of the (a) columns and (b) beam of Vogel's portal frame. Source: the author.

Figure 34 against the applied load factor. We can see that it agrees very well with the results of many works that analyzed this frame with different methods. In particular, it is found to be nearly identical to the curve obtained by Lavall et al. (2013), which is expected since the underlying kinematics is very similar. Although that work uses a model for plane frames, the lateral restrictions applied herein bring the fully three dimensional model developed here to the same conditions.

In Figure 35 we can see the ratios of column section areas that undergo plastification relative to the total section area with load factor of 1.01, compared to the works of Vogel (1985) with load factor 1.022, Barsan and Chiorean (1999) with load factor 1.03 and Lavall et al. (2013) with load factor 1.01. A very good agreement can be seen with

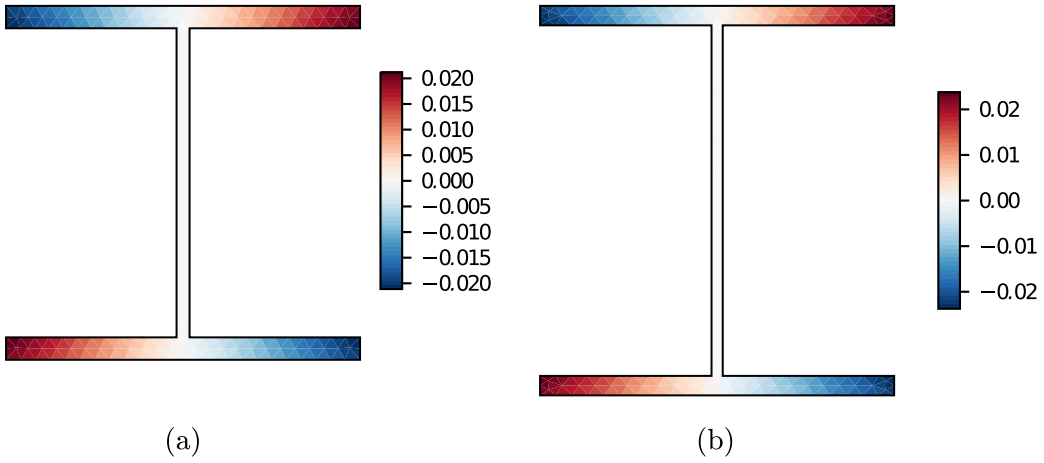

Figure 33: Warping function ψ for the sections of the (a) columns and (b) beam of Vogel's portal frame. Source: the author.

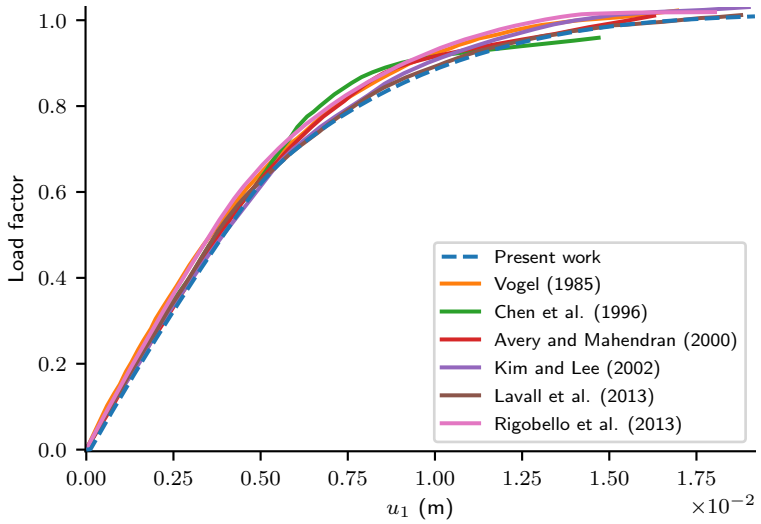

Figure 34: Displacement at the top of the right column of Vogel's portal frame. Source: the author.

the work of Vogel (1985). The pattern of plastification for the cross section of the rod element at the base of the right column for both works is compared in Figure 36. The values plastic strain for this section are shown in Figure 37, now with a color scale for the strain on each cell.

This example was also analyzed with both the three-dimensional and one-dimensional models of plastification. We can see in Figure 38 that the results are nearly identical, validating the hypothesis that the one-dimensional model is a good approximation for the behavior of rods in structural plane frames.

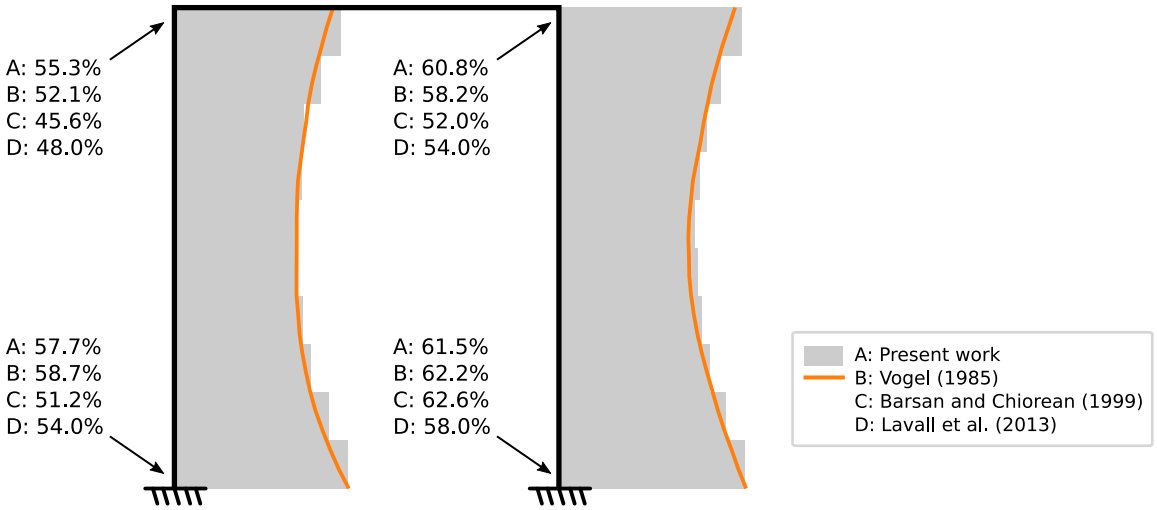

Figure 35: Ratios of column section areas that undergo plastification. Source: the author.

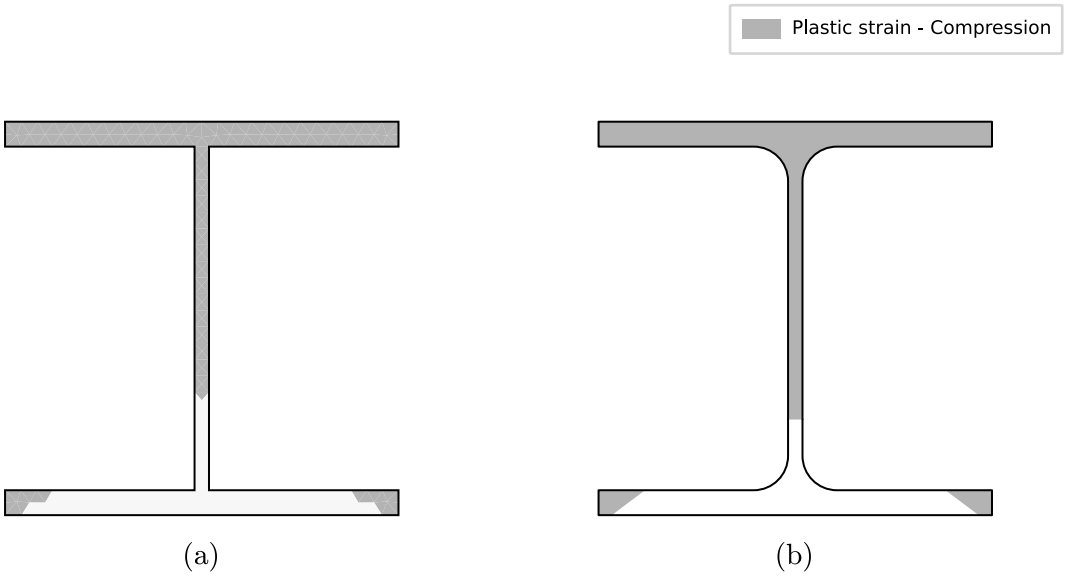

Figure 36: (a) Yield zone distribution for the cross section of the rod finite element at the base of the right column obtained in the present work; (b) yield zone distribution obtained by Vogel (1985) for the same cross section. Source: the author.

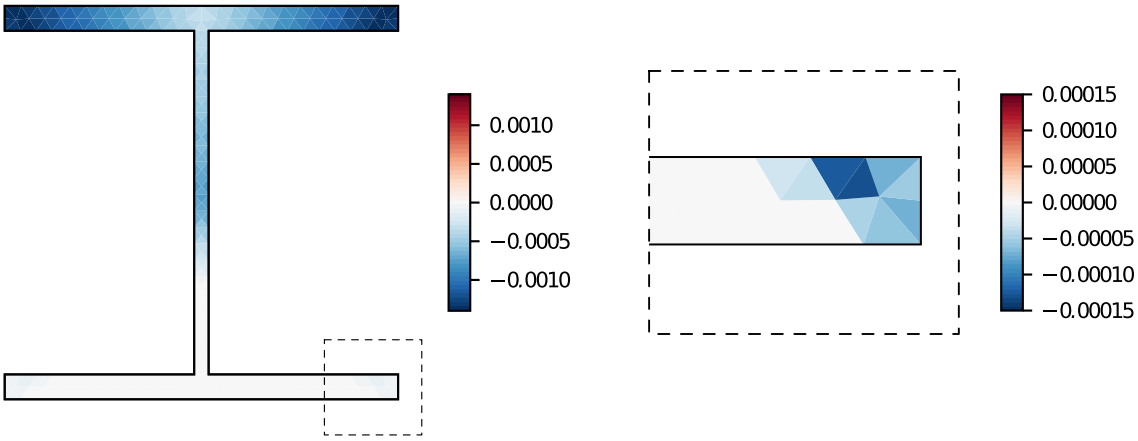

Figure 37: Yield zone distribution for the rod finite element at the base of the right column with color scale for the magnitude of the plastic strain. Source: the author.

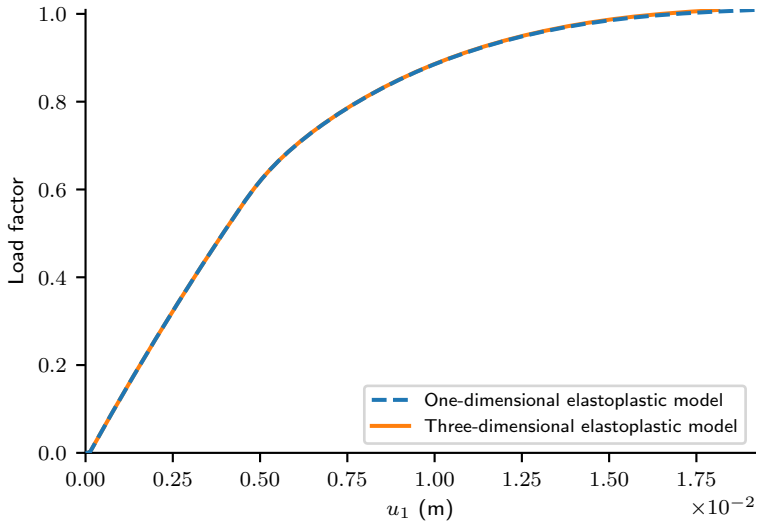

Figure 38: Displacement at the top of the right column of Vogel's portal frame comparing the plastification models with one and three dimensions. Source: the author.

4.6 Two-story space frame

This example analyzes an unbraced two-story space frame with configuration and problem data shown in Figure 39. The cross section, H150 x 160 x 6.5 x 10, is the same for all members of the frame. This frame was analyzed by Ngo-Huu (2007) and by Rigobello et al. (2013), and we follow the specifications made in those works. Accordingly, out-of-plumbness imperfections for the columns are given in Table 3 and are modeled directly in the rod mesh. The warping function for the cross section of the rods, obtained with the method described in section 2.1, can be seen in Figure 40. The residual stress distribution is the same as the one described in the previous example and its values for the cross section used here are shown in Figure 41. The frame was analyzed only with the one-dimensional elastoplastic constitutive model of section 3.5 and the material is considered perfectly plastic. We used a constant increment size of 8e-4 for the load factor.

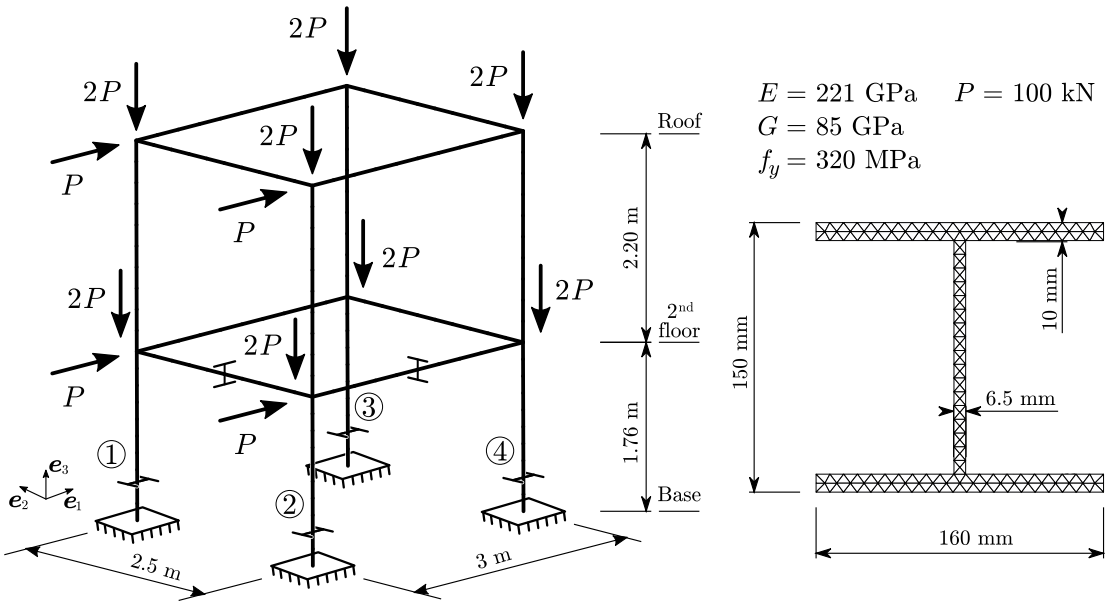

Figure 39: Configuration and problem data for two-story space frame example. Source: the author.

	Imperfections (mm)							
	Column 1		Column 2		Column 3		Column 4	
Level	$\boldsymbol{e}_1$	$\boldsymbol{e}_2$	$\boldsymbol{e}_1$	$\boldsymbol{e}_2$	$\boldsymbol{e}_1$	$\boldsymbol{e}_2$	$\boldsymbol{e}_1$	$\boldsymbol{e}_2$
Roof	4.51	11.08	5.49	11.41	-8.17	6.58	-4.31	12.04
2nd floor	1.39	6.88	-0.68	6.77	-5.11	2.11	-3.96	6.19
Base	0.0	0.0	0.0	0.0	0.0	0.0	0.0	0.0

Table 3: Out-of-plumbness imperfections for the columns of the two-story space frame.

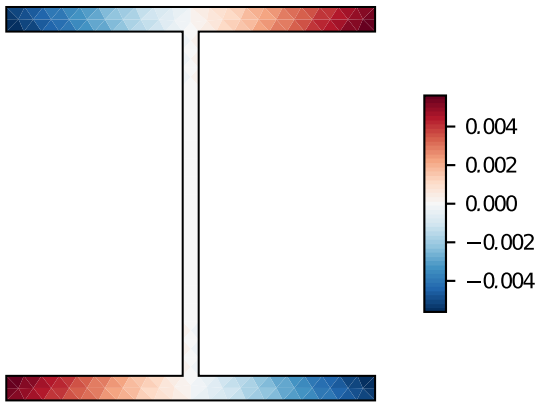

Figure 40: Warping function ψ for section H150 x 160 x 6.5 x 10. Source: the author.

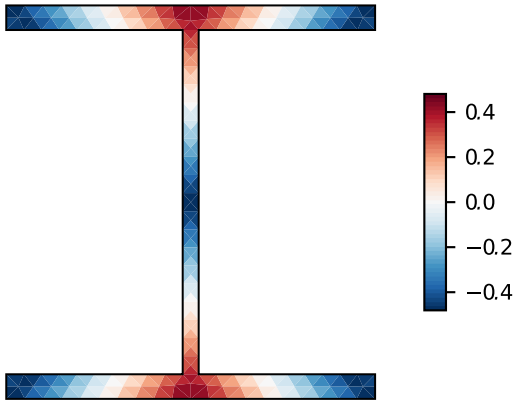

Figure 41: Residual stress factors $\hat{\sigma}_r$ for section H150 x 160 x 6.5 x 10. Source: the author.

The results for the displacements of column 4 in the direction of $\boldsymbol{e}_1$ are shown in Figure 42 for level of 2$^{\text{nd}}$ floor, and in Figure 43 for the roof level and have a very good agreement with the referenced works. The differences seen between the results of the present work and those of Ngo-Huu (2007) and Rigobello et al. (2013) may be attributed to a load step size too large to capture the asymptotic behavior of the displacements seen in the referenced works. Further testing with algorithms for automatic load step sizes must then be performed to check this hypothesis.

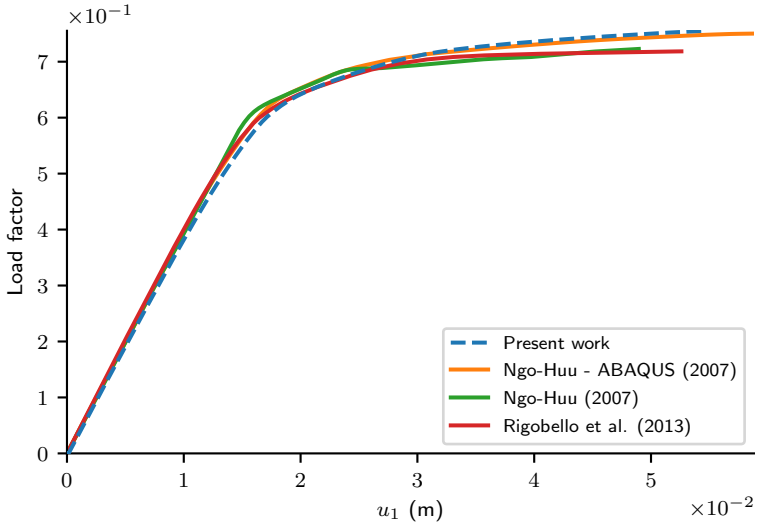

Figure 42: Displacement u_1 of column 4 at the level of 2$^{\text{nd}}$ floor. Source: the author.

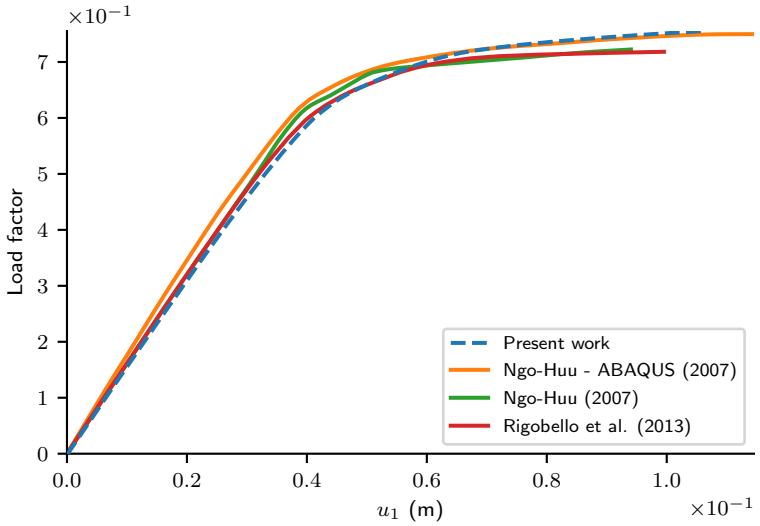

Figure 43: Displacement u_1 of column 4 at level of the roof. Source: the author.

5 Conclusion

This work presents the formulation of two elastoplastic constitutive models for small strains applied to a rod theory which features exact kinematics and consideration of cross sectional warping. Inelastic (ductile) rod structures, such as steel frame structures, experiencing large displacements and rotations but small strains are thereby possible to be analyzed. Furthermore, an implementation of these models with a variation of the plastic zone method is described, which allows the simulation of spread of plasticity along the rod axis and over the cross sections, capturing distributed stiffness degradation. Moreover, the existence of initial residual stresses is considered, as this is typical of steel structures.

To the author's knowledge, no such elastoplastic formulation for structural rod theories with consideration of cross sectional warping, i.e., for theories that treat the rod as one-dimensional idealization instead of a three-dimensional solid, and yet take warping into account, is available in the rod's literature so far, and we hope to have made a small contribution is this direction.

Several numerical tests were performed in order to validate the proposed scheme. The tests showed good consistency of the formulation with results from classic strength of materials in the linear elastic regime, and with results from the literature in more complex cases involving both geometric and material nonlinearities.

We note that, for cases involving structural frames under common, e.g., civil engineering, building loads, a one-dimensional plasticity model is an adequate simplification of the material behavior.

In particular, we hope this model may contribute with a simple, yet relatively robust, formulation for the so-called advanced analysis of steel structures, serving as a foundation on which variations of the method as well as several generalizations can be derived.

As for future paths, a better understanding of the constitutive models regarding their limitations, applicability and possible improvements would allow one to decide on the use of a simplified model. This may also help the understanding of heuristic measures, e.g., the reduction of material parameters by a certain factor, for the consideration of inelasticity and sensibility to nonlinearities as seen in many building standards.

References

ABNT (2008) *NBR 8800:2008 Projeto de estruturas de aço e de estruturas mistas de aço e concreto de edifícios*. Associação Brasileira de Normas Técnicas, Rio de Janeiro, Brasil.

AISC (2016) *ANSI/AISC 360-16 Specification for Structural Steel Buildings*. American Institute of Steel Construction, Chicago, United States of America.

ANTMAN, S. S. (1974) *Kirchhoff's problem for nonlinearly elastic rods*. Quarterly of Applied Mathematics XXXII (3), p. 221-240.

ANTMAN, J. J. (1979) *The eversion of thick spherical shells*. Archive for Rational Mechanics and Analysis. v. 70, p. 113-123.

ARGYRIS, J. (1982) *An excursion into large rotations*. Computer Methods in Applied Mechanics and Engineering v. 32. p. 85-155.

ARMERO, F.; ROMERO, I. (2003) *Energy-dissipative momentum-conserving time-stepping algorithms for the dynamics of nonlinear Cosserat rods*. Computational Mechanics 31. p. 3-26.

AVERY, P.; MAHENDRAN, M. (2000) *Distributed plasticity analysis of steel frame structures comprising non-compact sections*. Engineering Structures, v. 22, p. 901-919.

BALL, J. M. (1977) *Convexity Conditions and Existence Theorems in Non-linear Elasticity*. Archive for Rational Mechanics and Analysis, v. 63, p. 337-403.

BARSAN G.M.; CHIOREAN C. G. (1999) *Influence of residual stress on the carrying-capacity of steel framed structures*. Numerical investigation, Stability and Ductility of Steel Structures, Elsevier, p. 317-324.

BERTRAM, A. (2012) *Elasticity and Plasticity of Large Deformations: An Introduction*. 3. ed. (first edition in 2005) Springer, Berlin.

BETSCH, P.; STEINMAN P. (2003) *Constrained dynamics of geometrically exact beams*. Computational Mechanics 31. p. 49-59.

CAMPELLO, E. M. B. (2000) *Nonlinear Analysis of cold-formed steel members*. Dissertation (in Portuguese). Graduate Program in Civil Engineering, Polytechnic School,

University of São Paulo.

CAMPELLO, E. M. B.; LAGO, L. B. (2014) *Effect of higher order constitutive terms on the elastic buckling of thin-walled rods*. Thin-Walled Structures 77. p. 8-16.

CAMPELLO, E. M. B.; PIMENTA, P. M. (2001) *Geometrically nonlinear analysis of thin-walled space frames*. In: Proceedings of the Second European Conference on Computational Mechanics (II ECCM). Cracow.

CAMPELLO, E. M. B.; PIMENTA P. M. (2003) *A fully nonlinear multi-parameter rod model incorporating general cross sectional in-plane changes and out-of-plane warping*. Latin American Journal of Solids and Structures 1. p. 119-140.

CARDONA, A.; GÉRADIN, M. (1988) *A beam finite-element non-linear theory with finite rotations*. International Journal for Numerical Methods in Engineering, v. 26 (11), p. 2403-2438.

CARDONA, A.; HUESPE, A. (1998) *Continuation methods for tracing the equilibrium path in flexible mechanism analysis*. Engineering Computations, v. 15 (2),p. 190-220.

CARDONA, A.; HUESPE, A. (1999) *Evaluation of simple bifurcation points and post-critical path in large finite rotation problems*. Computer Methods in Applied Mechanics and Engineering 175. p. 137-156.

CHAVES, E. W. V. (2013) *Notes on continuum mechanics*. International Center for Numerical Methods in Engineering (CIMNE), Springer, Barcelona.

CHEN, W. F.; HAN, D. J. (1988) *Plasticity for structural engineers*. Springer-Verlag, Berlin.

CHEN, W.F.; GOTO, Y.; LIEW, J.Y.R. (1996) *Stability design of semi-rigid frames*. John Wiley & Sons, New York.

CIARLET, P. G. (1988) *Mathematical Elasticity Volume 1: Three-Dimensional Elasticity*. Elsevier, Netherlands, ISBN 978-0-444-70259-3

CORMEN, T. H.; LEISERSON, C. E.; RIVEST, R. L.; STEIN, C. (2001) *Introduction to Algorithms*. 2. ed. MIT Press, Cambridge.

CORRÊA, M. R. (2004) *Análise de estruturas reticuladas: rumo a uma teoria geometricamente exacta, cinematicamente completa e fisicamente não linear*. Tese (Doutorado em Engenharia Civil), Instituto Superior Técnico, Universidade Técnica de Lisboa.

DUNAVANT, D. A. (1985) *High degree efficient symmetrical Gaussian quadrature rules for the triangle*. International Journal for Numerical Methods in Engineering, v. 21(6), p. 1129-1148. ISSN 1097-0207.

DOWLING, N. E. (2013) *Mechanical behavior of materials. Engineering methods for deformation, fracture, and fatigue*. 4. ed. (first edition in) Pearson, Harlow, England.

ECCS. (1984) *Ultimate limit state calculation of sway frames with rigid joints*. Pub. 33. European Convention for Constructional Steelwork, Brussels.

GAMS, M.; PLANINC, I.; SAJE, M. (2007) *Energy conserving time integration scheme for geometrically exact beam*. Computer Methods in Applied Mechanics and Engineering 196. p. 2117-2129.

GAUSSMANN, F. (1951) *Uber die elastizitat poroser medien. (On elasticity of porous media)*. Vierteljahrsschrift der Naturforschenden Gesselschaft in Zurich, 96, p. 1-23.

GÉRADIN, M.; CARDONA, A. (2001) *Flexible Multibody Dynamics: A Finite Element Approach*. John Wiley & Sons, London.

GRUTTMANN, F.; SAUER, R.; WAGNER, W. (1999) *Shear stresses in prismatic beams with arbitrary cross sections*. International Journal for Numerical Methods in Engineering v. 45(7), p. 865-889.

GRUTTMANN, F.; SAUER, R.; WAGNER, W. (2000) *Theory and numerics of three-dimensional beams with elastoplastic material behaviour*. International Journal for Numerical Methods in Engineering 48. p. 1675-1702.

HAMMER, P. C.; MARLOWE, O. J.; STROUD, A. H. (1956) *Numerical integration over simplexes and cones*. In: Mathematical Tables and Other Aids to Computation, American Mathematical Society. v. 10, p. 130-137.

IBRAHIMBEGOVIĆ, A.; FREY, F.; ǨOZAR, I. (1995) *Computational aspects of vector-like parametrization of 3-dimensional finite rotations*. International Journal for Numerical

Methods in Engineering 38. p. 3653-3673.

IBRAHIMBEGOVIĆ, A.; MIKDAD, M. A. (2000) *Quadratically convergent direct calculation of critical points for 3d structures undergoing finite rotations.* Computer Methods in Applied Mechanics and Engineering 189. p. 107-120.

KIM S-E, LEE DH. (2002) *Second-order distributed plasticity analysis of space steel frames.* Engineering Structures, v. 24(6), p. 735-44.

KNOPS, R.J.; STUART, C. A. (1984) *Quasiconvexity and uniqueness of equilibrium solutions in nonlinear elasticity.* Arch. Rational Mech. Anal. Issue 86, p. 233-249.

LAVALL, A. C. C.; SILVA, R. G. L. da; COSTA, R. S.; FAKURY, R. H. (2013) Análise avançada de pórticos de aço conforme as prescrições da ABNT NBR 8800:2008. Revista da Estrutura de Aço, v. 2, n. 3, p. 146-165.

MEGSON, T. H. G. (2014) *Structural and stress analysis.* 3. ed. Elsevier Butterworth-Heinemann.

MESAROVIC, S. D. J. (1995) *Dynamic strain aging and plastic instabilities.* Journal of the Mechanics and Physics of Solids, v. 43, n. 5, p. 671-700.

MURDOCH, A. I. (2003) *Objectivity in classical continuum physics: a rationale for discarding the "principle of invariance under superposed rigid body motions" in favour of purely objective considerations.* Continuum Mechanics and Thermodynamics v. 15, p. 309-320.

NOLL, W. (2005a) *A Frame-Free Formulation of Elasticity.*

NOLL, W. (2005b) *The Theory of Surface Interactions.*

OGDEN, R. W. (1997) *Non-linear elastic deformations.* 2. ed. (first edition in 1984). Dover Publications Inc., New York, United States of America

OSAKADA, K. (2010) *History of plasticity and metal forming analysis.* Journal of Materials Processing Technology 210. p. 1436-1454.

PARK, R. J. T.; PRIESTLEY, M. J. N.; WALPOLE, W. R. (1983) *The seismic performance of steel encased reinforced concrete bridge piles.* Bulletin of the New Zealand

National Society for Earthquake Engineering, v. 16, n. 2, p. 123-140

PETROV, E.; GÉRADIN, M. (1998) *Finite element theory for curved and twisted beams based on exact solutions for three-dimensional solids. Part 2: Anisotropic and advanced beam models*. Computer Methods in Applied Mechanics and Engineering 165. p. 93-127.

PILKEY, W. D. (2002) *Analysis and design of elastic beams. Computational methods*. John Wiley and Sons.

PIMENTA, P. M. (1993) *On the geometrically-exact finite-strain rod model*. In: Proceeding of the third Pan-American Congress on Applied Mechanics, PACAM III, Escola Politécnica da Universidade de São Paulo, Brasil. p. 279-282.

PIMENTA, P. M.; CAMPELLO, E. M. B. (2001) *Geometrically nonlinear analysis of thin-walled space frames*. In: WASZCYSZYN Z.; STEIN, E. (eds.), Second European Conference On Computational Mechanics. Cracow, Poland.

PIMENTA, P. M.; CAMPELLO, E. M. B. (2003) *A fully nonlinar multi-parameter rod model incorporating general cross-section in-plane changes and out-of-plane warping*. Latin American Journal of Solids and Structures, v. 1 (1), p. 119-140.

PIMENTA, P. M.; YOJO, T. (1993a) *Geometrically exact analysis of spatial frames*. Applied Mechanics Reviews 46, n. 11, part 2, p. 118-128.

PIMENTA, P. M.; YOJO, T. (1993b) *Geometrically exact analysis of spatial frames with consideration of torsion warping*. In: Proceedings of the XVI Iberian-Latin-American Congress on Computational Methods in Engineering (XVI CILAMCE), São Paulo, p. 21-30.

PLANINC, I.; SAJE, M. (1999) *A quadratically convergent algorithm for the computation of stability points: The application of the determinant of the tangent stiffness matrix*. Computer Methods in Applied Mechanics and Engineering 169. p. 89-105.

PUZRIN, A. M. (2012) *Constitutive modeling in geomechanics*. Springer-Verlag, Berlin.

RAOULT, A. (1986) *Non-polyconvexity of the stored energy function of a Saint Venant-Kirchhoff material*. Aplikace Matemariky, Issue 6, p. 417-419.

REISSNER, E. (1972) *On one-dimensional finite-strain beam theory: the plane problem*.

Zeitschrift für Angewandte Mathematik und Physik, v. 23 (5), p. 795-804.

REISSNER, E. (1973) *On one-dimensional large displacement finite-strain beam theory.* Studies in Applied Mathematics, v. 52 (2), p. 87-95.

REISSNER, E. (1981) *On finite deformations of space-curved beams.* Zeitschrift für Angewandte Mathematik und Physik, v. 32 (6), p. 734-744.

RITTO-CORRÊA, M.; CAMOTIM, D. (2002) *On the differentiation of the rodrigues formula and its significance for the vector-like parameterization of Reissner-Simo beam theory.* International Journal for Numerical Methods in Engineering 55. p. 1005-1032.

RIGOBELLO, R.; CODA, H. B.; MUNAIAR NETO, J. (2013) *Inelastic analysis of steel frames with a solid-like finite element.* Journal of Constructional Steel Research, v. 86, p. 140-152.

SADOWSKI, A. J.; ROTTER, J. M.; STAFFORD, P. J.; REINKE, T.; UMMENHOFER, T. (2017) *On the gradient of the yield plateau in structural carbon steels.* Journal of Constructional Steel Research, v. 130, p. 120-130.

SAJE, M.; PLANINC I.; TURK G.; VRATANAR B. (1997) *A kinematically exact finite element formulation of planar elastic-plastic frames.* Computer Methods in Applied Mechanics and Engineering 144. p. 125-151.

SIMO, J. C. (1985) *A finite strain beam formulation. The three-dimensional dynamic problem.* Part I. Computer Methods in Applied Mechanics and Engineering 49. p. 55-70.

SIMO, J. C.; HUGHES, T. J. R. (1998) *Computational Inelasticity.* Springer, New York. (Interdisciplinary Applied Mathematics, v. 7).

TIAGO, C. M. (2007) *Meshless methods: Extending the linear formulation and its generalization to geometrically exact structural analysis.* Thesis. Instituto Superior Técnico, Universidade Técnica de Lisboa, Lisboa.

TIMOSHENKO; S. P. (1921) *On the correction factor for shear of the differential equation for transverse vibrations of bars of uniform cross-section.* Philosophical Magazine. p. 744.

TRUESDELL, C.; NOLL, W. (2004) *The Non-Linear Field Theories of Mechanics.* 3. ed. (first edition in 1965). Springer-Verlag, Berlin.

VLASOV, V. Z. (1959) *Thin-walled elastic bars*. 2. ed. (first edition in 1940) (in Russian), Fizmatgiz, Moscow.

VOGEL, U. (1985) *Calibrating frames*. Stahlbau 54. p. 295-311.

YOJO, T. (1993) *Análise não-linear geometricamente exacta de pórticos espaciais (com aplicação a torres de transmissão de alta tensão)*. Tese (Doutorado em Engenharia de Estruturas), Programa de Pós-graduação em Engenharia Civil, Escola Politécnica da Universidade de São Paulo.

Appendix A

Derivatives of $\boldsymbol{\eta}^r$ and $\boldsymbol{\kappa}^r$

First, we recall some elementary relations between skew-symmetric matrices and cross-products of vectors. Given vectors $\boldsymbol{a}$, $\boldsymbol{b}$ and $\boldsymbol{c}$, if $\boldsymbol{A} = \text{skew}(\boldsymbol{a})$ and $\boldsymbol{B} = \text{skew}(\boldsymbol{b})$, then

$$\boldsymbol{a} \times \boldsymbol{b} = -\,\boldsymbol{b} \times \boldsymbol{a} \tag{119}$$

$$\boldsymbol{A}\boldsymbol{b} = \boldsymbol{a} \times \boldsymbol{b} \tag{120}$$

$$\boldsymbol{A}^T\boldsymbol{b} = \boldsymbol{b} \times \boldsymbol{a} \tag{121}$$

$$\text{axial}(\boldsymbol{A}\boldsymbol{B} - \boldsymbol{B}\boldsymbol{A}) = \boldsymbol{a} \times \boldsymbol{b}. \tag{122}$$

And we also recall that the triple cross-product can be expanded as

$$\boldsymbol{a} \times (\boldsymbol{b} \times \boldsymbol{c}) = (\boldsymbol{c} \cdot \boldsymbol{a})\,\boldsymbol{b} - (\boldsymbol{a} \cdot \boldsymbol{b})\,\boldsymbol{c}. \tag{123}$$

Next, we restate, for reference, the definition of the tensor derivatives related to the rotation tensor:

$$\boldsymbol{\Omega} = \dot{\boldsymbol{Q}}\boldsymbol{Q}^T \qquad \dot{\boldsymbol{Q}} = \boldsymbol{\Omega}\boldsymbol{Q}, \tag{124}$$

$$\boldsymbol{K} = \boldsymbol{Q}'\boldsymbol{Q}^T \qquad \boldsymbol{Q}' = \boldsymbol{K}\boldsymbol{Q}, \tag{125}$$

$$\boldsymbol{G} = \delta\boldsymbol{Q}\boldsymbol{Q}^T \qquad \delta\boldsymbol{Q} = \boldsymbol{G}\boldsymbol{Q}, \tag{126}$$

$$\boldsymbol{H} = \Delta\boldsymbol{Q}\boldsymbol{Q}^T \qquad \Delta\boldsymbol{Q} = \boldsymbol{H}\boldsymbol{Q}, \tag{127}$$

and their axial vectors, products of $\boldsymbol{\Gamma}$ and derivatives of the vector of rotation parameters:

$$\boldsymbol{\omega} = \text{axial}(\boldsymbol{\Omega}) = \boldsymbol{\Gamma}\dot{\boldsymbol{\theta}} \tag{128}$$

$$\boldsymbol{\kappa} = \text{axial}(\boldsymbol{K}) = \boldsymbol{\Gamma}\boldsymbol{\theta}' \tag{129}$$

$$\boldsymbol{g} = \text{axial}(\boldsymbol{G}) = \boldsymbol{\Gamma}\delta\boldsymbol{\theta} \tag{130}$$

$$\boldsymbol{h} = \text{axial}(\boldsymbol{H}) = \boldsymbol{\Gamma}\Delta\boldsymbol{\theta}. \tag{131}$$

We can then find the axial vectors of combined derivatives of the rotation tensor. From

$$\dot{\boldsymbol{Q}}' = \dot{\overline{(\boldsymbol{K}\boldsymbol{Q})}} = \dot{\boldsymbol{K}}\boldsymbol{Q} + \boldsymbol{K}\dot{\boldsymbol{Q}} = \dot{\boldsymbol{K}}\boldsymbol{Q} + \boldsymbol{K}\boldsymbol{\Omega}\boldsymbol{Q} \tag{132}$$

$$\dot{\boldsymbol{Q}}' = (\boldsymbol{\Omega}\boldsymbol{Q})' = \boldsymbol{\Omega}'\boldsymbol{Q} + \boldsymbol{\Omega}\boldsymbol{Q}' = \boldsymbol{\Omega}'\boldsymbol{Q} + \boldsymbol{\Omega}\boldsymbol{K}\boldsymbol{Q}, \tag{133}$$

we have

$$\dot{\boldsymbol{K}}\boldsymbol{Q} = \boldsymbol{\Omega}'\boldsymbol{Q} + \boldsymbol{\Omega}\boldsymbol{K}\boldsymbol{Q} - \boldsymbol{K}\boldsymbol{\Omega}\boldsymbol{Q} \tag{134}$$

$$\dot{\boldsymbol{K}} = \boldsymbol{\Omega}' + \boldsymbol{\Omega}\boldsymbol{K} - \boldsymbol{K}\boldsymbol{\Omega} \tag{135}$$

$$\dot{\boldsymbol{\kappa}} = \boldsymbol{\omega}' + \boldsymbol{\omega} \times \boldsymbol{\kappa} \tag{136}$$

and

$$\boldsymbol{\Omega}'\boldsymbol{Q} = \dot{\boldsymbol{K}}\boldsymbol{Q} + \boldsymbol{K}\boldsymbol{\Omega}\boldsymbol{Q} - \boldsymbol{\Omega}\boldsymbol{K}\boldsymbol{Q} \tag{137}$$

$$\boldsymbol{\Omega}' = \dot{\boldsymbol{K}} + \boldsymbol{K}\boldsymbol{\Omega} - \boldsymbol{\Omega}\boldsymbol{K} \tag{138}$$

$$\boldsymbol{\omega}' = \dot{\boldsymbol{\kappa}} + \boldsymbol{\kappa} \times \boldsymbol{\omega}. \tag{139}$$

Analogously, from $\delta\boldsymbol{Q}' = \delta\boldsymbol{K}\boldsymbol{Q} + \boldsymbol{K}\boldsymbol{G}\boldsymbol{Q} = \boldsymbol{G}'\boldsymbol{Q} + \boldsymbol{G}\boldsymbol{K}\boldsymbol{Q}$, we obtain

$$\delta\boldsymbol{\kappa} = \boldsymbol{g}' + \boldsymbol{g} \times \boldsymbol{\kappa} \qquad \text{and} \qquad \boldsymbol{g}' = \delta\boldsymbol{\kappa} + \boldsymbol{\kappa} \times \boldsymbol{g}. \tag{140}$$

From $\Delta\boldsymbol{Q}' = \Delta\boldsymbol{K}\boldsymbol{Q} + \boldsymbol{K}\boldsymbol{H}\boldsymbol{Q} = \boldsymbol{H}'\boldsymbol{Q} + \boldsymbol{H}\boldsymbol{K}\boldsymbol{Q}$, we have

$$\Delta\boldsymbol{\kappa} = \boldsymbol{h}' + \boldsymbol{h} \times \boldsymbol{\kappa} \qquad \text{and} \qquad \boldsymbol{h}' = \Delta\boldsymbol{\kappa} + \boldsymbol{\kappa} \times \boldsymbol{h}. \tag{141}$$

And from $\Delta\delta\boldsymbol{Q} = \Delta\boldsymbol{G}\boldsymbol{Q} + \boldsymbol{G}\boldsymbol{H}\boldsymbol{Q} = \delta\boldsymbol{H}\boldsymbol{Q} + \boldsymbol{H}\boldsymbol{G}\boldsymbol{Q}$, we get

$$\Delta\boldsymbol{g} = \delta\boldsymbol{h} + \boldsymbol{h} \times \boldsymbol{g} \qquad \text{and} \qquad \delta\boldsymbol{h} = \Delta\boldsymbol{g} + \boldsymbol{g} \times \boldsymbol{h}. \tag{142}$$

With these, we can simplify the expressions for the variation and linearization of $\boldsymbol{\kappa}^r$, detailed step by step below:

$$\begin{aligned}
\boldsymbol{\kappa}^r &= \boldsymbol{Q}^T\boldsymbol{\kappa} && (143)\\
&= \boldsymbol{Q}^T\boldsymbol{\Gamma}\boldsymbol{\theta}' && (144)\\
&= \boldsymbol{\Gamma}^T\boldsymbol{\theta}' && (145)\\
\delta\boldsymbol{\kappa}^r &= \delta(\boldsymbol{Q}^T\boldsymbol{\kappa}) && (146)\\
&= \delta\boldsymbol{Q}^T\boldsymbol{\kappa} + \boldsymbol{Q}^T\delta\boldsymbol{\kappa} && (147)\\
&= \boldsymbol{Q}^T\boldsymbol{G}^T\boldsymbol{\kappa} + \boldsymbol{Q}^T\delta\boldsymbol{\kappa} && (148)\\
&= \boldsymbol{Q}^T(\boldsymbol{G}^T\boldsymbol{\kappa} + \delta\boldsymbol{\kappa}) && (149)\\
&= \boldsymbol{Q}^T(\delta\boldsymbol{\kappa} + \boldsymbol{\kappa}\times\boldsymbol{g}) && (150)\\
&= \boldsymbol{Q}^T\boldsymbol{g}' && (151)\\
&= \boldsymbol{Q}^T(\boldsymbol{\Gamma}\delta\boldsymbol{\theta})' && (152)\\
&= \boldsymbol{Q}^T(\boldsymbol{\Gamma}'\delta\boldsymbol{\theta} + \boldsymbol{\Gamma}\delta\boldsymbol{\theta}') && (153)\\
\Delta\delta\boldsymbol{\kappa}^r &= \Delta(\boldsymbol{Q}^T\boldsymbol{g}') && (154)\\
&= \Delta\boldsymbol{Q}^T\boldsymbol{g}' + \boldsymbol{Q}^T\Delta\boldsymbol{g}' && (155)\\
&= \boldsymbol{Q}^T\boldsymbol{H}^T\boldsymbol{g}' + \boldsymbol{Q}^T\Delta\boldsymbol{g}' && (156)\\
&= \boldsymbol{Q}^T(\boldsymbol{H}^T\boldsymbol{g}' + \Delta\boldsymbol{g}') && (157)\\
&= \boldsymbol{Q}^T(\boldsymbol{g}'\times\boldsymbol{h} + \Delta\boldsymbol{g}') && (158)\\
&= \boldsymbol{Q}^T\Big((\boldsymbol{\Gamma}\delta\boldsymbol{\theta})'\times\boldsymbol{\Gamma}\Delta\boldsymbol{\theta} + \Delta(\boldsymbol{\Gamma}\delta\boldsymbol{\theta})'\Big) && (159)\\
&= \boldsymbol{Q}^T\Big((\boldsymbol{\Gamma}'\delta\boldsymbol{\theta} + \boldsymbol{\Gamma}\delta\boldsymbol{\theta}')\times\boldsymbol{\Gamma}\Delta\boldsymbol{\theta} + \Delta\boldsymbol{\Gamma}'\delta\boldsymbol{\theta} + \boldsymbol{\Gamma}'\Delta\delta\boldsymbol{\theta} + \Delta\boldsymbol{\Gamma}\delta\boldsymbol{\theta}' + \boldsymbol{\Gamma}\Delta\delta\boldsymbol{\theta}'\Big) && (160)\\
&= \boldsymbol{Q}^T\Big((\boldsymbol{\Gamma}'\delta\boldsymbol{\theta} + \boldsymbol{\Gamma}\delta\boldsymbol{\theta}')\times\boldsymbol{\Gamma}\Delta\boldsymbol{\theta} + \Delta\boldsymbol{\Gamma}'\delta\boldsymbol{\theta} + \Delta\boldsymbol{\Gamma}\delta\boldsymbol{\theta}'\Big). && (161)
\end{aligned}$$

Notice that we can recombine the differentiations in equations (146) through (151) to obtain other back-rotated derivatives related to the rotation parameters, if needed:

$$\delta(\boldsymbol{Q}^T\boldsymbol{\kappa}) = \boldsymbol{Q}^T\boldsymbol{g}' \qquad (\boldsymbol{Q}^T\boldsymbol{g})' = \boldsymbol{Q}^T\delta\boldsymbol{\kappa} \qquad (162)$$

$$\Delta(\boldsymbol{Q}^T\boldsymbol{g}) = \boldsymbol{Q}^T\delta\boldsymbol{h} \qquad \delta(\boldsymbol{Q}^T\boldsymbol{h}) = \boldsymbol{Q}^T\Delta\boldsymbol{g} \qquad (163)$$

$$(\boldsymbol{Q}^T\boldsymbol{h})' = \boldsymbol{Q}^T\Delta\boldsymbol{\kappa} \qquad \Delta(\boldsymbol{Q}^T\boldsymbol{\kappa}) = \boldsymbol{Q}^T\boldsymbol{h}'. \qquad (164)$$

Finally, we do the same for $\boldsymbol{\eta}^r$:

$$\boldsymbol{\eta} = \boldsymbol{u}' + \boldsymbol{Q}^T\boldsymbol{e}_3 - \boldsymbol{e}_3 \tag{165}$$

$$\boldsymbol{\eta}^r = \boldsymbol{Q}^T\boldsymbol{\eta} \tag{166}$$

$$= \boldsymbol{Q}^T(\boldsymbol{u}' + \boldsymbol{e}_3^r) - \boldsymbol{e}_3^r \tag{167}$$

$$\delta\boldsymbol{\eta}^r = \delta(\boldsymbol{Q}^T\boldsymbol{\eta}) \tag{168}$$

$$= \delta\boldsymbol{Q}^T\boldsymbol{u}' + \boldsymbol{Q}^T\delta\boldsymbol{u}' + \delta\boldsymbol{Q}^T\boldsymbol{e}_3^r + \boldsymbol{Q}^T\delta\boldsymbol{e}_3^r - \delta\boldsymbol{e}_3^r \tag{169}$$

$$= \boldsymbol{Q}^T\delta\boldsymbol{u}' + \delta\boldsymbol{Q}^T(\boldsymbol{u}' + \boldsymbol{e}_3^r) \tag{170}$$

$$= \boldsymbol{Q}^T\delta\boldsymbol{u}' + \boldsymbol{Q}^T\boldsymbol{G}^T(\boldsymbol{u}' + \boldsymbol{e}_3^r) \tag{171}$$

$$= \boldsymbol{Q}^T\Big(\delta\boldsymbol{u}' + \boldsymbol{G}^T(\boldsymbol{u}' + \boldsymbol{e}_3^r)\Big) \tag{172}$$

$$= \boldsymbol{Q}^T\Big(\delta\boldsymbol{u}' + (\boldsymbol{u}' + \boldsymbol{e}_3^r) \times \boldsymbol{g}\Big) \tag{173}$$

$$= \boldsymbol{Q}^T\Big(\delta\boldsymbol{u}' + (\boldsymbol{u}' + \boldsymbol{e}_3^r) \times \boldsymbol{\Gamma}\delta\boldsymbol{\theta}\Big) \tag{174}$$

$$\Delta\delta\boldsymbol{\eta}^r = \Delta\Big(\boldsymbol{Q}^T\Big(\delta\boldsymbol{u}' + (\boldsymbol{u}' + \boldsymbol{e}_3^r) \times \boldsymbol{g}\Big)\Big) \tag{175}$$

$$= \Delta\boldsymbol{Q}^T\Big(\delta\boldsymbol{u}' + (\boldsymbol{u}' + \boldsymbol{e}_3^r) \times \boldsymbol{g}\Big) + \boldsymbol{Q}^T\Delta\Big(\delta\boldsymbol{u}' + (\boldsymbol{u}' + \boldsymbol{e}_3^r) \times \boldsymbol{g}\Big) \tag{176}$$

$$\begin{aligned} = \boldsymbol{Q}^T\boldsymbol{H}^T&\Big(\delta\boldsymbol{u}' + (\boldsymbol{u}' + \boldsymbol{e}_3^r) \times \boldsymbol{g}\Big) \\ &+ \boldsymbol{Q}^T\Big(\Delta\delta\boldsymbol{u}' + (\Delta\boldsymbol{u}' + \Delta\boldsymbol{e}_3^r) \times \boldsymbol{g} + (\boldsymbol{u}' + \boldsymbol{e}_3^r) \times \Delta\boldsymbol{g}\Big) \end{aligned} \tag{177}$$

$$= \boldsymbol{Q}^T\boldsymbol{H}^T\Big(\delta\boldsymbol{u}' + (\boldsymbol{u}' + \boldsymbol{e}_3^r) \times \boldsymbol{g}\Big) + \boldsymbol{Q}^T\Big(\Delta\boldsymbol{u}' \times \boldsymbol{g} + (\boldsymbol{u}' + \boldsymbol{e}_3^r) \times \Delta\boldsymbol{g}\Big) \tag{178}$$

$$= \boldsymbol{Q}^T\Big(\delta\boldsymbol{u}' \times \boldsymbol{h} - \boldsymbol{h} \times ((\boldsymbol{u}' + \boldsymbol{e}_3^r) \times \boldsymbol{g}) + \Delta\boldsymbol{u}' \times \boldsymbol{g} + (\boldsymbol{u}' + \boldsymbol{e}_3^r) \times \Delta\boldsymbol{g}\Big) \tag{179}$$

$$\begin{aligned} = \boldsymbol{Q}^T\Big(&\delta\boldsymbol{u}' \times \boldsymbol{h} - (\boldsymbol{g} \cdot \boldsymbol{h})(\boldsymbol{u}' + \boldsymbol{e}_3^r) + (\boldsymbol{h} \cdot (\boldsymbol{u}' + \boldsymbol{e}_3^r))\,\boldsymbol{g} \\ &+ \Delta\boldsymbol{u}' \times \boldsymbol{g} + (\boldsymbol{u}' + \boldsymbol{e}_3^r) \times \Delta\boldsymbol{g}\Big) \end{aligned} \tag{180}$$

$$\begin{aligned} = \boldsymbol{Q}^T\Big(&\delta\boldsymbol{u}' \times \boldsymbol{\Gamma}\Delta\boldsymbol{\theta} - (\boldsymbol{\Gamma}\delta\boldsymbol{\theta} \cdot \boldsymbol{\Gamma}\Delta\boldsymbol{\theta})(\boldsymbol{u}' + \boldsymbol{e}_3^r) + (\boldsymbol{\Gamma}\Delta\boldsymbol{\theta} \cdot (\boldsymbol{u}' + \boldsymbol{e}_3^r))\boldsymbol{\Gamma}\delta\boldsymbol{\theta} \\ &+ \Delta\boldsymbol{u}' \times \boldsymbol{\Gamma}\delta\boldsymbol{\theta} + (\boldsymbol{u}' + \boldsymbol{e}_3^r) \times (\Delta\boldsymbol{\Gamma}\delta\boldsymbol{\theta} + \boldsymbol{\Gamma}\Delta\delta\boldsymbol{\theta})\Big) \end{aligned} \tag{181}$$

$$\begin{aligned} = \boldsymbol{Q}^T\Big(&\delta\boldsymbol{u}' \times \boldsymbol{\Gamma}\Delta\boldsymbol{\theta} - (\boldsymbol{\Gamma}\delta\boldsymbol{\theta} \cdot \boldsymbol{\Gamma}\Delta\boldsymbol{\theta})(\boldsymbol{u}' + \boldsymbol{e}_3^r) + (\boldsymbol{\Gamma}\Delta\boldsymbol{\theta} \cdot (\boldsymbol{u}' + \boldsymbol{e}_3^r))\boldsymbol{\Gamma}\delta\boldsymbol{\theta} \\ &+ \Delta\boldsymbol{u}' \times \boldsymbol{\Gamma}\delta\boldsymbol{\theta} + (\boldsymbol{u}' + \boldsymbol{e}_3^r) \times \Delta\boldsymbol{\Gamma}\delta\boldsymbol{\theta}\Big). \end{aligned} \tag{182}$$

In this appendix, we used $\boldsymbol{\Gamma}$, $\boldsymbol{\Gamma}'$, $\Delta\boldsymbol{\Gamma}$, and $\Delta\boldsymbol{\Gamma}'$ as defined in equations (19), (24), (48), and (49) respectively.